DESIGN AND MODELING OF SPECIALTY OPTICAL FIBERS FOR SUPERCONTINUUM GENERATION

Type text here

Thesis submitted by

POOJA CHAUHAN

In Partial Fulfillment of the Requirements for the Degree of

DOCTOR OF PHILOSOPHY

Under the Joint Supervision of

Dr. AJEET KUMAR

&

Dr. YOGITA KALRA

Department of Applied Physics, Delhi Technological University

Shahbad Daulatpur, Main Bawana Road, Delhi, India

October-2020

DEDICATED

TO

MY BELOVED PARENTS

DELHI TECHNOLOGICAL UNIVERSITY
(Govt. of National Capital Territory of Delhi)
Shahbad Daulatpur, Main Bawana Road,
Delhi 110042, India

CERTIFICATE

This is to certify that the Ph.D. thesis entitled **"DESIGN AND MODELING OF SPECIALTY OPTICAL FIBERS FOR SUPERCONTINUUM GENERATION"** submitted to the Delhi Technological University, Delhi, India for the award of Doctor of Philosophy is based on the original research work carried out by me under the joint supervision of Dr. Ajeet Kumar, Assistant Professor and Dr. Yogita Kalra, Assistant Professor, Department of Applied Physics, Delhi Technological University, Delhi, India. It is further certified that the work embodied in this thesis has neither partially nor fully submitted to any other university or institution for the award of any degree or diploma.

Ms. Pooja Chauhan
PhD Scholar
(2K16/PhD/AP/16)

This is certify that the above statement made by the candidate is correct to the best of our knowledge.

Dr. Ajeet Kumar
(Supervisor)
Assistant Professor
Department of Applied Physics
Delhi Technological
University,

Dr. Yogita Kalra
(Supervisor)
Assistant Professor
Department of Applied Physics
Delhi Technological University,
Delhi, India

Prof. Rinku Sharma
(Head of the Department)
Department of Applied Physics
Delhi Technological University,
Delhi, India

ACKNOWLEDGEMENTS

It gives me an immense debt of gratitude to express my sincere thanks to my supervisors Dr. Ajeet Kumar, and Dr. Yogita Kalra, Department of Applied Physics, Delhi Technological University for being my doctoral research endeavor for past four years and providing me an opportunity to carry out my research under their guidance and support.

My sincere gratitude is reserved for Prof. Yogesh Singh, Vice-Chancellor, Delhi Technological University, and Prof. Rinku Sharma, Head of the Department, Applied Physics, Delhi Technological University for providing all necessary infrastructure, resources, and platforms to carry out my research work. Further, I place my special appreciation and thanks to the SRC, and DRC Committee members: Prof. S. C. Sharma (Chairman, DRC), Prof. Anurag Sharma (External Expert), Prof. Annapoorni (External Expert), Dr. Mukesh Jewariya (External Expert), Dr. M. Jayasimadri (Internal Expert), and Prof. Neeta Pandey (Internal Expert) who have served in my committee and gave their valuable time and suggestions on my thesis.

I also thank Prof. R.K. Sinha, Chapter Advisor and Dr. Yogita Kalra, Chapter Co-Advisor, SPIE and OSA Student Chapters at Delhi Technological University, India. I am extremely grateful and indebted to them for their constant support and encouragement extended to me.

I would like to give my heartfelt gratitude to Dr. Than Singh Saini (Postdoctoral Fellow, IISC, Bangalore) for his continuous support, scientific advices, continuous encouragement, and valuable input at all stages of my PhD journey. I put my special thanks to Dr. Sikandar Abbas (Postdoctoral Fellow, Carnegie Mellon University, USA), Dr. José Carlos Pérez (PhD, University of Rochester, USA), and Dr. Pawan Kumar (Assistant Professor, Tarsus University, Turkey) for their invaluable acumens and suggestions during the review process of my thesis.

Also, I thank all the faculty members and staff of Applied Physics Department for their constant help, co-operation and encouragement during my entire PhD period.

I thank my parents for their interminable support and encouragement. At the end, I would place on record, my sense of gratitude to everyone who, directly or indirectly have lent their support in this journey.

Date: 27/10/2020 **(Pooja Chauhan)**

Place: Delhi

ABSTRACT

This thesis work aims to design and modeling of specialty optical fibers for supercontinuum generation. Some novel photonic crystal fiber designs have been explored for the study of supercontinuum generation using highly nonlinear materials such as silica, tellurite, chalcogenide, and organic liquids in shorter fiber length with low input peak power and also focused on the coherence property to enhance the bandwidth of the supercontinuum broadband in the visible, near and mid-infrared wavelength regions.

Supercontinuum generation arises due to broadening of the high-intensity ultra-short pulses in a nonlinear optically active medium due to self-phase modulation, cross-phase modulation, solitons, high order dispersion, stimulated Raman scattering, self-steepening, and some optical losses. The various potential applications of supercontinuum sources include cancer detection, medical imaging, gas sensing, optical coherence tomography, wavelength-division multiplexing, spectroscopy, and metrology.

In this thesis, some sincere efforts have been made to numerically design the dispersion engineered photonic crystal fiber designs for supercontinuum generation in the visible, near, and mid-infrared wavelength regions. The computational analysis of the proposed fiber designs is based on the finite element method. We have tried to optimize the dispersion characteristics to reduce the effect of dispersion at the pump wavelength by tweaking the respective geometrical parameters of the core and cladding and also by changing the material composition in the core region. We have numerically analyzed the influence of input peak power, pulse width, peak power, and coherence on the supercontinuum broadening.

The proposed silica-based photonic crystal fibers can generate the broad supercontinuum spectrum of bandwidth 0.67 μm to 2.4 μm in the visible and the near-infrared wavelength region at low input power in shorter fiber length. Some newly reported chalcogenide glasses

have been numerically investigated for the ultra-broadband supercontinuum generation in the infrared wavelength region. We have attained the supercontinuum spanning, 1 μm to 14 μm and 2 μm to 11 μm in photonic crystal fibers composed of Ga-Sb-S and GAP-Se chalcogenides respectively. In a tellurite based photonic crystal fiber, we achieved a broadband supercontinuum ranging, 1 μm to 5.5 μm. We have also proposed a photonic crystal fiber based on liquid infiltration to increase the nonlinearity in silica fibers and able to produce highly coherent supercontinuum broadband of spanning, 1 μm to 2.6 μm in the near-infrared wavelength region by using a few centimeters fiber length with low peak power.

Keywords:

Specialty Optical Fibers, Photonic Crystal Fibers, Silica, Tellurite, Chalcogenides, Organic Liquids, Dispersion, Nonlinearity, Effective Mode Area, Supercontinuum Generation, Coherence

LIST OF PUBLICATIONS

Articles in Refereed International Journals (Thesis)

1. **P. Chauhan**, A. Kumar, and Y. Kalra, "Numerical exploration of coherent supercontinuum generation in multicomponent $GeSe_2$–As_2Se_3–PbSe chalcogenide based photonic crystal fiber", Optical Fiber Technology 54, p. 102100, 2020.

2. **P. Chauhan**, A. Kumar, and Y. Kalra, "Computational modeling of tellurite based photonic crystal fiber for infrared supercontinuum generation", Optik 187, pp. 92–97, 2019. ***(Commendable Research Award)***

3. **P. Chauhan**, A. Kumar, and Y. Kalra, "A dispersion engineered silica-based photonic crystal fiber for supercontinuum generation in near-infrared wavelength region", Optik 187, pp. 230–237, 2019. ***(Commendable Research Award)***

4. **P. Chauhan**, A. Kumar, and Y. Kalra, "Mid–infrared broadband supercontinuum generation in a highly nonlinear rectangular core chalcogenide photonic crystal fiber", Optical Fiber Technology 46, pp. 174–178, 2018. ***(Commendable Research Award)***

5. **P. Chauhan**, A. Kumar, and Y. Kalra, "Fluidic infiltrated core based photonic crystal fiber for coherent supercontinuum generation". (under communication)

Articles in Refereed International Journals (outside Thesis)

1. R. Sharma, S. Kaur, **P. Chauhan**, and A. Kumar, "Computational design & analysis of $GeSe_2$–As_2Se_3–PbSe based rib waveguide for mid-infrared supercontinuum generation", Optik 220, p. 165032, 2020.

Articles in Conference Proceedings (Thesis)

1. **P. Chauhan**, A. Kumar, and Y. Kalra, "Supercontinuum generation in a hollow-core methanol-silica based photonic crystal fiber: computational model and analysis", In Proc. of SPIE Vol. 11498, pp. 114980T-1, 2020.

2. **P. Chauhan**, A. Kumar, and Y. Kalra, "Ultra–coherent supercontinuum generation in isopropanol–silica based photonic crystal fiber at 1300 nm and 1600 nm wavelengths", In Photonic and Phononic Properties of Engineered Nanostructures X 11289, p. 1128923, International Society for Optics and Photonics, 2020.

3. **P. Chauhan**, A. Kumar, Y. Kalra, and T.S. Saini, "A multicomponent GAP–Se chalcogenide composition–based rectangular photonic crystal fiber for coherent supercontinuum generation", In Photonic Fiber and Crystal Devices: Advances in Materials and Innovations in Device Applications XIII 11123, p. 1112310, International Society for Optics and Photonics, 2019.

4. **P. Chauhan**, A. Kumar, and Y. Kalra, "Mid–infrared supercontinuum generation in highly nonlinear $AsSe_2$ chalcogenide circular photonic crystal fiber", In Frontiers in Optics, pp. JTu3A–34, Optical Society of America, 2019.

5. **P. Chauhan**, A. Kumar, Y. Kalra, and T.S. Saini, "Design and analysis of photonic crystal fiber in Ga–Sb–S chalcogenide glass for nonlinear applications", In AIP Conference Proceedings 2009(1), p. 020047, AIP Publishing LLC, 2018.

6. **P. Chauhan**, A. Kumar, Y. Kalra, and T.S. Saini, "Highly nonlinear spiral shaped photonic crystal fiber in a Ga–Sb–S chalcogenide glass for nonlinear applications", In Photonic Fiber and Crystal Devices: Advances in Materials and Innovations in Device Applications XII 10755, p. 1075510, International Society for Optics and Photonics, 2018.

7. **P. Chauhan**, A. Kumar, Y. Kalra, and T.S. Saini, "Rectangular core dispersion engineered photonic crystal fiber for supercontinuum generation", In Laser Science, pp. JW4A–69, Optical Society of America, 2018.

8. **P. Chauhan,** A. Kumar, Y. Kalra, and T.S. Saini, "A rectangular core photonic crystal fiber for nonlinear applications", International Conference on Advances in Science and Technology (ICAST), p. 109, SKIT, Jaipur, India, 2018.

9. **P. Chauhan**, A. Kumar, Y. Kalra, T.S. Saini, "Design and analysis of a chalcogenide step–index fiber for nonlinear applications", IEEE International Conference on Photonics and High Speed Optical Networks (ICPHON–2018), Department of Electronics and Communication Engineering, S.A. Engineering College, Chennai, Tamil Nadu, India, pp. 79-82, 2018.

10. **P. Chauhan**, A. Kumar, Y. Kalra, and T.S. Saini, "A rectangular-shaped photonic crystal fiber for nonlinear applications", National Student Conclave & Seminar on Science, Technology & Innovation, p. 79, Amity University, Noida, Uttar Pradesh, India, 2018.

11. **P. Chauhan**, A.t Kumar, Y. Kalra, "An organic liquid core photonic crystal fiber for nonlinear applications", Workshop on Optics & Photonics: Theory & Computational Techniques (OPTCT), p. 08, Department of Physics, Indian Institute of Technology Roorkee, Uttar Pradesh, India, 2018.

12. **P. Chauhan**, A. Kumar, T.S. Saini, and Y. Kalra, "Nanostructural-core photonic crystal fiber with very low negative dispersion for nonlinear applications", In Laser Science, pp. JW4A–120, Optical Society of America, 2017.

Articles in Conference Proceedings (Outside Thesis)

1. R. Sharma, S. Kaur, **P. Chauhan**, and A. Kumar, "Numerical modeling of rib waveguide of $GeSe_2$-As_2Se_3-PbSe chalcogenide glass for infrared supercontinuum generation", p. 43, International OSA Network of Students (IONS), Indian Institute of Technology Delhi, New Delhi, India, 2020. ***(Best Poster Presentation Award)***

2. R. Bansal, S. Pandey, **P. Chauhan**, and A.t Kumar, "Numerical analysis of linear and nonlinear aspects of chalcogenide based step–index fiber", p. 36, International OSA Network of Students (IONS), Indian Institute of Technology Delhi, New Delhi, India, 2020.

3. R. Sharma, S. Kaur, **P. Chauhan**, and A. Kumar, "Numerical modeling & analysis of GAP–Se chalcogenide based rib waveguide for nonlinear applications", pp. 126, International Conference on Atomic, Molecular, Optical and Nano Physics with Applications (CAMNP), Delhi Technological University, Delhi, India, 2019. ***(Best Poster Presentation Award)***

4. S. Pandey, R. Bansal, **P. Chauhan**, and A. Kumar, "Numerical modeling & analysis of $AsSe_2$–As_2S_5 chalcogenide based step–index optical fiber for nonlinear applications", Materials Today: Proceedings, 2020.

5. R. Aneja, A. Paliwal, J.S. Dham, **P. Chauhan**, and A. Kumar, "Polarimetrical optical sensing using plasmonic nanocrescent dimer based nanoantenna arrays", In Frontiers in Optics, pp. JTu4A–80, Optical Society of America, 2019.

6. A. Sharma, **P. Chauhan**, A. Kumar, Y. Kalra, and T.S. Saini, "Design and analysis of microstructured optical fiber for supercontinuum generation", In AIP Conference Proceedings 2136(1), p. 050002, AIP Publishing LLC, 2019.

7. A. Nagpal, A. Tomar, **P. Chauhan**, and A. Kumar, "Design and analysis of rectangular porous–core photonic crystal fibre for low–loss terahertz communication", International Conference on Optics & Electro–Optics (ICOL), Instruments Research & Development Establishment, Dehradun, India, 2019.

8. A. Tomar, A. Nagpal, **P. Chauhan**, A. Kumar, "Graduating hexagonal ring porous–core photonic crystal fibre for terahertz communication", International Conference on Optics & Electro–Optics (ICOL), Instruments Research & Development Establishment, Dehradun, India, 2019.

9. T. Garg, **P. Chauhan**, and A. Kumar, "Design and modeling of As_2Se_3 based golden spiral photonic crystal fiber for supercontinuum generation", FP027, PHOTONICS: International Conference on Fiber Optics and Photonics, Indian Institute of Technology Delhi, New Delhi, India, 2018.

10. S. Kumar, **P. Chauhan**, and A. Kumar, "Design and Analysis of Double V–Shaped Nanoantenna", FP067, PHOTONICS: International Conference on Fiber Optics and Photonics, Indian Institute of Technology Delhi, New Delhi, India, 2018.

11. R. Kumar, **P. Chauhan**, and A. Kumar, "A decagonal chalcogenide doped photonic crystal fiber for slow light generation", TP114, PHOTONICS: International Conference on Fiber Optics and Photonics, Indian Institute of Technology Delhi, New Delhi, India, 2018.

12. R. Kumar, **P. Chauhan,** and A. Kumar, "Slow light generation in decagonal liquid core photonic crystal fiber", In Laser Science, pp. JW3A–76, Optical Society of America, 2018.

13. S. Kumar, **P. Chauhan**, and A. Kumar, "Design and analysis of a cross V–shaped nanoantenna for visible region", In Laser Science, pp. JTu3A–68, Optical Society of America, 2018.

14. S. Kumar, **P. Chauhan**, and A. Kumar, "Design and analysis of double V–shaped nanoantenna", International Conference on Advances in Science and Technology (ICAST), p**.** 110, SKIT, Jaipur, India, 2018.

15. P. Chauhan, N. Shankhwar, Y. Kalra, and A. Kumar, "A comparative study of various types of nanoantennas for nearfield enhancement based applications", Research Scholar Day, SODHARTH, NIT Delhi, Delhi, India 2017.

CONTENTS

Title	Page No.
Certificate	I
Acknowledgements	II
Abstract	IV
List of Publications	VI
Contents	X
List of Figures	XII
List of Tables	XVI
List of Abbreviations	XVII
1. Introduction	1
References	10
2. Numerical Methods	15
References	20
3. A Dispersion Engineered Silica Based Photonic Crystal Fiber for Supercontinuum Generation in Near-Infrared Wavelength Region	
3.1 Introduction	21
3.2 Nonlinear PCF Designs	23
3.3 Numerical Results and Discussion	24
3.4 Conclusions	32
References	33
4. Computational Modeling of Tellurite Based Photonic Crystal Fiber for Infrared Supercontinuum Generation	
4.1 Introduction	37
4.2 Simulated PCF Design	38
4.3 Results and Discussion	39
4.4 Conclusions	47
References	48

5. Mid-Infrared Broadband Supercontinuum Generation in a Highly Nonlinear Rectangular Core Chalcogenide Photonic Crystal Fiber

5.1 Introduction 52
5.2 PCF Design 54
5.3 Results and Discussion 55
5.4 Conclusions 63
References 64

6. Numerical Exploration of Coherent Supercontinuum Generation in Multicomponent $GeSe_2$-$AsSe_3$-PbSe Chalcogenide Based Photonic Crystal Fiber

6.1 Introduction 67
6.2 Multicomponent PCF Model 70
6.3 Results and Discussion 71
6.4 Conclusions 80
References 81

7. Fluidic Infiltrated Core Based Photonic Crystal Fiber for Coherent Supercontinuum Generation

7.1 Introduction 86
7.2 Proposed PCFs Design 89
7.3 Results and Discussion 90
7.4 Conclusions 103
References 104

8. Concluding Remarks and Future Research Scope 108

LIST OF FIGURES

Fig. 3.1 Transverse cross-sectional view of different proposed PCF structures in silica glass. ……...(23)

Fig. 3.2 Dispersion characteristics curves corresponding to proposed PCF1, PCF2, PCF3, and PCF4 designs for Λ =1.1 µm. ……...(25)

Fig. 3.3 Dispersion characteristics curves corresponding to proposed PCF1, PCF2, PCF3, and PCF4 designs for Λ =1.4 µm. ……...(25)

Fig. 3.4 Dispersion characteristics curves corresponding to proposed PCF1, PCF2, PCF3, and PCF4 designs for Λ =1.7 µm. ……...(26)

Fig. 3.5 Dispersion characteristics curves corresponding to proposed PCF2 design for variation in diameters of smaller air-holes (d_1=d_3=d_4) with Λ and d_2 fixed as 1.4 µm and 0.8 µm respectively. ……...(27)

Fig. 3.6 Dispersion characteristics curves corresponding to proposed PCF2 design for variation in diameter of bigger air-holes (d_2) with Λ and d_1=d_2=d_3 fixed as1.4 µm and 0.5 µm respectively. ……...(27)

Fig. 3.7 Plot of nonlinear coefficient and effective mode area with wavelength. ……...(28)

Fig. 3.8 Effect of fiber length on generated SC with peak power of 8 kW. ……...(29)

Fig. 3.9 Effect of pulse width on generated SC with peak power of 8 kW. ……...(30)

Fig. 4.1 A transverse geometrical view of designed PCF. ……...(39)

Fig. 4.2 Spectral variation of n_{eff} for r_0 when af=1.4 fixed. ……...(40)

Fig. 4.3 Spectral variation of n_{eff} for af with r_0=0.9 µm constant. ……...(41)

Fig. 4.4 Spectral variation dispersion characteristics curves for r_0 with af=1.4. ……...(42)

Fig. 4.5 Spectral variation dispersion characteristics curves for af with r_0=0.9 µm fixed. ……...(42)

Fig. 4.6 Effect of **(a)** r_0, and **(b)** af on effective mode area. ……...(43)

Fig. 4.7 Spectral variation of nonlinear coefficient for **(a)** r_0, and **(b)** af. ……...(44)

Fig. 4.8 Simulated spectral broadening of SCG in a 5.5 cm long PCF.
……...…...(45)
Fig. 4.9 Spectral evolution of SCG with fiber length.
……...(45)
Fig. 5.1 Transverse cross-sectional view of proposed fiber design.
……...(54)
Fig. 5.2 Effect of variation of diameter of bigger air-holes (d_1) on chromatic dispersion, and kept d_2 = 0.5 µm and Λ = 2.5 µm.
……...(55)
Fig. 5.3 Effect of variation of diameter of smaller air-holes (d_2) on chromatic dispersion, and kept d_1 = 1.6 µm, and Λ = 2.5 µm constant.
……...(56)
Fig. 5.4 Effect of Λ on chromatic dispersion (with d_1 = 1.6 µm, and d_2 = 0.5 µm constant).
……...(57)
Fig. 5.5 Combined effect of nonlinear coefficient and effective mode area with wavelength.
……...(58)
Fig. 5.6 Generated SC spectra in different propagating fiber lengths at 4000 nm with 8.19 kW pump power.
……...(60)
Fig. 5.7 Generated SC spectra in a 9 mm fiber length using different pulse durations at 4000 nm.
……...(61)
Fig. 5.8 Generated SC spectra with different peak powers in 9 mm long fiber at 4000 nm.
……...(62)
Fig. 6.1 Proposed multicomponent PCF model. Inset top: a small cross-section of PCF with parameter definitions and material used; and Inset down: fundamental mode confinement at 3.1 µm.
……...(70)
Fig. 6.2 Study of dispersion characteristics with a variation of d and keeping Λ=2.5 µm as constant.
……...(71)
Fig. 6.3 Study of dispersion characteristics with a variation of Λ and keeping d =1.3 µm as constant.
……...(72)
Fig. 6.4 Study of effect of variation of d parameter on **(a)** nonlinear coefficient, and **(b)** effective mode area with wavelength.
……...(73)
Fig. 6.5 Effect of spectral broadening of SCG, spectral evolution of SCG, degree of coherence and spectral coherence evolution with wavelength (from top to bottom) in 5 mm long PCF with E_{pulse}= 0.092 nJ (pulse width= 85 fs, and peak power= 950 W).
……...(74)
Fig. 6.6 Effect of spectral broadening of SCG, spectral evolution of SCG, degree of coherence and spectral coherence evolution with wavelength (from top to bottom) in **(a)** 10 mm, and **(b)** 15 mm long PCF with E_{pulse}= 0.092 nJ (pulse width= 85 fs, and peak power= 950 W).
……...(75)

Fig. 6.7 Effect of spectral evolution of SCG with wavelength **(a)** peak power= 150 W (E_{pulse}= 0.014 nJ), 950 W (E_{pulse}= 0.092 nJ), 1750 W (E_{pulse}= 0.169 nJ), and 2550 W (E_{pulse}= 0.246 nJ) when pulse width fixed as 85 fs and pump wavelength as 3.1 µm, and **(b)** pulse width= 45 fs (E_{pulse}= 0.049 nJ), 85 fs (E_{pulse}= 0.092 nJ), 125 fs (E_{pulse}= 0.135 nJ), and 165 fs (E_{pulse}= 0.178 nJ) when peak power is fixed as 950 W and pump wavelength as 3.1 µm in 10 mm long PCF.
……...(76)
Fig. 6.8 Effect of spectral evolution of SCG at pump wavelength **(a)** 2.6 µm **(b)** 3.1 µm **(c)** 3.6 µm and, **(d)** 4.1 µm with 85 fs pulse width and peak power of 950 W.
……...(77)
Fig. 6.9 Time-wavelength spectrogram generated for fiber lengths **(a)** 5 mm, **(b)** 10 mm and, and **(c)** 15 mm.
……...(77)
Fig. 6.10 Effect of variation of f_R, τ_1 and τ_2 on SC spectrum with pump wavelength of 3.1 µm having pulse width of 85 fs and peak power of 950 W.
……...(78)
Fig. 7.1: Schematic cross-sectional view of proposed fiber designs.
……...(89)
Fig. 7.2: Spectral variation of refractive indices of fused silica and organic liquids (nitrobenzene and ethanol).
……...(90)
Fig. 7.3: The spectral variation of parameters d/Λ with Λ=2.8 µm constant in PCF_A to study the dispersion characteristics.
……...(92)
Fig. 7.4: The spectral variation of parameters d/Λ with Λ=2.8 µm, and d_{c1}=2.514 µm fixed in PCF_B to study the dispersion characteristics.
……...(92)
Fig. 7.5: The spectral variation of parameters d_{c1} with d/Λ=0.5000 (Λ=2.8 µm constant) in PCF_B to study the dispersion characteristics.
……...(93)
Fig. 7.6: The spectral variation of parameters d/Λ while keeping Λ=2.8 µm, d_{c1}=2.514 µm, and d_{c2}=4 µm fixed in PCF_C to study the dispersion characteristics.
……...(94)
Fig. 7.7: The spectral variation of parameters d_{c1} when d/Λ=0.5000 with Λ=2.8 µm, and d_{c2}=4 µm constant in PCF_C to study the dispersion characteristics.
……...(94)
Fig. 7.8: The spectral variation of parameters d_{c2} by keeping d/Λ=0.5000 (Λ=2.8 µm), and d_{c1}=2.514 µm in PCF_C to study the dispersion characteristics.
……...(95)
Fig. 7.9: Spectral variation of **(a)** effective mode index; **(b)** chromatic dispersion in PCF_A, PCF_B, and PCF_C.
……...(96)
Fig. 7.10: Spectral variation of **(a)** effective mode area; **(b)** nonlinear coefficient chromatic in PCF_A, PCF_B, and PCF_C.
……...(97)
Fig. 7.11: (a) Spectra of generated SC, and **(b)** pulse spectrograms for different peak power variation using pulse width as 75 fs in 2.5 cm long fiber length at 1.55 µm.
……....(100)
Fig. 7.12: (a) Spectra of generated SC, and **(b)** pulse spectrograms for different pulse width using peak power as 5 kW in 2.5 cm long fiber length at pump wavelength of 1.55 µm.
……...…..(101)

Fig. 7.13 (a) Generated spectral SC broadband at 1.55 µm with peak power 5 kW and pulse width 75 fs in 2.5 cm long PCF_C, **(b)** plot of SCG span obtained in different fiber length, **(c)** evolution of coherence in the proposed fiber design, and **(d)** plot of average coherence vs fiber length.
…….....(101)

LIST OF TABLES

Table 3.1. Optimized geometrical parameters of PCF2 design used in simulations. ……..…(28)

Table 3.2 Comparison table of previously reported and reported work. ……..…(31)

Table 4.1. Simulated propagation constant values. ……..…(40)

Table 4.2. Comparison table of previously reported work in tellurite based PCF. ……..…(46)

Table 5.1. Optimized geometrical parameters of the proposed PCF design. ……..…(58)

Table 6.1: Comparison of SC spectrum generated in proposed PCF with previously reported in chalcogenide PCFs. ……..…(79)

Table 7.1: List of parameters defined in different PCFs during computational simulations. ……..…(91)

Table 7.2: Numerical findings of linear and nonlinear parameters in optimized PCF_C design. ……..…(98)

Table 7.3: Comparison table for the justification of uniqueness of the proposed fiber design with previously reported results based on organic liquid infiltration fibers. ……(102)

LIST OF ABBREVIATIONS

- SC: Supercontinuum
- SCG: Supercontinuum Generation
- SPM: Self-Phase Modulation
- CPM: Cross-Phase Modulation
- SRS: Stimulated Raman Scattering
- FWM: Four Wave Mixing
- PCF:Photonic Crystal Fiber
- PCFs: Photonic Crystal Fibers
- NLSE: Nonlinear Schrödinger Equation
- GNLSE: Generalized Nonlinear Schrödinger Equation
- FEM: Finite Element Method
- ZDW: Zero Dispersion Wavelength
- ZDWs: Zero Dispersion Wavelengths

CHAPTER-1

INTRODUCTION

The study of light-matter interaction at high power is referred as nonlinear optics. A nonlinear media deals with optical nonlinearities, and the material properties are no longer act linearly with the incident electric field. Laser light is an intense power source of light due to its unique characteristics such as its monochromatic behaviour, divergence, and coherence in comparison to ordinary light sources. Laser sources have the potential to transform the optical response of any system with the electric field. A well-known phenomenon from decades known as the superposition principle doesn't exist for the pulse propagation in nonlinear optics.

The invention of laser (i.e., light amplification by stimulated emission of radiation) is credited to great physicist T. H. Maiman [1]. He observed the first laser action in 1960 when he performed an experiment to generate a laser light pulse based on the stimulated emission of the atoms in the ruby crystal. With this discovery of lasers, continuous efforts are made to increase the output efficiency of the lasers, and the field of nonlinear optics has been developed. Javan et al. experimentally developed a continuous beam of light of power 15 mW using a He-Ne gaseous active medium at 1.15 μm [2]. In 1962, McClung et al. used the Q-switching technique to produce the giant pulses of peak power 100 times that of existed ruby lasers [3]. In 1963, the first mode-locked laser i.e., the combination of He-Ne laser and acoustic-optic modulator, was demonstrated by Hangrove et al. [4]. The mode-locking technique is used by Mocker et al. for the investigation of mode competition and mode coupling of passive Q-switched ruby laser [5]. Demaria et al. performed the mode-locking of Nd^{3+} doped glass lasers

and studied the effects of optical length [6]. The first Nd:YAG laser was reported by Geusic et al., and the laser operation was based on Q-switching mode [7]. In 1987, an erbium-doped fiber amplifier was introduced by Mears et al. near at 1.55 μm wavelength [9]. These amplifiers were widely in practice in the fiber optical telecommunication for longer distances but were proven least suitable for the generation of high output power in fiber lasers and amplifiers.

The commercially available solid and gas lasers can produce the more massive laser output in the kilowatt range. Some major consequences such as the compactness and management of thermal property are observed in these lasers. The most efficient way to overcome these issues is the development of fiber laser of comparable output power level. In 1961, E. Snitzer reported the first operation of laser oscillation in Nd^{3+} doped optical fiber cavity system [8]. The fiber lasers consist of the optical fiber with the doped concentration of rare-earth elements as the gain medium for lasing action. The major advantages of fiber laser include 95% optical conversion efficiency, high optical gain and quality, and their compact size in comparison with solid or gas lasers.

The laser technology has revolutionized the development of efficient high power laser systems with the shortest, controllable, human-made pulse durations, and moderate pulse energies. In 1962, Franken et al. observed the first nonlinear optical process named as a second harmonic generation. The frequency mixing was observed by Bass et al. in 1962 from the second harmonic of two ruby lasers in the ultraviolet region [10]. In 1964, the effect of intensity on the index of refraction i.e., Kerr effect of liquids was first demonstrated by Maker et al. [14]. In 1965, Giordmaine et al. showed the results against coherent, tunable, optical parametric oscillation using lithium metaniobate crystal [11]. Maker et al. presented the experimental results of nonlinear optical effects that occurred due to induced polarization third order in the electric field strength using a giant pulsed ruby laser in 1965 [12]. In 1967, New et al. reported the optical third-harmonic generation in the noble gases based on nonlinear susceptibilities

[13]. Lallemand et al. performed the self-focusing of laser beams and calculated the stimulated Raman gain in liquids [15]. In 1966, Carman et al. observed the four-wave mixing concept and stimulated four-photon interaction using a Q-switched ruby laser [16]. Eckhardt et al. investigated the existence of stimulated Raman scattering in some organic liquids using giant-pulse of ruby laser [17]. In 1967, Shimizu et al. theoretically observed broadening of frequency components due to self-phase modulation and stimulated Rayleigh scattering [18]. All these theoretical and experimental investigations of optical phenomena were well-thought-out just after the invention of laser technology.

Supercontinuum generation (SCG) was first coined by Alfano and Shapiro in 1970 with double frequency generation experiment of photons in the presence of nonlinear medium [19-21]. SCG is an optical process in which an intense ultrashort pulse gets broadened during interaction with a nonlinear medium. SCG leads by optical linear and nonlinear effects i.e., group velocity dispersion, nonlinearity, self-phase modulation (SPM), cross-phase modulation (CPM), stimulated Raman scattering (SRS), four-wave mixing (FWM), and solitons generation [19, 20].

The optical fibers based on total internal reflection were in practice during the period of 1990s for the confinement and guidance of light in core over a long propagating length of the fiber. The special characteristics of maintaining the high intensity of input light along the entire length of fiber make these optical fibers an ideal choice to study the nonlinear effect of SCG.

Specialty fibers are those fibers in which the modification of structure and material properties are practiced for the rendering of new optical properties and characteristics [19]. The fundamental aspects by which one can propose an effective design of specialty fibers are glass composition and geometry. Glass composition is the most important key feature to study the nonlinear properties of proposed specialty fibers. This factor is related to the type of glass used with high linear and nonlinear refractive index, and has a wide transparency window which in

result, produces an ultra-broadband SCG. The most commonly used glasses are silica, tellurite, fluoride, and chalcogenides. And, the geometry of fibers also plays a vital role in analyzing the nonlinear properties. The geometrical parameters of the specialty fibers help in the optimization process for the generation of ultra-broadband supercontinuum (SC).

Photonic crystal fibers (PCFs) are specialty optical fiber which have been widely in practice to study the nonlinear effects due to their unique property of better confinement of fundamental mode in small core size and tailored dispersion characteristics [19, 20]. PCFs are generally characterized by the symmetric air holes pattern in cladding drawn throughout the entire fiber length. Photonic crystal fiber (PCF) is a developing technology that has great potential to revolutionize nonlinear devices by replacing optical fibers in the near future.

The PCFs are generally composed of pure/fused silica, liquids, tellurite, fluoride, and chalcogenide glasses, and are useful for nonlinear optical devices. Many theoretical and experimental studies of the generation of SC have been reported in fibers and PCFs based on these materials [22-40]. The foremost requirements of SCG in PCFs include the high nonlinear coefficient and the transparency of the material. The transmission range of silica glass is 0.3─2.5 μm due to the multiphonon transmission edge. Transparent material like pure silica has been used to obtain a SC spectrum in both visible and near-infrared wavelength regions [51]. The fundamental reasons to use silica are – they can be synthesized with great purity at low-cost factor, and the chemical processes used in the synthesis of silica are simple and efficient. Price et al. reported the SCG spanning, 0.3─1.6 μm in a 15 cm long pure silica holey fiber at 50 kW pump power [56]. Labruyère et al. demonstrated 0.37─1.75 μm broadband SCG using a peak power 10 kW in a 55 cm long Ge-doped silica PCF [57]. Begum et al. numerically explored a silica-based PCF and reported the broadband of SCG spanning, 0.96─1.89 μm in 1 m long fiber length at 1.06 μm, 1.31 μm, and 1.55 μm pump wavelengths [58]. Vindas et al. generated effectively a SCG of bandwidth 1200 nm in a 5 m long silica-based fiber [59]. During

the literature review of above studies, we found that the SCG reported in these silica-based fibers were generated in longer fiber length at high pump power. This could be improved either by designing the novel PCF designs that can give flattened dispersion profile or one can infiltrate the organic liquids in the core or cladding regions of the PCF to increase nonlinearity which in result able to produce broad bandwidth of SC spectrum in visible and near-infrared wavelength region at low input power and in the shorter length of fibers.

Silica fibers have limited exposure in the broadening of spectra till 2.5 μm due to high material absorption and fails to generate the SC spectra in the mid-infrared region. To overcome this failure, soft glasses are proven most promising to further extend the continuum in near and mid-infrared wavelength regions. Tellurite and fluoride glasses have the property to grow in the mid-infrared domain because high value of nonlinear coefficient in comparison of pure silica, broad optical transparency window but restricted up to ~5-7 μm wavelengths, and also limit the high losses in comparison to silica-based PCFs [51, 53]. Nowadays, chalcogenides are widely in practice and proven to be superior to other choices to generate the mid-infrared SC broadband. Chalcogenide glasses belong to chalcogens present in the group 16. Such glasses hold very high-linear and nonlinear refractive index and excellent transmission in the mid-infrared region up to 20 μm [54, 55]. Due to these reasons, chalcogenide glasses are considered as an ideal choice for nonlinear photonic devices in the mid-infrared region. Chalcogenides glasses such as As-S, As-Se, Ge-As-S, and Ge-As-Se are widely in practice for the fabrication of optically active and passive materials in the mid-infrared region [23-27, 44-50]. Many novel fiber glass compositions are coming into focus. New highly nonlinear Ga-Sb-S and GeSe-AsSe-PbSe chalcogenide glasses have been reported for nonlinear applications recently [46, 52]. The chalcogenide glass-based PCFs are nowadays in practice for the generation of broader bandwidth in the mid-infrared wavelength region because of film-forming property and optical stability. Such fibers can generate an ultra-

broadband of SCG using fiber of a few millimeters length at low pump power. The broadband SC reported so far was achieved by using relatively longer fiber propagation length.

Hence, this work aims to numerically model the PCFs design based on highly nonlinear materials to achieve the ultr-broadband SCG using low peak power aand smaller fiber length in the visible, near, and mid-infrared wavelengths. Smaller length fiber has smaller propagation and bending loss; hence, requires lower input pump power. The demand of broadband laser source is very high in major applications which includes spectroscopy, gas sensing, medical, optical coherence tomography, wavelength-division multiplexing, and free space communications [41-43].

The main objectives are:

1. To design and model the silica-based PCFs for ultra-broadband SCG in visible and near-infrared wavelength region with shorter fiber length and low input power.
2. To design and model the chalcogenide-based PCFs for SCG using the existing and newly reported highly nonlinear chalcogenide glasses at low pump power and fibers of shorter length.
3. To design and model the tellurite-based PCF for coherent ultra-broadband SCG in fibers of shorter length at low power level.
4. To design and model the liquid filled PCF for the generation of broader SC bandwidth in visible, and infrared wavelengths.
5. To design and model the PCF for study of coherence property to increase the bandwidth of ultra-broadband SCG in visible, near and mid-infrared regions.

In this thesis, we present some novel photonic crystal fiber designs for study of ultra-broadband SCG and coherence using silica glass, tellurite glasses, organic liquids, and with new chalcogenide glasses in the visible, near-infrared, and mid-infrared wavelength regions for shorter fiber length and low input power.

We have performed the numerical simulations using the "COMSOL Multiphysics" based on finite element method. in the proposed PCF structures. We have adopted the time domain and frequency domain-dependent generalized nonlinear Schrödinger wave equation (GNLSE) to study the process of SCG in fiber design.

The outline of the thesis is organized as follows:

C**hapter 1** is dedicated to a brief introduction about the progress in nonlinear optics field, and the overview about specialty optical fibers and supercontinuum generation are also discussed in detail.

In **chapter 2**, the numerical method of the supercontinuum generation in fibers is presented.

In **chapter 3**, the computational modeling of photonic crystal fiber in silica glass for near-infrared supercontinuum generation has been reported. Optical parameters like chromatic dispersion, nonlinearity and the effective area of the fundamental mode have been computed and tailored. At a pump wavelength of 1300 nm, a flat dispersion profile has been attained with +0.6402 ps/nm/km dispersion in the anomalous region. The reported structure offers a high nonlinear coefficient 26.27 W^{-1} km^{-1} at the pump wavelength. An ultra-broadband supercontinuum spanning, from 0.67─2.4 μm can be easily achieved by the proposed fiber of 37 cm length using a 63 fs secant laser pulse source with 8 kW peak power in the near-infrared wavelength region.

In **chapter 4**, a golden spiral photonic crystal fiber using tellurite glass has been reported for the supercontinuum generation. Dispersion engineering has been used for the optimization of geometrical parameters of the fiber. At 1.35 μm central wavelength, the proposed fiber offers the high value of nonlinear coefficient as 884 W^{-1} km^{-1}. A supercontinuum band ranging 1000-5500 nm has been generated using proposed fiber of length 5.5 cm in the infrared wavelength region.

In **chapter 5**, the numerical modeling of a highly nonlinear rectangular core Ga-Sb-S chalcogenide-based photonic crystal fiber has been reported for supercontinuum generation in the mid-infrared region. Numerical investigation of linear and nonlinear optical processes has been performed. Optimization of geometrical parameters, i.e., pitch, the diameter of bigger and smaller air-holes has been done to achieve small and normal dispersion at the pump wavelength. The proposed design is capable of generating supercontinuum spanning 1-14 μm in 9 mm fiber length pumped with 90 fs pulse, and peak power of 8.19 kW. Such Ga-Sb-S based chalcogenide fibers can be proven effective for nonlinear applications.

In **chapter 6**, the computational analysis of a photonic crystal fiber made up of a multicomponent chalcogenide glass (GAP-Se) system has been reported for highly coherent supercontinuum generation in the mid-infrared spectral region. Dispersion engineering has been adopted to minimize the dispersion effect at pump wavelength by alteration of geometrical parameters of designed fiber. By injecting an input pulse of 85 fs durations in the normal dispersion region, a coherent ultra-broadband supercontinuum spectrum ranging from ~2 to11 μm obtained in a 10 mm fiber length using low input peak power of 950 W at 3.1 μm.

In **chapter 7**, a novel silica photonic crystal fiber made up of composite core formation of highly nonlinear liquids has been reported for the coherent supercontinuum generation. The proper optimization process has been adopted to achieve the ultra-flat chromatic dispersion curve (by tailoring the geometrical parameters and changing the core materials of the designed fiber). We have thoroughly studied the influence of different core compositions, i.e. silica core, nitrobenzene core, and composite nitrobenzene-ethanol core on dispersion, nonlinearity, and effective mode area. We have achieved an ultra-flat dispersion curve with a core composition of nitrobenzene and ethanol together in a comparison of other core compositions. We have attained the ultra-broadband highly coherent supercontinuum spanning, 1-2.6 μm in a 2.5 cm

long designed fiber by injecting a femtosecond laser pulse (pulse-width 75 fs) with input peak power of 5 kW at 1.55 μm.

Chapter 8 provides the concluding remarks of the present thesis and the outlook of the future research scope.

References:

1. T.H. Maiman, "Stimulated optical radiation in ruby", Nature 187, pp. 493-494, 1960.

2. A. Javan, W.R. Bennett Jr, and D.R. Herriott, "Population inversion and continuous optical maser oscillation in a gas discharge containing a He-Ne mixture", Physical Review Letters 6(3), p. 106, 1961.

3. F.J. McClung, and R.W. Hellwarth, "Giant optical pulsations from ruby", Journal of Applied Physics 33(3), pp. 828-829, 1962.

4. L.E. Hargrove, R.L. Fork, and M.A. Pollack, "Locking of He–Ne laser modes induced by synchronous intracavity modulation", Applied Physics Letters 5(1), pp. 4-5, 1964.

5. H.W. Mocker, and R.J. Collins, "Mode competition and self-locking effects in a Q-switched ruby laser", Applied Physics Letters 7(10), pp. 270-273, 1965.

6. A.J. DeMaria, C.M. Ferrar, and G.E. Danielson Jr, "Mode locking of a Nd^{3+}-doped glass laser", Applied Physics Letters 8(1), pp. 22-24, 1966.

7. J.E. Geusic, H.M. Marcos, and LeGrand Van Uitert, "Laser oscillations in Nd-doped yttrium aluminum, yttrium gallium and gadolinium garnets", Applied Physics Letters 4(10), pp.182-184, 1964.

8. E. Snitzer, "Proposed fiber cavities for optical masers", Journal of Applied Physics 32(1), pp. 36-39, 1961.

9. R.J. Mears, L. Reekie, I. M. Juancey, and D.N. Payne, "Low-noise erbium-doped fiber amplifier operating at 1.54 μm," Electronics Letters 23, pp. 1026-1028, 1987.

10. M. Bass, P.A. Franken, A.E. Hill, C.W. Peters, and G. Wein reich, "Optical mixing", Physical Review Letters 8(1), p. 18, 1962.

11. J.A. Giordmaine, and Robert C. Miller, "Tunable coherent parametric oscillation in LiNbO3 at optical frequencies", Physical Review Letters 14(24) p. 973, 1965.

12. P.D. Maker, and R.W. Terhune, "Study of optical effects due to an induced polarization third order in the electric field strength", Physical Review Letters 137(3A), p. A801, 1965.

13. G.H.C. New, and J.F. Ward, "Optical third-harmonic generation in gases", Physical Review Letters 19(10), p. 556, 1967.

14. P.D. Maker, R.W. Terhune, and C.M. Savage, "Intensity-dependent changes in the refractive index of liquids", Physical Review Letters 12(18), p. 507, 1964.

15. P. Lallemand, and N. Bloembergen, "Self-focusing of laser beams and stimulated Raman gain in liquids", Physical Review Letters 15(26), p. 1010, 1965.

16. R.L. Carman, R.Y. Chiao, and P.L. Kelley, "Observation of degenerate stimulated four-photon interaction and four-wave parametric amplification", Physical Review Letters 17(26), p. 1281, 1966.

17. G. Eckhardt, R.W. Hellwarth, F.J. McClung, S.E. Schwarz, D. Weiner, and E.J. Woodbury, "Stimulated Raman scattering from organic liquids", Physical Review Letters 9(11), p. 455, 1962.

18. F. Shimizu, "Frequency broadening in liquids by a short light pulse", Physical Review Letters 19(19), p. 1097, 1967.

19. G.P. Agrawal, "Nonlinear Fiber Optics", 5th ed., Elsevier Academic Press, 2013.

20. P. Russell, "Photonic crystal fibers", Science 299, pp. 358–362, 2003.

21. J.M. Dudley, G. Genty, S. Coen, "Supercontinuum generation in photonic crystal fiber", Reviews of Modern Physics 78, pp. 1135–1184, 2006.

22. J.K. Ranka, R.S. Windeler, and A.J. Stentz, "Visible continuum generation in air-silica microstructure optical fibers with anomalous dispersion at 800 nm", Optics Letters 25, pp. 25–27, 2000.

23. M.R. Karim, B.M.A. Rahman, and G.P. Agrawal, "Dispersion Engineered $Ge_{11.5}As_{24}Se_{64.5}$ nanowire for supercontinuum generation: a parametric study", Optics Express 22, pp. 31029–31040, 2014.

24. T.S. Saini, A. Kumar, and R.K. Sinha, "Broadband mid-infrared supercontinuum spectra spanning 2 – 15 μm using As_2Se_3 chalcogenide glass triangular-core graded-index photonic crystal fiber", Journal of Lightwave Technolnology 33(18), pp. 3914 – 3920, 2015.

25. T.S. Saini, A. Kumar, and R.K. Sinha, "Broadband mid-IR supercontinuum generation in As_2Se_3 based chalcogenide photonic crystal fiber: A new design and analysis", Optics Communications 347, pp. 13 – 19, 2015.

26. T.S. Saini, A. Bailli, A. Kumar, R. Cherif, M. Zghal, and R.K. Sinha, "Design and analysis of equiangular spiral photonic crystal fiber for mid-infrared supercontinuum generation", Journal of Modern Optics 62(19), pp. 1570 – 1576, 2015.

27. A.G.N. Chaitanya, T.S. Saini, A. Kumar, R.K. Sinha, "Ultra-broadband mid-IR supercontinuum generation in $Ge_{11.5}As_{24}Se_{64.5}$ based chalcogenide graded-index photonic crystal fiber: design and analysis", Applied Optics 55(36), pp. 10138 – 10145, 2016.

28. J. Swiderski and M. Michalska, "Mid-infrared supercontinuum generation in a single-mode thulium-doped fiber amplifier", Laser Physics Letters 10(3), p. 035105, 2013.

29. J.H.V. Price, T.M. Monro, K. Furusawa, W. Belardi, J.C. Baggett, S. Coyle, C. Netti, J.J. Baumnerg, R. Paschotta and D.J. Richardson, "UV generation in a pure-silica holey fiber", Applied Physics B 77(2-3), pp. 291-298, 2003.

30. C. Xia, M. Kumar, M.Y. Cheng, O.P. Kulkarni, M.N. Islam, A. Galvanauskas, F.L. Terry, M.J. Freeman, D.A. Nolan and W.A. Wood, "Supercontinuum Generation in Silica Fibers by Amplified Nanosecond Laser Diode Pulses", IEEE Journal of Selected Topics in Quantum Electronics 13(3), pp. 789-787, 2007.

31. A. Labruyère, P. Leproux, V. Couderc, V.Tombelaine, J. Kobelke, K. Schuster, H. Bartelt, S. Hilaire, G. Huss, and G. Mélin, "Structured-Core GeO_2-Doped Photonic-Crystal Fibers for Parametric and Supercontinuum Generation", IEEE Photonics Technology Letters 16, 2010.

32. D. Ghosh, S. Roy, Mrinmay Pal, A. Pal, S.K. Bhadra, J. McCarthy, H. Bookey, and A. Kar, "Generation of supercontinuum and its theoretical study in three-ring silica microstructured optical fibers", Applied Optics 48, 2009.

33. J.C. Vindas, S.T. Piero, A. Diez and M.V. Andres, "Supercontinuum generation in highly Ge-doped core Y-shaped microstructured optical fiber", Applied Physics B 98, pp. 371-376, 2010.

34. T. Taru, M. Hirano, T. Sasaki and Knight, "Supercontinuum generation in pure silica core cut-off shifted single-mode fibers", Conference on Quantum electronics and Laser Science Conference, IEEE, pp. 1-2 2009.

35. K.M. Hilligsøe, T.V. Andersen, H.N. Paulsen, C.K. Nielsen, and K. Mølmer, "Supercontinuum generation in a photonic crystal fiber with two zero dispersion wavelengths", Optics Express 12, pp. 1045-1054, 2004.

36. A. Agrawal, M. Tiwari, Y.O. Azabi, V. Janyani, B.M.A. Rahman, and K.T.V. Grattan, "Ultrabroad supercontinuum generation in tellurite equiangular spiral photonic crystal fiber", Journal of modern Optics 60(12), pp. 956-962, 2013.

37. B. Wanjun, X.L. Juanjuan, X. Liangming, and L. Meisong, "Mid-infrared SCG in silica photonic crystal fibers", Applied Optics 55, pp. 6355-6362, 2016.

38. M.R. Karim, B.M.A. Rahman, Y.O. Azabi, A. Agrawal, and G.P. Agrawal, "Ultra broadband mid-infrared supercontinuum generation through dispersion engineering of chalcogenide microstructured fibers", Journal of the Optical Society of America B 32(11), pp. 2343-2351, 2015.

39. I. Kubat, C.S. Agger, U. Moller, A.B. Seddon, Z. Tang, S. Sujecki, T.M. Benson, D. Furniss, S. Lamrini, K. Scholle, P. Fuhrberg, B. Napier, M.Farries, J. Ward, P.M. Moselund, and O. Bang, "Mid-infrared supercontinuum generation to 12.5μm in large NA chalcogenide step-index fibers pumped at 4.5μm", Optics Express 22, pp. 19169–19182, 2014.

40. A. Agrawal, N. Kejalakshmy, B.M.A. Rahman, and K.T.V. Grattan, "Soft glass equiangular spiral photonic crystal fiber for supercontinuum generation", IEEE Photonics Technology Letters 21(22), pp. 1722-1724, 2009.

41. I. Hartl, X.D. Li, C. Chudoba, R.K. Ghanta, T.H. Ko, J.G. Fujimoto, J.K. Ranka, and R.S. Windeler, "Ultrahigh-resolution optical coherence tomography using continuum generation in an air-silica microstructure optical fiber", Optics Letters 26, pp. 608–610, 2001.

42. P. Hsiung, Y. Chen, T.H. Ko, J.G. Fujimoto, C.J.S. De Matos, S.V. Popov, J.R. Taylor, and V.P. Gapontsev, "Optical coherence tomography using a continuous-wave, high-power, Raman continuum light source", Optics Express 12, pp. 5287–5295, 2004.

43. H. Takara, T. Ohara, T. Yamamoto, H. Masuda, M. Abe, H. Takahashi, and T. Morioka, "Field demonstration of over 1000-channel DWDM transmission with supercontinuum multi-carrier source", Electronics Letters 41, pp. 270–271, 2005.

44. M. Liao, C. Chaudhari, G. Qin, X. Yan, C. Kito, T. Suzuki, Y. Ohishi, M. Matsumoto, and T. Misumi, "Fabrication and characterization of a chalcogenide-tellurite composite microstructure fiber with high nonlinearity", Optics Express 17, 21608–21614, 2009.

45. J.W. Choi, Z. Han, B.U. Sohn, G.F.R. Chen, C. Smith, L.C. Kimerling, K.A. Richardson, A.M. Agarwal, and D.T.H. Tan, "Nonlinear characterization of GeSbS chalcogenide glass waveguides", Scientific Reports 6, 39234, 2016.

46. A. Yang, M. Zhang, L. Li, Y. Wang, B. Zhang, Z. Yang, and D. Tang, "Ga–Sb–S chalcogenide glasses for mid-infrared applications", Journal of the American Ceramic Society 99, pp. 1–4, 2015.

47. B. Ung and M. Skorobogatiy, "Chalcogenide microporous fibers for linear and nonlinear applications in the mid-infrared", Optics Express 18(8), pp. 8647–8659, 2010.

48. M.R. Karim, B.M.A. Rahman, "Numerical investigation of mid-infrared supercontinuum generation in Ge-As-Se based chalcogenide photonic crystal fiber using low peak power", Applied Physics Research 8, pp. 29-37, 2016.

49. X. Gai, S. Madden, D.Y. Choi, D. Bulla, B.L. Davies, "Dispersion engineered $Ge_{11.5}As_{24}Se_{64.5}$ nanowires with a nonlinear parameter of $136W^{-1}m^{-1}$ at 1550nm", Optics Express 18(18), pp. 18866-18874, 2010.

50. S. Haxha, H. Ademgil, “Novel design of photonic crystal fibers with low confinement losses, nearly zero ultra-flattened chromatic dispersion, negative chromatic dispersion and improved effective mode area”, Optics Communications 281(2), pp. 278–286, 2008.

51. J.M. Dudley, and J.R. Taylor, eds. “Supercontinuum generation in optical fibers”, Cambridge University Press, 2010.

52. C. Goncalves, M. Kang, B.U. Sohn, G. Yin, J. Hu, D. Tan, and K. Richardson, "New candidate multicomponent chalcogenide glasses for supercontinuum generation”, Applied Sciences 8(11), p. 2082, 2018.

53. V.A.G. Rivera, and D. Manzani “Technological Advances in Tellurite Glasses”, Springer International Publishing, 2017.

54. N. Granzow, S.P. Stark, M.A. Schmidt, A.S. Tverjanovich, L. Wondraczek, and J. Russell, "Supercontinuum generation in chalcogenide-silica step-index fibers", Optics Express 19(21), pp. 21003-21010, 2011

55. J. Sanghera, and D. Gibson, "Optical properties of chalcogenide glasses and fibers", In Chalcogenide Glasses, Woodhead Publishing, pp. 113-138, 2014.

56. J.H.V. Price, T.M. Monro, K. Furusawa, W. Belardi, J.C. Baggett, S. Coyle, C. Netti, J.J. Baumnerg, R. Paschotta and D.J. Richardson, “UV generation in a pure-silica holey fiber”, Applied Physics B, 2003.

57. A. Labruyère, P. Leproux, V. Couderc, V. Tombelaine, J. Kobelke, K. Schuster, H. Bartelt, S. Hilaire, G. Huss, and G. Mélin, “Structured-Core GeO_2-Doped Photonic-Crystal Fibers for Parametric and Supercontinuum Generation”, IEEE Photonics Technology Letters 22(16), pp. 1259-1261, 2010.

58. F. Begum, and P.E. Abas, “Near-infrared supercontinuum generation in silica-based photonic crystal fiber”, Progress in Electromagnetics Research 89, pp.149-159, 2019.

59. J.C. Vindas, S.T. Piero, A. Diez, and M.V. Andres, “Supercontinuum generation in highly Ge-doped core Y-shaped microstructured optical fiber”, Appied Physics B 98, pp. 371-376, 2010.

CHAPTER-2

NUMERICAL METHODS

The pulse propagation of the electromagnetic wave in a medium encounters loss and dispersion during interaction with the atoms. In the nonlinear medium, the Kerr effect and Raman effect together lead the wave propagation when the field intensity is high in the optical waveguide. Under these effects, the refractive index shows dependence on intensity (called Kerr effect) and the interaction between the photons and phonons becomes possible due to molecular vibrations (called Raman effect). Both the frequency and time domains are considered for the derivation of corresponding nonlinear pulse propagation equations. The frequency dependent form is mostly in practice due to methodical resemblance with the nonlinear Schrödinger equation (NLSE) and it also shows direct dependence of frequency on the linear and nonlinear effects i.e., loss, chromatic dispersion, nonlinearity, and the electric field mode area. We have used both formulations for the effective computational study of the SCG process in different photonic crystal fiber designs. Now, we will discuss both the methods here in brief.

A full vectorial finite element method (FEM) based software 'COMSOL Multiphysics' has been used for numerical simulations of effective mode index in the fundamental mode of the proposed PCFs.

The group velocity dispersion is responsible for the determination of range up to which the spectral components of an ultra-short pulse propagates in the PCF structure at different phase velocities.

It is a function of wavelength which depends on the effective indices of propagating mode and can be calculated as follows [1]:

$$D(\lambda) = -\frac{\lambda}{c}\frac{d^2 Re\left(n_{eff}\right)}{d\lambda^2} \quad (1)$$

where c is the velocity of light in free space and $Re\ (n_{eff})$ is the real part of the effective index of mode.

Nonlinearity depends upon the nonlinear refractive index of the material and is formulated as [1, 2]:

$$\gamma = \frac{2\pi n_2}{\lambda A_{eff}} \quad (2)$$

where n_2 is the nonlinear refractive index of material, and the pump wavelength is represented as λ. The effective area of the fundamental mode is denoted as A_{eff} and is another important vital parameter that controls the electric field intensity in the core of fiber at different wavelengths [1]. It is governed by relation below:

$$A_{\text{eff}} = \frac{\left(\int\int_{-\infty}^{\infty}|E|^2 dxdy\right)^2}{\left(\int\int_{-\infty}^{\infty}|E|^4 dxdy\right)} \quad (3)$$

where, the symbol of E corresponds to the electric field distribution in x-y plane of fiber.

To study the process of SCG, a tunable femtosecond laser with secant field profiles has been used for the generation of pump pulses. This hyperbolic secant pulse [2] is expressed as:

$$\mathrm{A(z = 0, T)} = \sqrt{\mathrm{P_0}}\ \mathrm{sech}\left(\frac{\mathrm{T}}{\mathrm{T_0}}\right) \quad (4)$$

In the above equation, $T_0 = T_{FWHM}/1.7627$ and P_0 corresponds to the peak power of the applied input pulse.

The following time-domain GNLSE has been solved using Split-Step Fourier Method [2] for the numerical simulations of SCG in chapters 3, 4, and 5:

$$\frac{\partial A}{\partial z}+\frac{\alpha}{2}A-\left(\sum_{n\geq 2}\frac{i^{n+1}}{n!}\beta_n\frac{\partial^n A}{\partial T^n}\right)=i\gamma\left(1+\frac{i}{\omega_0}\frac{\partial}{\partial T}\right)\left(A(z,t)\int_{-\infty}^{\infty}R(T')\times|A(z,T-T')|^2dT'+i\Gamma_R(z,T)\right) \quad (5)$$

where A(z,t) is the output pulse envelope, α is the attenuation coefficient of the fiber, γ is the nonlinear coefficient and β_n is related to the n^{th} derivative of the propagation constant β. In our simulations, the effect of noise is neglected ($\Gamma_R = 0$).

Due to the effect of electronic and nuclear contribution [2], the nonlinear response i.e. R(t) is expressed as:

$$R(t)=(1-f_R)\delta(t)+f_R h_R(t) \quad (6)$$

where f_R is related to the fractional contribution of Raman response in accordance with the total linear response. The Raman response function, h_R (t) describes the vibration of the molecules of the matter during interaction with light. It is generally given by the following relation [2]:

$$h_R(t)=\frac{\tau_1^2+\tau_2^2}{\tau_1\tau_2^2}exp\left[-\frac{t}{\tau_2}\right]sin\left(\frac{t}{\tau_1}\right) \quad (7)$$

where Raman period is given by τ_1 and the damping time of vibrations is denoted as τ_2. Both τ_1 and τ_2 are the characteristics properties of the nonlinear material.

In the numerical analysis of SCG in chapters 6 and 7, we have implemented the frequency domain-dependent GNLSE to study the pulse propagation and SC generation in the proposed PCFs which is framed as [2]:

$$\frac{\partial\tilde{A}'}{\partial z}=i\bar{\gamma}(\omega)\exp\left(-\hat{L}(\omega)z\right)\mathbb{F}\times\left\{\bar{A}(z,T)\int_{-\infty}^{\infty}R(T')|\bar{A}(z,T-T'|^2dT'\right\} \quad (8)$$

This includes the combined effects of dispersion and other nonlinear processes. The transformation of $\tilde{A}'$ i.e. output pulse envelop, from the frequency domain to time domain is given by the following relation:

$$\bar{A}(z,T) = \mathrm{F}^{-1}\left\{\frac{\tilde{A}'(z,\omega)}{A_{\mathrm{eff}}^{\frac{1}{4}}(\omega)}\right\} \tag{9}$$

and, the frequency-dependent nonlinear coefficient is framed as:

$$\bar{\gamma}(\omega) = \frac{n_2 n_0 \omega}{c n_{\mathrm{eff}}(\omega) A_{\mathrm{eff}}^{\frac{1}{4}}(\omega)} \tag{10}$$

In the above equations, the F^{-1}, z, n_0, n_2, A_{eff}, and c correspond to the inverse Fourier transform, propagation distance, linear refractive index of material, nonlinear refractive index, effective mode area, and speed of light in vacuum respectively. The change of variable relation is given below:

$$\tilde{A}'(z,\omega) = \tilde{A}(z,\omega) exp\left[-\hat{L}(\omega)z\right] \tag{11}$$

In the previous equation, $\hat{L}(\omega)$ refers to the linear operation and has the definition given below:

$$\hat{L}(\omega) = i[\beta(\omega) - \beta(\omega_0) - (\beta_1(\omega_0)(\omega - \omega_0))] - \frac{\alpha(\omega)}{2} \tag{12}$$

The terms β, β_1, ω_0, and α have the definition of the propagation constant, reciprocal of envelope v_g, reference frequency, and material loss. The organic liquids have a negligible material loss as a consequence of low absorption coefficients. We have considered the material loss of silica in the simulations due to smaller fiber propagating length [5].

The Raman response function has the dependence of fractional Raman response (f_{R}), Raman period (τ_1), and damping time (τ_2). In chapter 6, it is composed as follows:

$$R(t) = (1 - f_R)\delta(t) + f_R \frac{\tau_1^2 + \tau_2^2}{\tau_1 \tau_2^2} exp\left(-\frac{t}{\tau_2}\right) sin\left(\frac{t}{\tau_1}\right) H(t) \tag{13}$$

We have considered f_R=0.115, τ_1=23.1 fs, and τ_2=195 fs of As_2Se_3 chalcogenide glass system [4].

The Raman response function in chapter 7 considered as follows:

$$R(t) = (1 - f_R)\delta(t) + f_R h_R(t)\, H(t) \tag{14}$$

where, H(t) refers as the Heaviside step function that has values as H(t) =0 for $t < 0$ and $H(t)$ =1 for t > 0, f_R=0.86, and h_R (t) for the nitrobenzene is taken as [3]:

$$\begin{aligned} h_R(t) = {} & 0.0288 \times exp\left(-\frac{t}{31.8}\right)\left(1 - exp\left(-\frac{t}{0.15}\right)\right) + 0.0930 \ldots\ldots \\ & \times exp\left(-\frac{t}{0.51}\right)\left(1 - exp\left(-\frac{t}{0.15}\right)\right) + 1.475 \ldots\ldots \\ & \times exp\left(-\frac{t^2}{2 \times 0.08^2}\right) sin\left(\frac{t}{0.10}\right) \end{aligned} \tag{15}$$

Coherence property of the generated SCG gives more flexibility to increase the applications of designed PCF structures. The temporal coherence property is an important factor in the study of SCG in fibers. It is very sensitive to the quantum noise during pulse propagation. Generally, a one-photon-per-mode theory is applied to measure the instability in the phase with respect to wavelength.

So, the measurement of the complex degree of coherent property [2] is governed by:

$$\left|g_{12}^{(1)}(\lambda, t_1 - t_2)\right| = \left|\frac{E_1^*(\lambda, t_1)E_2(\lambda, t_2)}{\sqrt{|E_1(\lambda, t_1)|^2}\sqrt{|E_2(\lambda, t_2)|^2}}\right| \tag{16}$$

where, E_1 and E_2 represent the electric fields of consecutive originated SC spectrums in the designed fiber.

References:

1. G.P. Agrawal, “Nonlinear Fiber Optics”, 5th ed., Elsevier Academic Press, 2013.

2. J.M. Dudley, G. Genty, and S. Coen, “Supercontinuum generation in photonic crystal fiber”, Review of Modern Physics 78, pp. 1135–1184, 2006.

3. S. Kedenburg, A. Steinmann, R. Hegenbarth, T. Steinle, and H. Giessen, "Nonlinear refractive indices of nonlinear liquids: wavelength dependence and influence of retarded response", Applied Physics B 117(3), pp. 803-816, 2014.

4. B. Ung, and M. Skorobogatiy, “Chalcogenide microporous fibers for linear and nonlinear applications in the mid infrared”, Optics Express 18 (8), pp. 8647–8659, 2010.

5. R. Raei, Rasoul, M.E. Heidari, and H. Saghaei, "Supercontinuum generation in organic liquid-liquid core-cladding photonic crystal fiber in visible and near-infrared regions", Journal of Optical Society of America B 35(2), pp. 323-330, 2018.

CHAPTER-3

A DISPERSION ENGINEERED SILICA-BASED PHOTONIC CRYTAL FIBER FOR SUPERCONTINUUM GENERATION IN NEAR-INFRARED WAVELENGTH REGION*

3.1 Introduction

Photonic crystal fibers are fascinating due to their unique linear and nonlinear properties such as dispersion management, high birefringence, high power delivery, and SCG [1-3]. Such PCFs have the ability to guide light with some alterations in refractive index, and structural parameters of the fiber [6]. Due to these special advantages over conventional optical fiber, PCFs are good source to generate the broadband laser sources because of their high nonlinearity property.

During the past few years, several methods have been explored to achieve an ultra-broadband SC spectrum in the near-infrared and mid-infrared wavelength regions [7-10]. For various nonlinear applications, many silica-based fibers have been reported for the generation of ultra-broadband SC spectra spanning from the visible to the infrared range of electromagnetic spectrum [2-3, 11].

*** Pooja Chauhan**, Ajeet Kumar, and Yogita Kalra, "A dispersion engineered silica-based photonic crystal fiber for supercontinuum generation in near-infrared wavelength region", Optik, 187, pp. 230–237, 2019.

Many experimental and theoretical works have been carried out in the field of photonics using conventional and non-conventional silica glass fibers, tellurite, fluoride, and chalcogenide [12-31]. Price et al. [12] obtained a broad spectrum of SCG in a pure silica holey fiber by launching ultra-short pulses from an amplified Ti: Sapphire laser. Xia et al. [13], used amplified nanosecond laser diode pulses for SCG in silica fibers. Alexis et al. [14] showed an efficient broadband four-wave mixing in doped PCFs. Debashri et al. [15] investigated theoretically a three-ring silica fiber for the generation of SC. Vindas et al. [16] used silica for a Y-shaped fiber optimized for SCG. T. Taru et al. [17] reported a flat and single mode SCG in pure silica core cut-off shifted single-mode fibers using a nanosecond microchip laser. Karen et al. [25] carried out experimental and theoretical work for SCG in the highly nonlinear silica PCF with two zero dispersion wavelengths. Yu et al. [26] fabricated and characterized a new type of silica-based all solid fiber with a two-dimensional nanostructure core for SCG. Wanjun et al. [27] numerically investigated a silica PCF for SCG and coherence.

In this chapter, a novel design of photonic crystal fiber in silica glass is numerically modeled for ultra-broadband visible and near-infrared SCG. The proposed structure offers very low and flat dispersion with high nonlinearity in the near-infrared region and is able to produce an ultra-broadband SC spanning of range ~ 0.67 – 2.4 μm by using a 37 cm long fiber pumped with a femtosecond secant laser pulse of 8 kW peak power at a pump wavelength of 1300 nm.

This chapter is categorized into four sections. Section 1 discusses in detail previous research works on PCFs and SCG. Section 2 gives an idea about the design of proposed nonlinear PCF structures with parameters definition. Section 3 presents and debates the numerical results. Lastly, in section 4 some conclusions regarding the effectiveness of the proposed PCF structure have been drawn.

3.2 Nonlinear PCF Designs:

We present four different hexagonal-shaped PCF structures that consist periodic arrangement of air-holes in the cladding region made from silica glass as shown in fig 3.1. We have designed four different hexagonal shaped fibers and named them as PCF1, PCF2, PCF3, and PCF4. In order to construct the core, one air-hole has been removed from the center of each PCF. The wavelength-dependent refractive index of silica is taken from Malitson et al. [4].

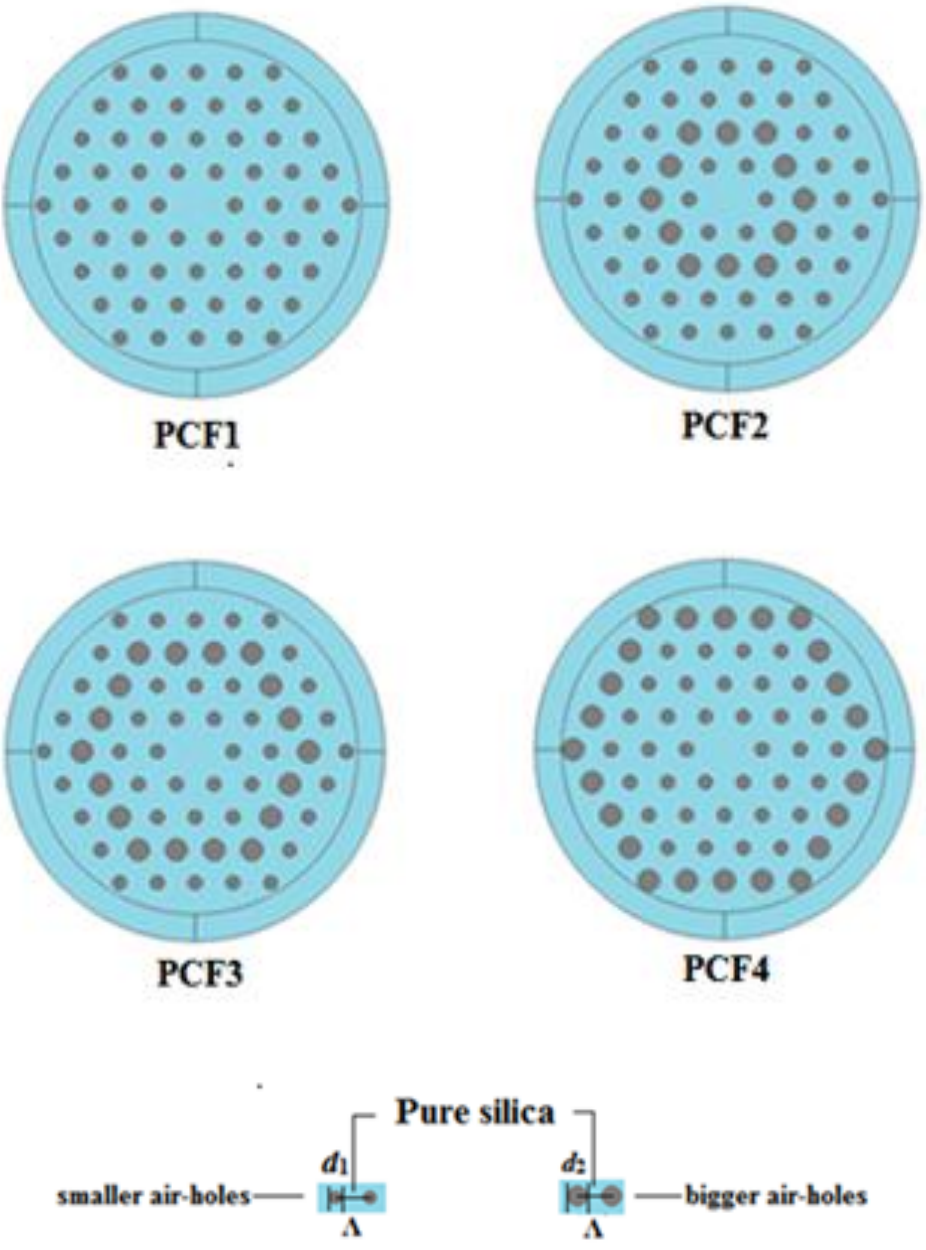

Fig. 3.1 Transverse cross-sectional view of different proposed PCF structures in silica glass.

The aim behind designing these four PCFs is to inquire the effect of increased diameter of air-holes in the second, third and fourth layers of air-holes in PCF2, PCF3 and PCF4 respectively in comparison of regular hexagonal shape PCF1. We also aim to control the dispersion effect in normal and anomalous dispersion regions. The geometrical dimensions of air-holes in first ring, second ring, third ring, and fourth ring are denoted as d_1, d_2, d_3, and d_4 respectively in each proposed PCF. The air-holes are placed periodically with center-to-center distance (pitch) between air-holes that is represented by the parameter Λ.

3.3 Numerical Results and Discussion:

We have performed the computational modal analysis in the FEM-based software named as "COMSOL Multiphysics" and considered the GNLSE for generation of the ultra-broadband SC in proposed fiber design. The chromatic dispersion in PCFs can be controlled and tailored with little modifications in the geometrical parameters such as air-hole arrangement, shape, pitch, and diameter.

In our study, the parameters d_1, d_2, d_3, d_4, and Λ of the designed PCF1, PCF2, PCF3, and PCF4 structures are tailored to obtain the flat dispersion profile in the anomalous region and to get the minimum dispersion at the pump wavelength.

Initially, we have studied the effect of pitch parameter Λ by varying it from 1.1 μm to 1.7 μm with steps of 0.3 μm and keeping diameters of smaller and bigger air-holes as $d_1=d_3=d_4=0.5$ μm and $d_2=0.8$ μm respectively. The dispersion curves corresponding to the effect of variation of Λ on PCF1, PCF2, PCF3, and PCF4 are shown in figs. 3.2-3.4.

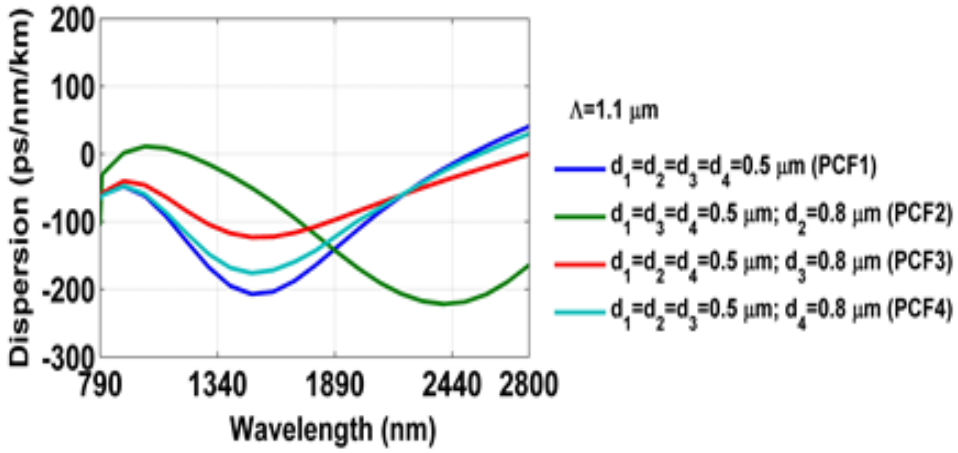

Fig. 3.2 Dispersion characteristics curves corresponding to proposed PCF1, PCF2, PCF3, and PCF4 designs for Λ =1.1 μm.

For the pitch value of Λ=1.1μm, a huge change in the nature of dispersion profile has been observed with a larger shift in zero dispersion wavelengths (ZDWs) towards longer wavelength side for PCF1, PCF3, and PCF4 in comparison with the dispersion curve for PCF2 as demonstrated in fig 3.2. For Λ=1.4 μm there is a smaller shift in ZDWs and the dispersion curve is shifted towards the anomalous regime as shown in fig 3.3. The dispersion curve of PCF1 lies in a higher dispersion range, and among PCF2, PCF3 and PCF4, the dispersion range of PCF2 is lower relative to PCF3 and PCF4.

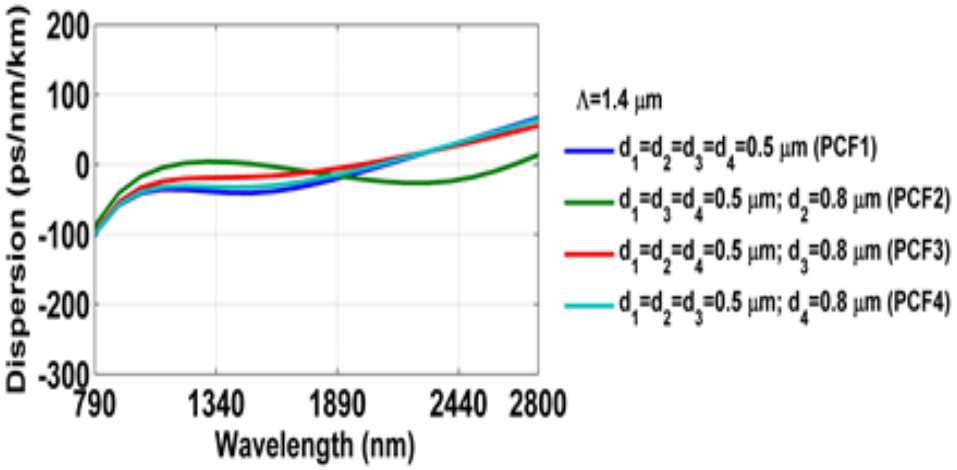

Fig. 3.3 Dispersion characteristics curves corresponding to proposed PCF1, PCF2, PCF3, and PCF4 designs for Λ =1.4 μm.

At Λ=1.7 µm, there is a larger change in the dispersion curve when compared to the case of Λ=1.4 µm, as seen in fig. 3.4. We have achieved the lower dispersion range in the case of PCF2 while the dispersion values are higher in the cases of PCF1, PCF3, and PCF4, for Λ ranging 1.1-1.7 µm.

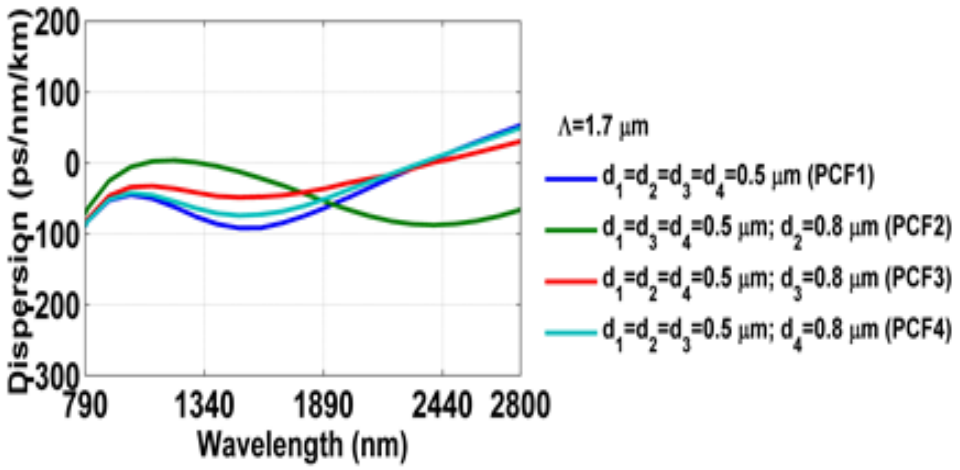

Fig. 3.4 Dispersion characteristics curves corresponding to proposed PCF1, PCF2, PCF3, and PCF4 designs for Λ =1.7 µm.

Next, the effect of diameters of smaller air-holes (d_1=d_3=d_4) and bigger air-holes (d_2) have been studied and shown in figs. 3.5-3.6. Figure 3.5 represents the dispersion characteristics curves for increased diameter dimensions of smaller air-holes i.e., d_1=d_3=d_4 while keeping d_2=0.8 µm and Λ=1.4 µm fixed for PCF2. It is noticed that with the increment in the diameter of smaller air-holes, the dispersion curve is shifted drastically from normal to anomalous dispersion side. The ZDWs for d_1=d_3=d_4=0.3 µm, d_1=d_3=d_4=0.5 µm, and d_1=d_3=d_4=0.7 µm are also shifted towards the shorter wavelength region.

Next, the diameters of bigger air-holes of PCF2 is increased from 0.6 to 1.0 µm as presented in fig. 3.6. With increased diameter values of d_2, there is a bigger shift in ZDWs towards the longer wavelength side while keeping d_1=d_3=d_4=0.5 µm and Λ=1.4 µm fixed for PCF2.

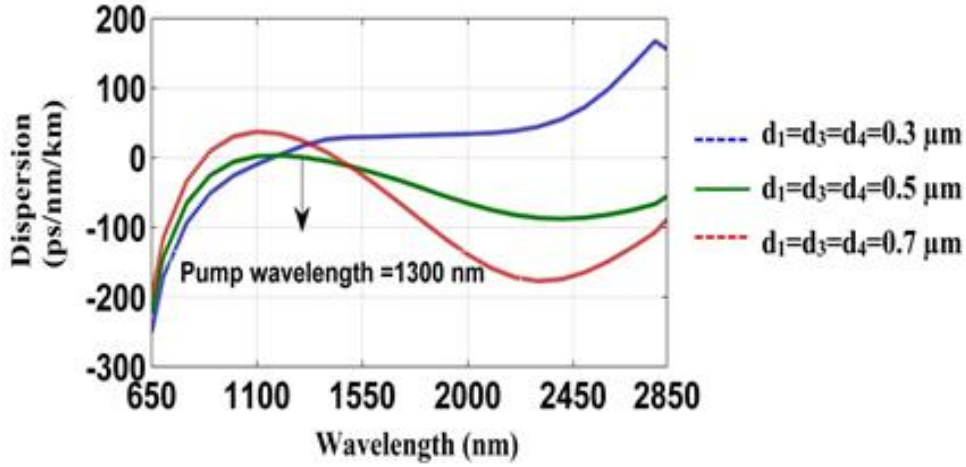

Fig. 3.5 Dispersion characteristics curves corresponding to proposed PCF2 design for variation in diameters of smaller air-holes (d_1=d_3=d_4) with Λ and d_2 fixed as 1.4 µm and 0.8 µm respectively.

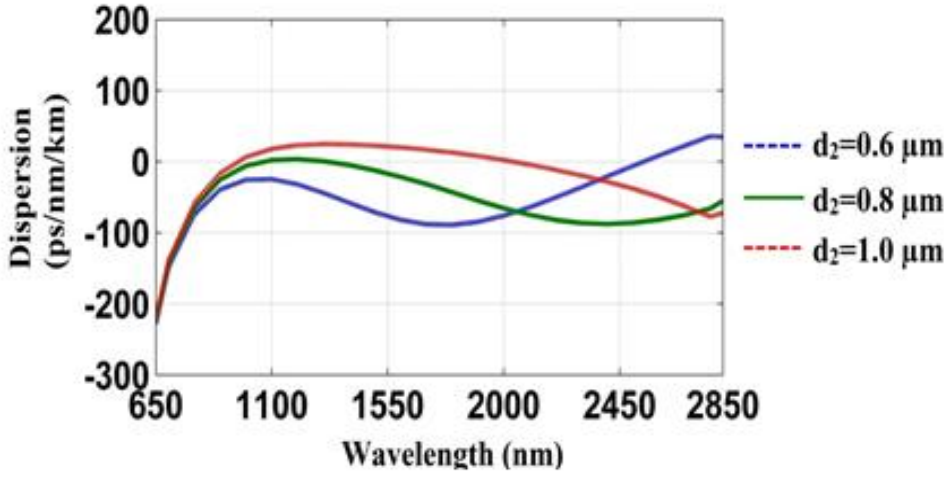

Fig. 3.6 Dispersion characteristics curves corresponding to proposed PCF2 design for variation in diameter of bigger air-holes (d_2) with Λ and d_1=d_2=d_3 fixed as1.4 µm and 0.5 µm respectively.

The computational analysis of the chromatic dispersion reveals that the dispersion curve obtained for PCF2 structure with optimized parameters (d_1=d_3=d_4=0.5 µm, d_2=0.8 µm, and Λ=1.4 µm) is flatter in comparison with PCF1, PCF3, and PCF4 design. A flat dispersion profile with low dispersion value +0.6402 ps/nm/km in PCF2 has been achieved at 1300 nm (central wavelength) to get stable ultra-broadband SC. The optimized parameters dimensions of PCF2 is tabulated in table 3.1.

Optimized geometrical dimensions of PCF2			Dispersion @ 1300nm
Diameter of smaller air-holes	**Diameter of bigger air-holes**	**Pitch**	
$d_1=d_3=d_4$=0.5 µm	d_2=0.8 µm	Λ=1.4 µm	+ 0.6402 ps/nm/km

Table 3.1. Optimized geometrical parameters of PCF2 design used in simulations.

The combined effect of the nonlinearity and effective mode area is shown in fig. 3.7 for the optimized geometrical parameters of the PCF2 structure. The value of nonlinear coefficient n_2= 2.36×10^{-20}m^2/W [6]. As wavelength increases, the nonlinearity coefficient decreases while the effective mode area increases. In the proposed PCF2 structure, we found the value of nonlinear coefficient as 26.27 W^{-1}km^{-1} at 1.3 µm. The propagating fundamental mode confinement is controlled by the high index contrast of the core-cladding regions. This results in a high nonlinear coefficient with a low effective area at the pump wavelength.

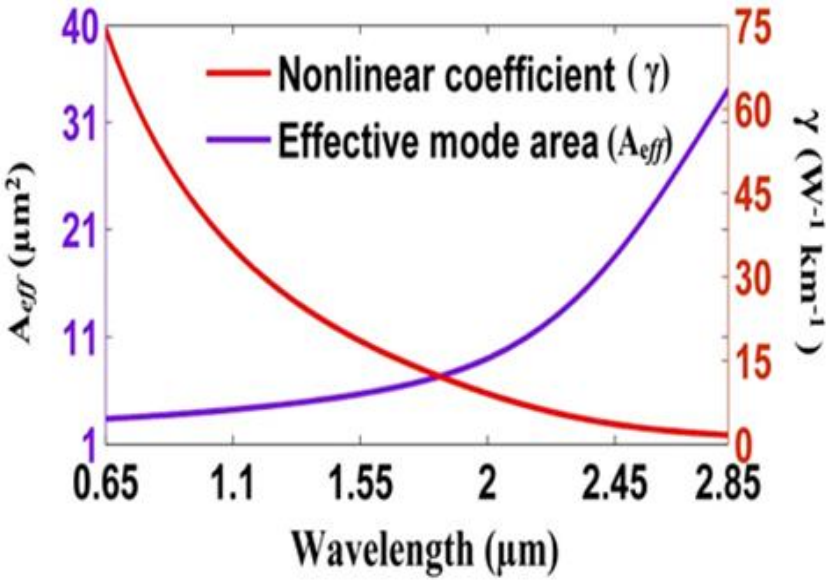

Fig. 3.7 Plot of nonlinear coefficient and effective mode area with wavelength.

The determining elements responsible for SCG in fibers are the dispersion, pump wavelength, the pulse duration, the peak power, and the fiber length.

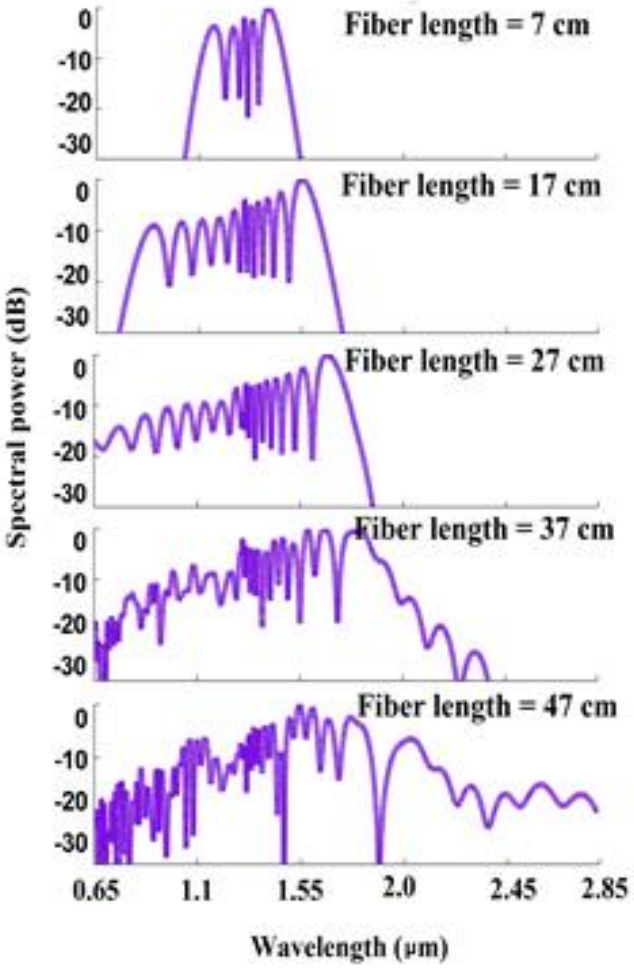

Fig. 3.8 Effect of fiber length on generated SC with peak power of 8 kW.

The simulated spectra of stable ultra-broadband SC with a different propagating fiber lengths in the PCF2 design are shown in fig. 3.8. In the simulation process, the propagating lengths of the proposed PCF structure have been taken as 7 cm, 17 cm, 27 cm, 37 cm, and 47 cm with an input power of 8 kW and an input pulse width of 63 fs. The spectral broadening of the SC spectra has increased as the propagating length of the fiber goes up. The group velocity dispersion effect is responsible for broadening the SC spectrum in fibers of shorter length. In the proposed PCF2 structure, the output SC spectrum becomes constant in the spectral range of ~0.67 – 2.4μm in a propagating fiber length of 37 cm. The symmetrical broadening of the input pulse is due to SPM. The Raman effect dictates limit of propagating length which in turn extends the SC spectrum.

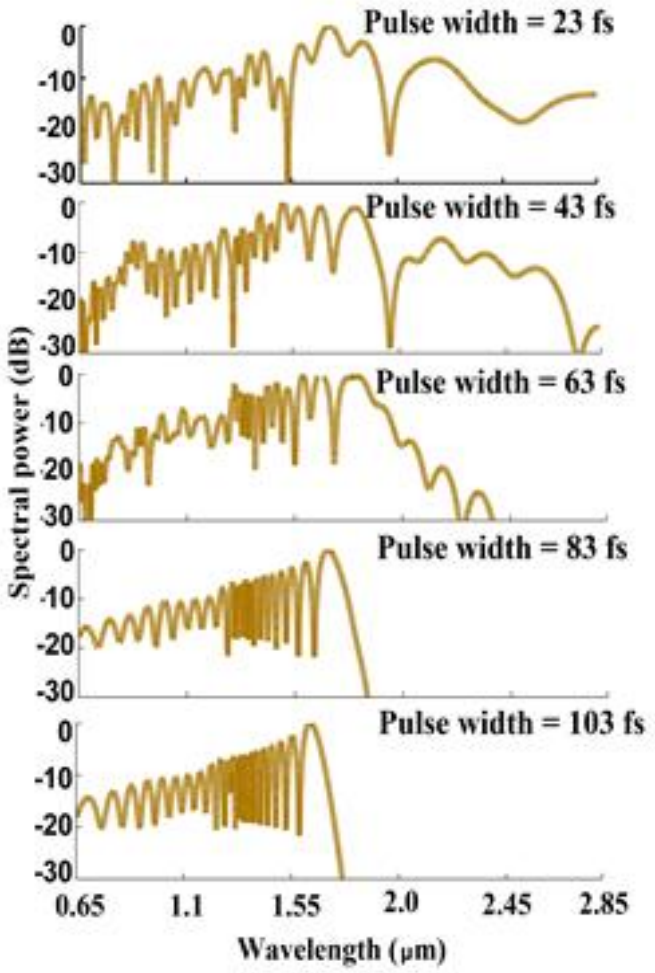

Fig. 3.9 Effect of pulse width on generated SC spectra with peak power of 8 kW.

Lastly, the influence of pulse width on the bandwidth of the SC spectra in the 37 cm long PCF2 design has been illustrated in fig. 3.9. With input power of 8 kW, the pulse width was assigned several different values 23 fs, 43 fs, 63 fs, 83 fs, and 103 fs. The shorter pulses provide broader SC spectra. The output SC spectrum gets narrower with as pulse width increases due to SPM effect. When pumping is chosen in the anomalous dispersion region, the broadening of the SC spectrum is controlled by Raman scattering due to a soliton decay process. For a 63 fs laser pulse, the nonlinear length [L_{NL}=(γ×Peak power)$^{-1}$], and dispersion length, L_D= T_0^2/β_2 are calculated as 4.7×10^{-3} m, and 5.54×10^{-1} m respectively at 1.3 μm. The soliton dynamics defined by their order $N \approx L_D/L_{NL}$, and fission lengths $L_{fission} = L_D/N$ are found to be 11 and 5

mm. The dispersive waves (i.e. non-solitonic radiation) may appear due to the presence of two ZDWs, which further controls the broadening of SC in the anomalous region

In table 3.2, we have compared the obtained result of SCG in proposed PCF with some previously reported silica-based PCFs for SCG. With the simulation results, it is clear that a stable ultra-broadband SC spectrum spanning ~0.67 – 2.4 μm has been obtained using a 37 cm long fiber length of PCF2 pumped with a 63 fs secant laser pulse of 8 kW at an operating wavelength of 1300 nm which is broader in comparison of other reported SCG in silica based-PCFs.

S. No.	**Previously reported work**	**Pump wavelength (μm)**	**Fiber length**	**SCG spanning (μm)**	**Ref.**
1.	Silica PCF	1.31	70 m	1.0-1.8	[32]
2.	Ge-doped Silica PCF	1.31	120 m	1.26-1.38	[33]
3.	Silica PCF	1.3	3.40 cm	1.1-1.7	[34]
4.	Silica PCF	1.3	1 m	1.4-1.52	[35]
5.	**Silica PCF**	**1.3**	**37 cm**	**0.67-2.4**	**Reported work**

Table 3.2 Comparison table of previously reported and reported work.

3.4 Conclusions:

In summary, we have numerically modeled photonic crystal fibers using dispersion engineering techniques for SCG in the visible and near infrared regions using silica glass. The effect of increased diameter of air-holes in the second, third and fourth layers of air-holes has been analyzed thoroughly in order to control the dispersion effect. For the optimized geometrical parameters i.e., smaller air-holes (d_1=d_3=d_4=0.5 µm), bigger air-holes (d_2=0.8 µm) and pitch (Λ=1.4 µm) of PCF2, we have achieved a very low dispersion +0.6402 ps/nm/km, and the nonlinear coefficient value 26.27 $W^{-1}km^{-1}$ at 1300 nm. An ultra-broadband supercontinuum ranging from 0.67 to 2.4 µm is obtained in a 37 cm long proposed fiber using a 63 fs pulse width and 8 kW.

References:

1. G.P. Agrawal, "Nonlinear Fiber Optics", 5th ed., Elsevier Academic Press, 2013.

2. P. Russell, "Photonic crystal fibers", Science 299, pp. 358–362, 2003.

3. J.M. Dudley, G. Genty, S. Coen, "Supercontinuum generation in photonic crystal fiber", Review of Modern Physics 78, pp. 1135–1184, 2006.

4. I.M. Malitson, "Interspecimen comparison of the refractive index of fused silica" Journal of Optical Society of America 55(10), pp. 1205-1209, 1965.

5. J.M. Dudley, and J.R. Taylor, eds. "Supercontinuum generation in optical fibers", Cambridge University Press, 2010.

6. P. Jamatia, T.S. Saini, A. Kumar, and R.K. Sinha, "Design and analysis of a highly nonlinear composite photonic crystal fiber for supercontinuum generation: visible to mid-infrared", Applied Optics 55(24), pp. 6775-6781, 2016.

7. T.S. Saini, A. Kumar, and R.K. Sinha, "Broadband mid-infrared supercontinuum spectra spanning 2 – 15 μm using As_2Se_3 chalcogenide glass triangular-core graded-index photonic crystal fiber", Journal of Lightwave Technology 33(18), pp. 3914 – 3920, 2015.

8. T.S. Saini, A. Kumar, and R.K. Sinha, "Broadband mid-IR supercontinuum generation in As_2Se_3 based chalcogenide photonic crystal fiber: A new design and analysis", Optics Communications 347, pp. 13 – 19, 2015.

9. T.S. Saini, A. Bailli, A. Kumar, R. Cherif, M. Zghal, and R.K. Sinha, "Design and analysis of equiangular spiral photonic crystal fiber for mid-infrared supercontinuum generation", Journal of Modern Optics 62(19), pp. 1570 – 1576, 2015.

10. A.G.N. Chaitanya, T.S. Saini, A. Kumar, R.K. Sinha, "Ultra-broadband mid-IR supercontinuum generation in $Ge_{11.5}As_{24}Se_{64.5}$ based chalcogenide graded-index photonic crystal fiber: design and analysis", Applied Optics 55(36), pp. 10138 – 10145, 2016.

11. J. Swiderski and M. Michalska, "Mid-infrared supercontinuum generation in a single-mode thulium-doped fiber amplifier", Laser Physics Letters, 2013.

12. J.H.V. Price, T.M. Monro, K. Furusawa, W. Belardi, J.C. Baggett, S. Coyle, C. Netti, J.J. Baumnerg, R. Paschotta and D.J. Richardson, "UV generation in a pure-silica holey fiber", Applied Physics B, 2003.

13. C. Xia, M. Kumar, M.Y. Cheng, O.P. Kulkarni, M.N. Islam, A. Galvanauskas, F.L. Terry, M.J. Freeman, D.A. Nolan and W.A. Wood, "Supercontinuum Generation in Silica Fibers by Amplified Nanosecond Laser Diode Pulses", IEEE Journal of Selected Topics in Quantum Electronics 13(3), pp. 789-787, 2007.

14. A. Labruyère, P. Leproux, V. Couderc, V. Tombelaine, J. Kobelke, K. Schuster, H. Bartelt, S. Hilaire, G. Huss, and G. Mélin, "Structured-Core GeO_2-Doped Photonic-Crystal Fibers for Parametric and Supercontinuum Generation", IEEE Photonics Technology Letters 22(16), pp. 1259-1261, 2010.

15. D. Ghosh, S. Roy, Mrinmay Pal, A. Pal, S.K. Bhadra, J. McCarthy, H. Bookey, and A. Kar, "Generation of supercontinuum and its theoretical study in three-ring silica microstructured optical fibers", Applied Optics 48(31), pp. G12-G20, 2009.

16. J.C. Vindas, S.T. Piero, A. Diez, and M.V. Andres, "Supercontinuum generation in highly Ge-doped core Y-shaped microstructured optical fiber", Appied Physics B 98, pp. 371-376, 2010.

17. T. Taru, M. Hirano, T. Sasaki and Knight, "Supercontinuum generation in pure silica core cut-off shifted single-mode fibers", Conference on Quantum electronics and Laser Science Conference, 2009.

18. P. Siwach, A. Kumar, and T.S. Saini, "Broadband supercontinuum generation-spanning 1.5–13 μm in $Ge_{11.5}As_{24}Se_{64.5}$ based chalcogenide glass step index optical fiber", Optik 156, pp. 564-570, 2018.

19. T.S. Saini, A. Kumar, and R.K. Sinha, "Design and modelling of dispersion-engineered rib waveguide for ultra-broadband mid-infrared supercontinuum generation", Journal of Modern Optics 64(2), pp. 143-149, 2017.

20. P. Chauhan, A. Kumar, and Y. Kalra, "Mid-infrared broadband supercontinuum generation in a highly nonlinear rectangular core chalcogenide photonic crystal fiber", Optical Fiber Technology 46, pp. 174-178, 2018.

21. P. Chauhan, A. Kumar, Y. Kalra, and T. S. Saini, "Design and analysis of photonic crystal fiber in Ga-Sb-S chalcogenide glass for nonlinear applications", AIP Conference Proceedings, AIP Publishing, 2009(1), p. 020047, 2018.

22. M.R. Karim, H. Ahmad, S. Ghosh, and B.M.A. Rahman, "Mid-infrared supercontinuum generation using As_2Se_3 photonic crystal fiber and the impact of higher-order dispersion parameters on its supercontinuum bandwidth", Optical Fiber Technology 45, pp. 255-266, 2018.

23. Y. Yu, X. Gai, T. Wang, P. Ma, R. Wang, Z. Yang, D.K. Choi, S. Madden, and B.L. Davies, "Mid-infrared supercontinuum generation in chalcogenides", Optical Materials Express 3(8), pp. 1075-1086, 2013.

24. A. Ghanbari, A. Kashaninia, and H. Saghaei, "Supercontinuum generation for optical coherence tomography using magnesium fluoride photonic crystal fiber", Optik 140, pp. 545-554, 2017.

25. K.M. Hilligsøe, T.V. Andersen, H.N. Paulsen, C.K. Nielsen, and K. Mølmer, "Supercontinuum generation in a photonic crystal fiber with two zero dispersion wavelengths", Optics Express 12, pp. 1045-1054, 2004.

26. X. Yu, P. Shum, N.Q. Ngo, W.J. Tong, J. Luo, G.B. Ren, Y.D. Gong, and J.Q. Zhou, "Silica-Based Nanostructure Core Fiber", IEEE Photonics Technology Letters 20, pp. 162-164, 2008.

27. B. Wanjun, X.L. Juanjuan, X. Liangming, and L. Meisong, "Mid-infrared SCG in silica photonic crystal fibers", Applied Optics 55, pp. 6355-6362, 2016.

28. A. Ghatak, K. Thyagarajan, "Introduction to Fiber Optics", Cambridge University Press, 2000.

29. I. Kubat, C.S. Agger, U. Moller, A.B. Seddon, Z. Tang, S. Sujecki, T.M. Benson, D. Furniss, S. Lamrini, K. Scholle, P. Fuhrberg, B. Napier, M. Farries, J. Ward, P.M. Moselund, and O. Bang, "Mid-infrared supercontinuum generation to 12.5μm in large NA chalcogenide step-index fibers pumped at 4.5μm", Optics Express 22, pp. 19169–19182, 2014.

30. K.S. Kim, R.H. Stolen, W.A. Reed and K.W. Quoi, "Measurement of the nonlinear index of silica-core and dispersion-shifted fibers", Optics Letters 19, pp. 257-259, 1994.

31. Q. Lin and G.P. Agrawal, "Raman response function for silica fibers", Optics Letters 31 (21), pp. 3086-3088, 2006.

32. F. Begum, and Y. Namihira, "Design of supercontinuum generating photonic crystal fiber at 1.06, 1.31 and 1.55 μm wavelengths for medical imaging and optical transmission systems", Natural Science 3(05), p.401, 2011.

33. Y. Namihira, M.A. Hossain, T. Koga, M.A. Islam, S.A. Razzak, S.F. Kaijage, Y. Hirako, and H. Higa, "Design of highly nonlinear dispersion-flattened hexagonal photonic crystal fibers for dental optical coherence tomography applications", Optical review 19(2), pp.78-81, 2012.

34. M.L. Ferhat, L. Cherbi, and I. Haddouche, "Supercontinuum generation in silica photonic crystal fiber at 1.3 μm and 1.65 μm wavelengths for optical coherence tomography", Optik 152, pp.106-115, 2018.

35. F. Begum, and P.E. Abas, "Near-infrared supercontinuum generation in silica-based photonic crystal fiber", Progress in Electromagnetics Research 89, pp.149-159, 2019.

CHAPTER-4

COMPUTATIONAL MODELING OF TELLURITE BASED PHOTONIC CRYSTAL FIBER FOR INFRARED SUPERCONTINUUM GENERATION*

4.1 Introduction:

Photonic crystal fibers are eminently growing in the field of photonics for development of SCG in infrared wavelength region. Initially, the theoretical interest started with the silica based PCFs because of low cost and broad transparency window that covers the visible and near-infrared region. Later, silica fibers are failed to generate SC in mid-infrared region due to very high optical losses beyond 2 μm wavelength [1]. Silica fibers are replaced by tellurite-based glass because of their high linear and nonlinear refractive index with extended optical transparency window till 5.5 μm in infrared wavelength region [1, 22].

Researchers, and scientists have reported many fibers using silica glass, tellurite, fluoride, and chalcogenide glasses for SCG [2-35]. Saini et al. [2] reported a step index fiber using tellurite glass for mid-infrared SCG, spanning 1340-2840 nm using a 6.3 cm fiber length at 2000 nm. A 2900 nm SC span is generated in a 5 cm long hexagonally shaped tellurite-based PCF by Huang et al. [3].

*** Pooja Chauhan**, Ajeet Kumar, and Yogita Kalra, "Computational modeling of tellurite based photonic crystal fiber for infrared supercontinuum generation", Optik, 187, pp. 92–97, 2019.

A tellurite PCF with all-normal dispersion profile has been numerically engineered for octave-spanning SC in 5 cm long fiber length at different pump wavelength in ref. [4]. Numerical investigation of tellurite glass PCF for SCG has been presented by Klimczak et al. [5] using a 2 cm fiber sample with pumping of 150 fs⁄36 nJ⁄1580 nm pulses in the infrared region. In ref [6], a highly nonlinear tellurite PCF with three ZDWs has been numerically simulated for SCG and demonstrated SC spectrum of bandwidth 3030 nm and 2400 at 1.55 μm and 1.93 μm respectively. Qin et al. [7] have experimentally demonstrated a flattened SCG in a tellurite microstructured fiber of length 36 cm at 1550 nm wavelength. A step-index fiber has been presented experimentally by Froidevaux et al. [8] for SCG spanning 1.5-4.4 μm using a 12 cm long segment with sub-nanojoule femtosecond pump pulse at 2300 nm pump wavelength.

In this chapter, our study has been restricted to the numerical analysis of highly nonlinear tellurite-based PCF for infrared SCG. The proposed idea has been thoroughly discussed in forthcoming sections. Section 1 briefs about the introduction of the SCG and its related research ideas reported so far. In section 2, the design of the proposed PCF has been discussed with geometrical parameters. The interpretation of the results of numerical analysis has been framed in section 3. Finally, the major conclusions of the work have been drawn in section 4.

4.2 Simulated PCF Design

A photonic crystal fiber in tellurite glass is designed and represented in fig. 4.1. The air-holes are organized in golden spiral geometry in cladding made up of tellurite. The diameter of air-holes is denoted by d_h (= $af \times r_0$; where af = air-filling fraction and r_0 = spiral radius). The position of each air-hole is marked from center of the PCF according to the relations $x = r_0\sqrt{n} \times \cos(n\beta)$ and $y = r_0\sqrt{n} \times \sin(n\beta)$ where β represents the angle formed between the

n^{th} and $(n+1)^{th}$ ring's center of air-holes. The fabrication challenges of spiral-shaped PCF design are expected to be covered by techniques reported in reference [36].

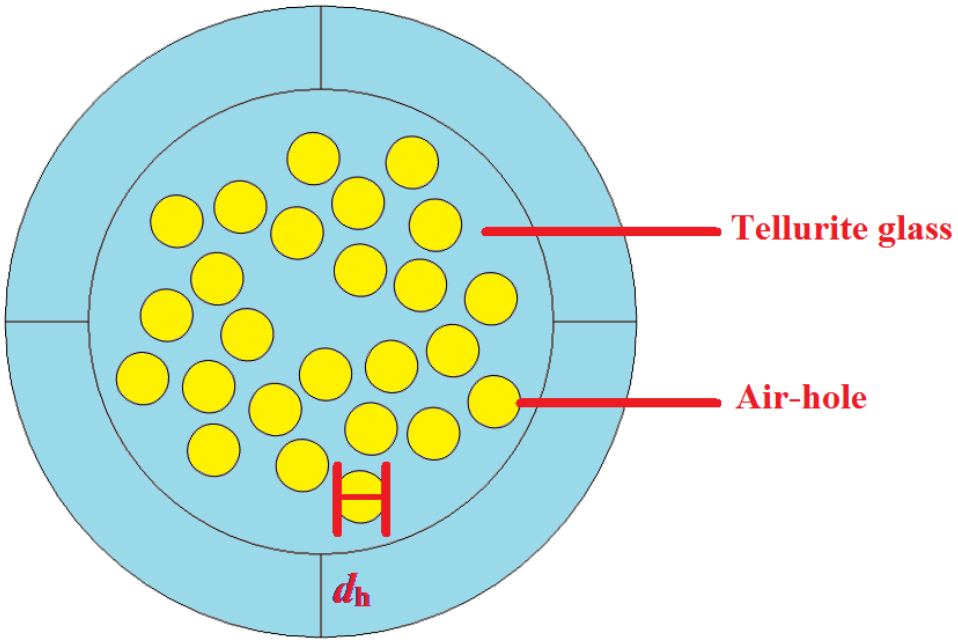

Fig. 4.1 A transverse geometrical view of designed PCF.

4.3 Results and Discussion:

The numerical investigation of modal and dispersive properties has been done using the finite element method. The dispersive property (i.e. group velocity dispersion) is a very sensitive parameter that directly affects the process of nonlinear interactions in designed fiber.

In our study, we have considered the chromatic dispersion only for the optimization process of geometrical parameters of proposed PCF design. The chromatic dispersion and other higher order dispersion terms are directly dependent on propagation constant which directly calculated using Taylor's series expansion and reported in table 4.1. A step by step numerical approach has been adopted for the optimization of r_0 and af parameters in order to attain the zero-dispersion wavelength (ZDW) and minimum dispersion at 1350 nm with high nonlinearity with low effective mode area for ultra-broadband SCG in the infrared region.

β_n (λ_p=1350nm)	Optimized parameters r_0=0.9 µm; af=1.4
β_2 (ps^2/nm)	3.9376×10^{-11}
β_3 (ps^3/nm)	7.3588×10^{-13}
β_4 (ps^4/nm)	6.4308×10^{-16}
β_5 (ps^5/nm)	-2.0717×10^{-17}
β_6 (ps^6/nm)	-8.7779×10^{-20}
β_7 (ps^7/nm)	1.2267×10^{-21}
β_8 (ps^8/nm)	2.9093×10^{-24}
β_9 (ps^9/nm)	-3.7788×10^{-26}

Table 4.1. Simulated propagation constant values.

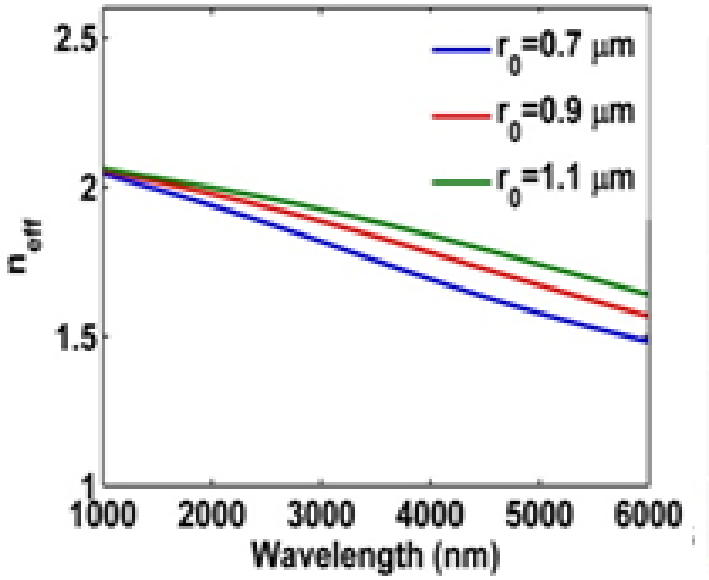

Fig. 4.2 Spectral variation of n_{eff} for r_0 when af=1.4 fixed.

The spectral variations of effective mode index (n_{eff}) with little modification in geometrical parameters (r_0 and af) are shown in figs. 4.2 and 4.3. With increase of r_0, the values of n_{eff} varied from 2.045-1.483 for r_0=0.7 µm, 2.057-1.568 for r_0=0.9 µm, and 2.063-1.64 for r_0=1.1 µm.

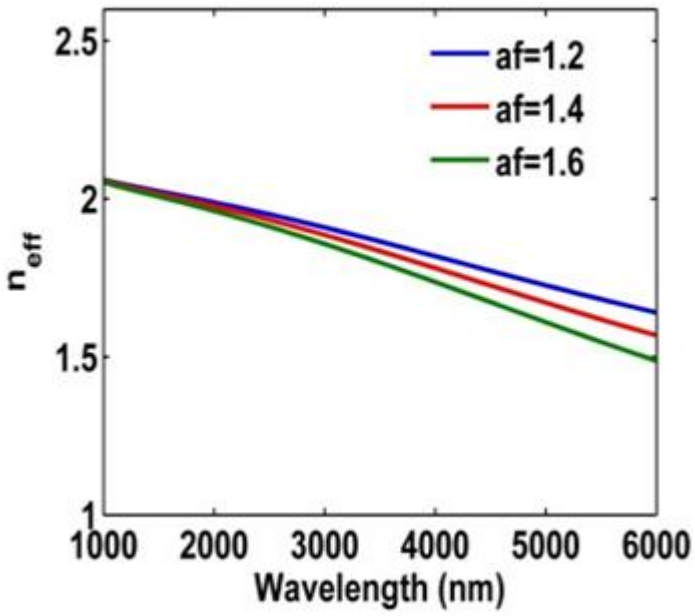

Fig. 4.3 Spectral variation of n_{eff} for *af* with r_0=0.9 µm constant.

Now, we have increased the value of parameter *af* and studied the effect on the effective mode index. The values of n_{eff} are found as 2.06-1.64 for *af*=1.2, 2.057-1.568 for *af*=1.4, and 2.052-1.488 for *af*=1.6.

With increased values of r_0, the values of n_{eff} changed drastically with the longer difference in comparison of n_{eff} values of increased values of *af* in the spectral wavelength region of 1000-6000 nm.

The optical property i.e. dispersion management is the most important aspect for the process of SCG over a broad wavelength range. The tailoring of geometrical parameters (r_0 and *af*) of proposed PCF design is necessary for the dispersive property to achieve ZDW in the shorter wavelength range. The process of optimization is lead in order to minimize the dispersion at the pump wavelength.

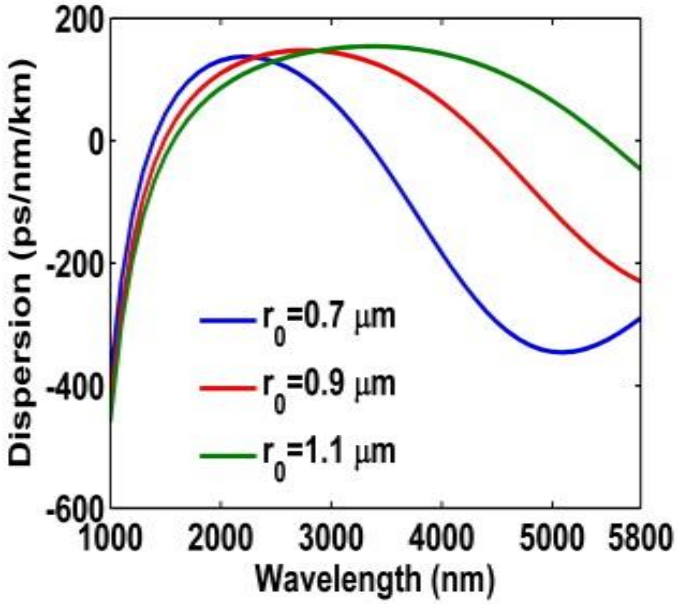

Fig. 4.4 Spectral variation dispersion characteristics curves for r_0 with *af*=1.4.

Firstly, the effect of the increased value of parameter r_0 on chromatic dispersion has been studied which is demonstrated in fig 4.4. The value of r_0 is varied from 0.7-1.1 μm with the increased step of 0.2 μm and keeping *af* constant as 1.4. With increased value of r_0, the ZDWs have been shifted vigorously towards the longer wavelength region. For the different set of values of r_0 as 0.7 μm, 0.9 μm, and 1.1 μm, the two ZDWs have been observed at around 1386 nm & 3299 nm, 1475 nm & 4426 nm, and 1589 nm & 5528 nm respectively.

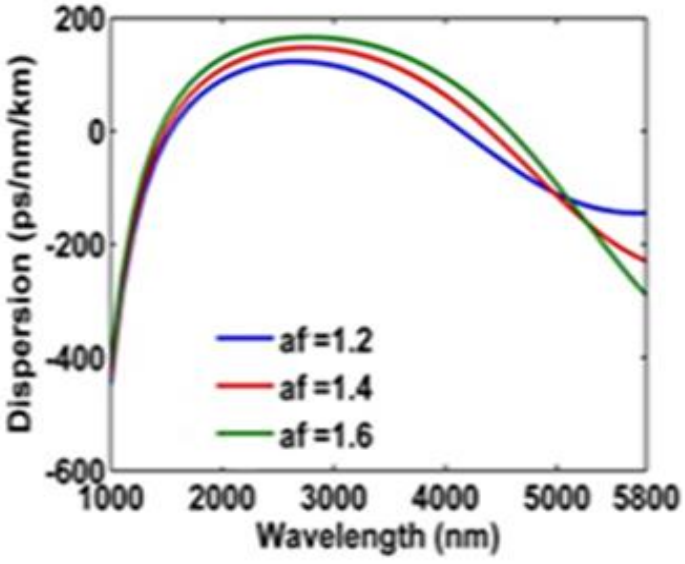

Fig. 4.5 Spectral variation dispersion characteristics curves for *af* with r_0=0.9 μm fixed.

In order to get an ultra-broadening of SCG, we have chosen the commercially available laser pump source of 1350 nm wavelength. At 1350 nm, the values of chromatic dispersion are found as -48.38 ps/nm/km for r_0=0.7 µm, -92.08 ps/nm/km for r_0=0.9 µm, and -121.2 ps/nm/km for r_0=1.1 µm.

Then, the value of parameter *af* has been increased to study the effect on dispersion characteristics curve. For increased values of *af* from 1.2-1.6, there is a slight shift of ZDWs towards the shorter wavelength side while keeping r_0=0.9 µm fixed as shown in fig. 4.5. The two ZDWs are originated at 1567 nm & 4156 nm for *af*=1.2, 1475 nm & 4426 nm for *af*=1.4, and 1418 nm & 4603 nm for *af*=1.6. At pump wavelength 1350 nm, the values of dispersion for *af* values 1.2, 1.4, and 1.6 are found as -109.4 ps/nm/km, -92.08 ps/nm/km, and -71.91 ps/nm/km respectively.

Nonlinearity is measured in terms of the nonlinear coefficient (γ) that is interlinked with the nonlinear refractive index (n_2) and effective mode area (A_{eff}) of propagating mode. Tellurite glasses have a high value of n_2 [7] as compared to pure silica glass.

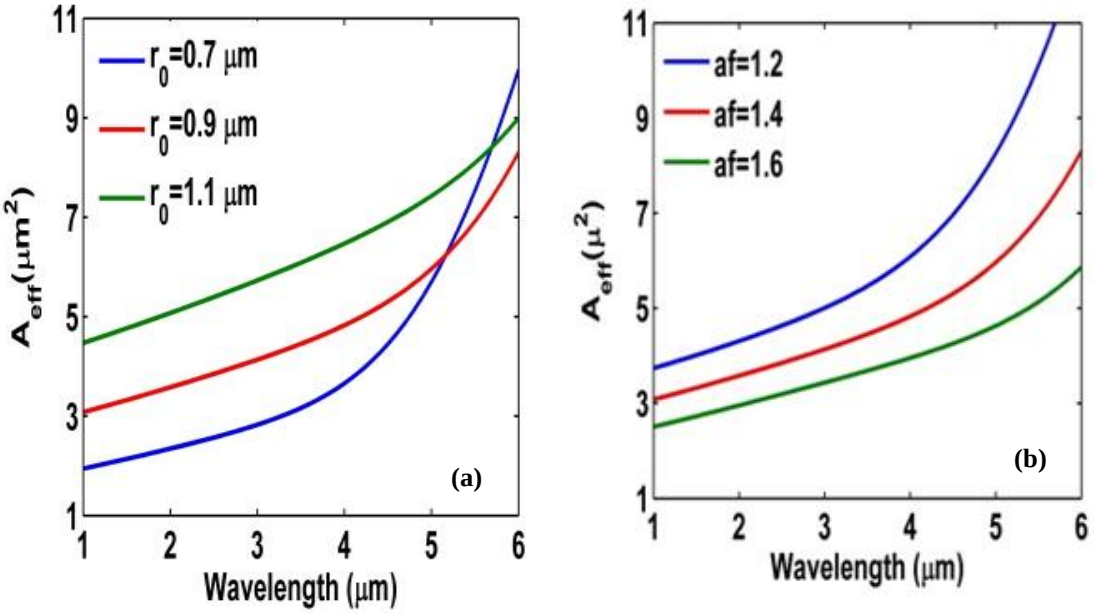

Fig. 4.6 Effect of **(a)** r_0, and **(b)** *af* on effective mode area.

The combined effect of γ and A_{eff} with variation of wavelength is illustrated in figs. 4.6 (a-b), and figs. 4.7 (a-b). For increased value of r_0,the the values of γ are changed sharply due to larger variation in A_{eff} values in comparison of γ for increased value of *af* due to lesser variation in A_{eff} values.

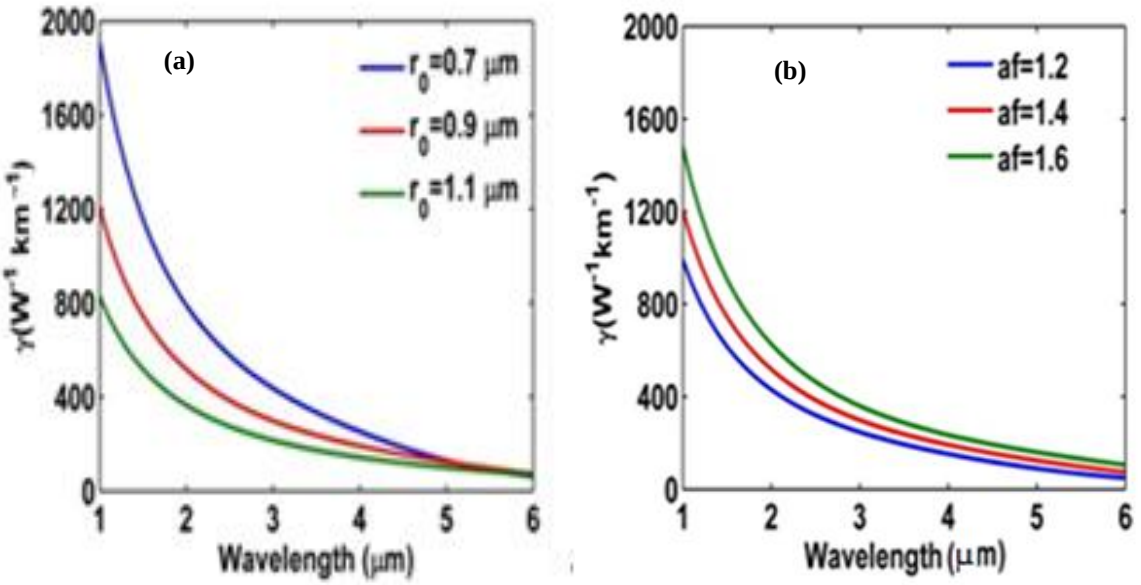

Fig. 4.7 Spectral variation of nonlinear coefficient for **(a)** r_0, and **(b)** *af*.

To study the process of SCG, it is necessary to optimize the geometrical parameters of proposed PCF design in accordance to minimize the effective mode area and maximize the effective mode area at the pump wavelength. The factors like dispersion management, high nonlinearity, propagating fiber length, pulse width, and peak power are generally responsible for ultra-broadening of SCG. For femtosecond laser pulse, evolution of solitons are responsible for the broadening of SC while, FWM and Kerr nonlinearity are dominated in case of input laser pulse of pico and nanosecond pulse width. The presence of higher order of propagation constants i.e. $\boldsymbol{\beta_n}$ play an important role in tuning of SC bandwidth.

A hyperbolic secant femtosecond pulse laser of wavelength 1350 nm is able to generate an ultra-broadband SCG, spanning 4500 nm in an infrared wavelength region in propagating fiber length of 5.5 cm with peak power 5 kW and pulse width 75 fs as shown in figs 4.8 and 4.9. For

the designed fiber, L_{NL} (i.e. nonlinear length) is given by (γ×Peak power)$^{-1}$ and L_D (i.e. dispersion length) is calculated by T_0^2/β_2 in which T_0 = *Pulse width/1.763* the numerically calculated values are found as 2.26×10^{-4} m and 4.66×10^{-2} m respectively at pump wavelength of 1.35 μm.

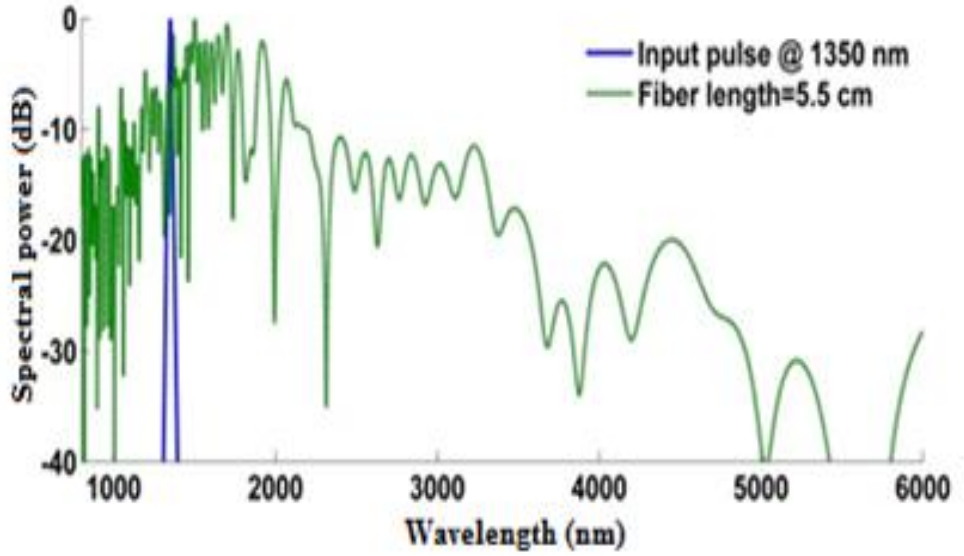

Fig. 4.8 Simulated spectral broadening of SCG in a 5.5 cm long PCF.

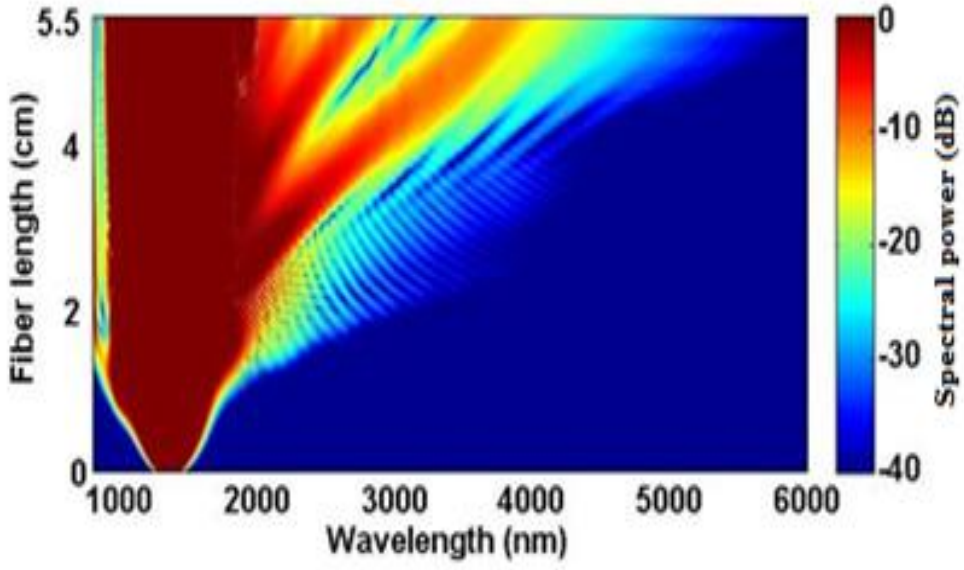

Fig. 4.9 Spectral evolution of SCG with fiber length.

The process of solitons generation defined by their order ($N \approx L_D / L_{NL}$=15) and fission length ($L_{fission} = L_D / N$=3 mm) for the generated SC spectrum. Since, the optical input laser pulse is chosen in normal region, the initial broadening occurred because of SPM and some transfer of pulse energy in anomalous region due to presence of higher values of β_n. The transfer of energy leads formation of dispersive waves (called non-solitonic radiations) which remarkably control the bandwidth of SC spectrum in longer wavelength region.

We have compared the obtained broadband SC in proposed tellurite PCF with some previously reported PCFs for SCG in infrared wavelength region. A broader SC of spanning, 1000-5500 nm is generated in our proposed tellurite-based PCF in comparison with SCG results tabulated in table 4.2.

S. No.	**Previously reported work**	**Pump wavelength (μm)**	**Fiber Length (cm)**	**SCG (nm)**
1.	PCF [10]	2.8	2	800-2600
2.	PCF [11]	1.55	10	970-4100
3.	PCF [9] (Core:TeO_2-Li_2O-WO_3-MoO_3-Nb_2O_5; Cladding: TeO_2-ZnO-Na_2O-La_2O_3)	3.0	5 &15	1500-4000
4.	PCF [8] (60TeO_2- 20PbO-20$PbCl_2$)	2.45	5	2000-4900
5.	**PCF [Reported] (TeO₂-Li₂O-WO₃-MoO₃-Nb₂O₅)**	**1.35**	**5.5**	**1000-5500**

Table 4.2. Comparison table of previously reported work in tellurite based PCF.

4.4 Conclusions:

In summary, we have reported a golden spiral shaped photonic crystal fiber with tellurite glass as cladding material for infrared supercontinuum generation. The reported fiber possesses a very high nonlinear coefficient and low effective mode area at a pump wavelength of 1350 nm. At nearly -40 dB power level, a SCG spanning, 4500 nm is achieved in the 5.5 cm long fiber length.

References:

1. J.M. Dudley, V.G. Genty, and S. Coen, "Supercontinuum generation in photonic crystal fiber", Review of Modern Physics 78, pp. 1135–1184, 2006.

2. T.S. Saini, T.H. Tuan, L. Xing, N.P.T. Hoa, T Suzuki, and Y. Ohishi, "Coherent mid-infrared supercontinuum spectrum using a step-index tellurite fiber with all-normal dispersion", Applied Physics Express 11 (10), p. 102501, 2018.

3. T. Huang, P. Huang, Z. Cheng, J. Liao, X. Wu, and J. Pan, "Design and analysis of a hexagonal tellurite photonic crystal fiber with broadband ultra-flattened dispersion in mid-IR", Optik 167, pp. 144-149, 2018.

4. F. Xu, C. Mei, J. Yuan, F. Li, Z. Kang, B. Yan, K. Wang, X. Sang, X. Zhou, K. Zhong, and C. Yu, "Supercontinuum Generation in an All-Normal Dispersion Tellurite Photonic Crystal Fiber", Conference on Lasers and Electro-Optics/Pacific Rim, Optical Society of America, pp. W3A-30, 2018.

5. M. Klimczak, G. Stepniewski, H. Bookey, A. Szolno, R. Stepien, D. Pysz, A. Kar, A. Waddie, M. R. Taghizadeh, and R. Buczynski, "Broadband infrared supercontinuum generation in hexagonal-lattice tellurite photonic crystal fiber with dispersion optimized for pumping near 1560 nm", Optics letters 38(22), pp. 4679-4682, 2013.

6. A. Agrawal, M. Tiwari, Y. O. Azabi, V. Janyani, B. M. A. Rahman, and K. T. V. Grattan, "Ultrabroad supercontinuum generation in tellurite equiangular spiral photonic crystal fiber", Journal of Modern Optics 60(12), pp. 956-962, 2013.

7. G. Qin, Y. Xin, K. Chihiro, L. Meisong, S. Takenobu, M. Atsushi and O. Yasutake , "Highly nonlinear tellurite microstructured fibers for broadband wavelength conversion and flattened supercontinuum generation", Journal of Applied Physics 107, p. 043108, 2010.

8. P. Froidevaux, L. Arnaud, K. Bertrand, D. Frédéric, M. Pierre, G. Grégory et al., "Dispersion-engineered step-index tellurite fibers for mid-infrared coherent supercontinuum generation from 1.5 to 4.5 μm with sub-nanojoule femtosecond pump pulses", Applied Sciences 8(10), p. 875, 2018.

9. X. Feng, W.H. Loh, J.C. Flanagan, A. Camergo, S. Dasgupta, P. Petropoulos, P. Horak, K.E. Frampton, N.M. White, J.H. Price, H.N. Rutt, and D.J. Richardson, "Single-mode tellurite glass holey fiber with extremely large mode area for infrared nonlinear applications," Opt. Express 16(18), pp. 13651–13656, 2008.

10. M. Liao, X. Yan, G. Qin, C. Chaudhari, T. Suzuki, T. Ohishi, "A highly non-linear tellurite microstructure fiber with multi-ring holes for supercontinuum generation", Opt. Express 17(18), pp. 15481-15490, 2009.

11. M. Klimczak, G. Stępniewski, H. Bookey, A. Szolno, R. Stępień, D. Pysz, A. Kar, A. Waddie, M. R. Taghizadeh, R. Buczyński, "Broadband infrared supercontinuum generation in hexagonal-lattice tellurite photonic crystal fiber with dispersion optimized for pumping near 1560 nm", Optics Letters 38(22), pp. 4679-4682, 2013.

12. S. Kedenburg, C. Strutynski, B. Kibler, P. Froidevaux, F. Désévédavy, G. Gadret, J.C. Jules, T. Steinle, F. Mörz, A. Steinmann, H. Giessen, and F. Smektala, "High repetition rate mid-infrared supercontinuum generation from 1.3 to 5.3 µm in robust step-index tellurite fibers," Journal of Optical Society of America B 34(3), pp. 601-607, 2017.

13. P. Froidevaux, A. Lemière, B. Kibler, F. Désévédavy, P. Mathey, G. Gadret, J.-Ch. Jules, K. Nagasaka, T. Suzuki, Y. Ohishi, and F. Smektala, "Dispersion-Engineered Step-Index Tellurite Fibers for Mid-Infrared Coherent Supercontinuum Generation from 1.5 to 4.5 µm with Sub-Nanojoule Femtosecond Pump Pulses," Applied Sciences 8(10), 1875 (2018).

14. F. Begum, and Y. Namihira, "Design of supercontinuum generating photonic crystal fiber at 1.06, 1.31 and 1.55 µm wavelengths for medical imaging and optical transmission systems", Natural Science 3(05), p. 401, 2011.

15. Y. Namihira, M.A. Hossain, T. Koga, M.A. Islam, S.A. Razzak, S.F. Kaijage, Y. Hirako, and H. Higa, "Design of highly nonlinear dispersion flattened hexagonal photonic crystal fibers for dental optical coherence tomography applications", Optical review 19(2), pp. 78-81, 2012.

16. M.L. Ferhat, L. Cherbi and I. Haddouche, " Supercontinuum generation in silica photonic crystal fiber at 1.3 µm and 1.65 µm wavelengths for optical coherence tomography, Optik 152, pp. 106-115, 2018.

17. F. Begum, and P.E. Abas, "Near infrared supercontinuum generation in silica based photonic crystal fiber", Progress in Electromagnetics Research 89, p. 149-159, 2019.

18. L.B. Shaw, V.Q. Nguyen, J.S. Sanghera, I.D. Aggarwal, P.A. Thiele, and F.H. Kung, "IR supercontinuum generation in As-Se photonic crystal fiber", Advanced Solid State Photonics Vienna, Austria, Paper TuC5, 2005.

19. I. Kubat, C.S. Agger, U. Moller, A.B. Seddon, Z. Tang, S. Sujecki, T.M . Benson, D. Furniss, S. Lamrini, K. Scholle , P. Fuhrberg, B. Napier, M. Farrie, J. Ward, P.M . Moselund, and O . Bang, "Mid-infrared supercontinuum generation to 12.5µm in large NA chalcogenide step-index fibres pumped at 4.5µm", Opt. Express 22, pp. 19169-19182, 2014.

20. X. Gai, S. Madden, D.Y. Choi, D. Bulla, and B.L. Davies, "Dispersion engineered $Ge_{11.5}As_{24}Se_{64.5}$ nanowires with a nonlinear parameter of $136W^{-1}m^{-1}$ at 1550nm", Optics Express 18.18, pp. 18866-18874, 2010.

21. N. Granzow, S.P. Stark, M.A. Schmidt, A.S. Tverjanovich, L. Wondraczek, and P. Russell, "Supercontinuum generation in chalcogenide silica step-index fibers", Opt. Express 19, pp. 21003-21010, 2011.

22. J.M. Dudley, and J.R. Taylor, "Ten years of nonlinear optics in photonic crystal fiber", Nature Photonics 3, pp. 85-90, 2009.

23. T. S. Saini, N.P.T. Hoa, T.H. Tuan, X. Luo, T. Suzuki, and Y. Ohishi, "Tapered tellurite step-index optical fiber for coherent near-to-mid-IR supercontinuum generation: experiment and modeling", Applied optics 58(2), pp 415-421, 2019.

24. N.A. Wolchover, F. Luan, A.K. George, J.C. Knight and F.G. Omenetto, "High nonlinearity glass photonic crystal nanowires", Optics Express 15, pp. 829-833, 2007.

25. K.M. Hilligsøe, T.V. Tndersen, H.N. Paulsen , C.K. Nielsen , K. Mølmer, S. Keiding, R. Kristiansen, K.P. Hansen, and J.J. Larsen, "Supercontinuum generation in photonic crystal fiber with two zero dispersion wavelength", Optics Express 12, pp. 1045–1054, 2004.

26. J. Hu, C.R. Menyuk, L.B. Shaw, J.S. Sanghera, and I.D. Aggarwal, "Maximizing bandwidth of supercontinuum generation in As_2Se_3 chalcogenide fibers", Optics Express 18, pp. 6722–6739, 2010.

27. B. Dabas, and R.K. Sinha, "Design of highly birefringent chalcogenide glass PCF: a simplest design", Optics Communications 284, pp. 1186–1191, 2011.

28. H. Ademgil, and S. Haxha, "Highly nonlinear birefringent photoniccrystal fiber", Optics Communications 282, pp. 2831–2835, 2009.

29. P. Siwach, A. Kumar, and T.S. Saini, "Broadband supercontinuum generation spanning 1.5–13 μm in $Ge_{11.5}As_{24}Se_{64.5}$ based chalcogenide glass step index optical fiber", Optik 156, pp. 564-570, 2018.

30. T.S. Saini, A. Kumar, and R.K. Sinha, "Design and modelling of dispersion-engineered rib waveguide for ultra broadband mid-infrared supercontinuum generation", Journal of Modern Optics 64(2), pp. 143-149, 2017.

31. P. Chauhan, A. Kumar, and Y. Kalra, "Mid-infrared broadband supercontinuum generation in a highly nonlinear rectangular core chalcogenide photonic crystal fiber", Optical Fiber Technology 46, pp. 174-178, 2018.

32. P. Chauhan, A. Kumar, Y. Kalra, and T.S. Saini, "Design and analysis of photonic crystal fiber in Ga-Sb-S chalcogenide glass for nonlinear applications", AIP Conference Proceedings, AIP Publishing, 2009(1), p. 020047, 2018.

33. M.R. Karim, H. Ahmad, S. Ghosh, and B.M.A. Rahman, "Mid-infrared supercontinuum generation using As_2Se_3 photonic crystal fiber and the impact of higher-order dispersion parameters on its supercontinuum bandwidth." Optical Fiber Technology 45, pp. 255-266, 2018.

34. Y. Yu, X. Gai, T. Wang, P. Ma, R. Wang, Z. Yang, D.K. Choi, S. Madden, and B.L. Davies, "Mid-infrared supercontinuum generation in chalcogenides", Optical Materials Express 3(8), pp. 1075-1086, 2013.

35. A. Ghanbari, A. Kashaninia, and H. Saghaei, "Supercontinuum generation for optical coherence tomography using magnesium fluoride photonic crystal fiber", Optik 140, pp. 545-554, 2017.

36. A. Agrawal, Y.O. Azabi, and B.M.A. Rahman, " Stacking the equiangular spiral", IEEE Photonics Technology Letters,25(3), pp. 291-294, 2013.

CHAPTER-5

MID-INFRARED BROADBAND SUPERCONTINUUM GENERATION IN A HIGHLY NONLINEAR RECTANGULAR CORE CHALCOGENIDE PHOTONIC CRYSTAL FIBER*

5.1 Introduction:

Photonic crystal fiber is an emerging technology which has great potential to revolutionize nonlinear devices by replacing conventional optical fibers in near future. They have the upper hand over conventional fibers because they are endlessly single mode and hence exhibit better confinement of light in the core region [1, 2]. Enhanced field confinement and engineered dispersion characteristics result in enhanced support for nonlinear phenomena [3, 4]. Chalcogenide glasses are suitable for the SCG process due to their broad mid-infrared transmission window and high nonlinear refractive index which is nearly 100-1000 times larger than pure silica [5-6].

Tremendous numerical and experimental results have been reported by researchers using chalcogenides optical fibers and PCFs to study SCG [7-14]. Shaw et al. experimentally showed the broadening of SC covering from 2.1-3.1 μm using a PCF in As_2Se_3 chalcogenide glass [7]. Hu et al. maximized the bandwidth of SCG using As_2Se_3 chalcogenide

---

*** Pooja Chauhan**, Ajeet Kumar, and Yogita Kalra, "Mid–infrared broadband supercontinuum generation in a highly nonlinear rectangular core chalcogenide photonic crystal fiber", Optical Fiber Technology, 46, pp. 174–178, 2018.

PCF for input pulse at the wavelength of 2.5 μm [8]. Petersen et.al reporte mid-infrared SC spectra, spanning 1.4 to 13.3 μm in a chalcogenide-based fiber [9]. Liao et al. modeled a composite PCF of As_2Se_3 glass and tellurite to get high nonlinearity at 1.55 μm [10]. Saini et al. presented the theory of an equiangular spiral shaped PCF structure to generate the SC spectrum, spanning 1.2 to 15 μm [11]. Salem et al. have done the numerical investigations of a tapered As_2S_3 PCF design at 4.7 μm for generation of ultra-broadband SC spectrum [12]. Saini et al. also reported on the numerical modeling of an As_2Se_3 rib waveguide for SCG [13]. Choi et al. carried out a nonlinear characterization using a Ge-Sb-S chalcogenide-based waveguide for the demonstration of the SC spectrum [14].

There are many nonlinear applications of SCG possible in the mid-infrared region, including spectroscopy, medical, telecommunications, security, and meteorology [15-21]. Previously silica, tellurite, and fluoride based photonic crystal fibers have been dedicated to the numerical and theoretical study of SCG. Due to low nonlinearity and high material absorption loss beyond 2.4 μm, silica glasses constrained the development of SCG in the mid-infrared region. Tellurite and fluoride glasses have the properties to grow in the mid-infrared domain because of their high optical transparency with high nonlinearity but are restricted to at most a ~5 μm wavelength. Nowadays, chalcogenides are in practice and proven to be superior to other choices for the generation of SCG in mid-infrared region. Recently, a highly nonlinear $Ga_8Sb_{32}S_{60}$ based chalcogenide glass has been reported by Yang et al. with a nonlinear refractive index, $n_2 = 12.4\times10^{-18}$ m^2/W at 1.55 μm and a broad transparency mid-infrared range 0.8─14 μm [22]. These glasses are easily bonded with heavy metals and capable of generating the multi-photon spectra for laser sources. Chalcogenide glasses made up of Ga are stable and less toxic than As-chalcogenide glasses [23]. All these properties make Ga-Sb-S chalcogenide glass most suitable for the mid-infrared applications.

In this chapter, we have proposed a rectangular core $Ga_8Sb_{32}S_{60}$ chalcogenide-based PCF structure for SCG in mid-infrared range. The designed chalcogenide PCF exhibits a flat dispersion profile and high nonlinearity with low effective mode area. At pump wavelength of 4000 nm, this PCF structure produced an ultra-broadening of SC, spanning from 1-14 μm in a 9 mm long designed PCF.

Our study is divided into four sections. Section 1 includes an overview of SCG. Section 2 details the proposed design of the PCF. Section 3 outlines the theoretical results. At the end, the conclusion is outlined in section 4.

5.2 PCF Design:

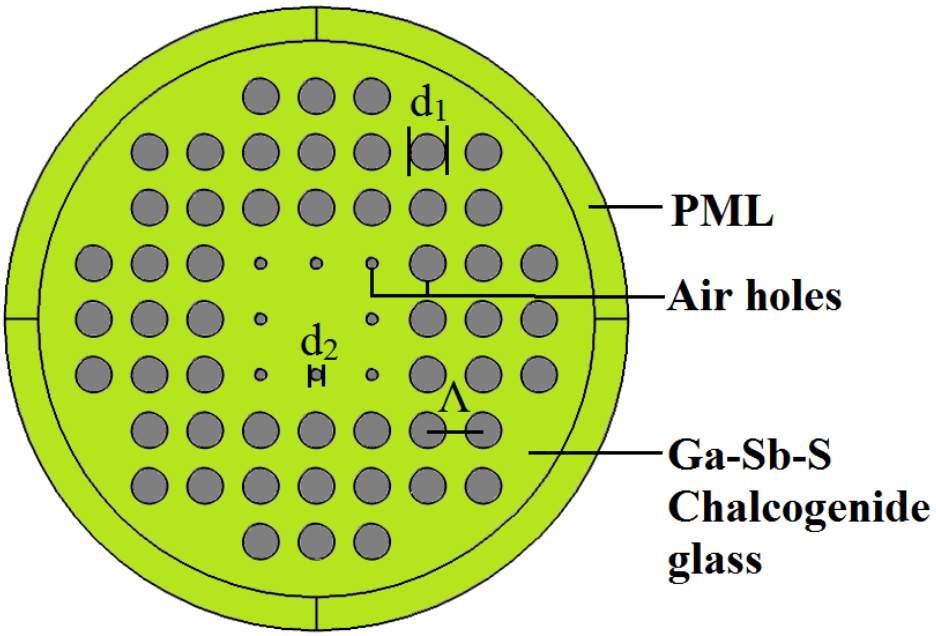

Fig. 5.1 Transverse cross-sectional view of proposed fiber design.

A novel $Ga_8Sb_{32}S_{60}$ chalcogenide-based PCF has been computationally designed to generate a broadband SC as shown in fig. 5.1. The Sellmeier equation of $Ga_8Sb_{32}S_{60}$ chalcogenide glass is taken from Yang et al. [22]. Four rings of air-holes are arranged periodically in the rectangular pattern. One air-hole has been removed for the confinement of the propagating fundamental mode in PCF design. The diameter of larger air-holes in the second, third and

fourth ring is denoted by d_1 and the diameter of smaller air-holes in the first ring around the core is represented by d_2. The center-to-center distance between air-holes is kept constant and denoted as Λ. The PCF is surrounded by a perfectly matched layer of thickness 1.5 µm. The proposed PCF design can be fabricated by the commonly used method of stack and draw [24].

5.3 Results and Discussion:

We have employed a FEM-based software "COMSOL Multiphysics" to simulate the fundamental mode propagating in the proposed PCF. And, we have implemented the GNLSE to generate the broadband SC in the infrared wavelength region. Dispersion management property is basically controlled by the geometrical parameters (pitch and size of air-holes) of the proposed PCF design. Optimization of these parameters will result in the minimum dispersion effect, and minimum effective mode area in the proposed PCF design.

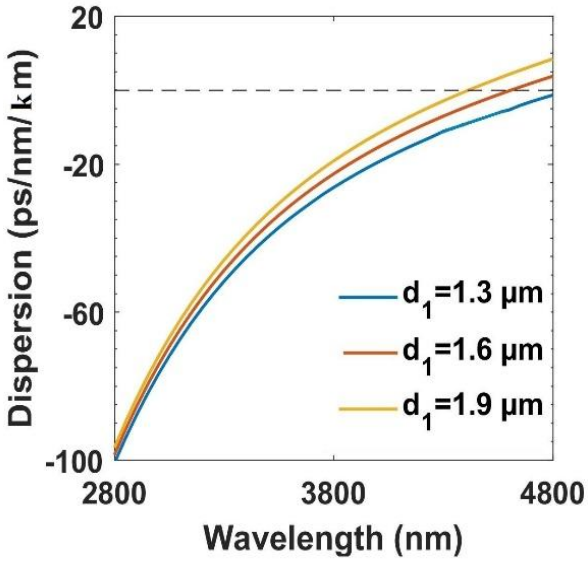

Fig. 5.2 Effect of variation of diameter of bigger air-holes (d_1) on chromatic dispersion, and kept d_2 = 0.5 µm and Λ = 2.5 µm.

Initially, the effect of variation in the diameter of bigger air-holes has been studied and shown in fig. 5.2. With an increase of the d_1 parameter, the ZDW shifted towards the shorter

wavelength side by keeping d_2=0.5 µm and Λ =2.5 µm fixed. The diameter of the bigger air-holes is varied from 1.3 µm to 1.9 µm to obtain low dispersion at the pump wavelength. The effective mode area is increased for increased values of d_1 while keeping other parameters (i.e., d_2 and Λ) fixed. The dispersion at the pump wavelength of 4000 nm is varied from -19.52 ps/nm/km to -11.78 ps/nm/km as diameter d_1 is increased from 1.3 to 1.9 µm in the normal dispersion regime.

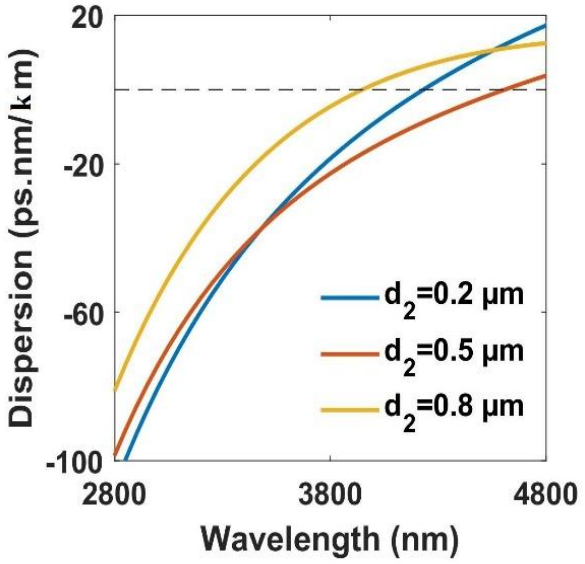

Fig. 5.3 Effect of variation of diameter of smaller air-holes (d_2) on chromatic dispersion, and kept d_1 = 1.6 µm, and Λ = 2.5 µm fixed.

The optimization of parameter d_2 is important due to its pivotal role in controlling the dispersion. The bandwidth of the SC spectrum in the proposed design is broader than what would have been obtained in case of the regular arrangement of air-holes having diameter d_1. Small modifications in the diameter d_2, were observed to have a great influence on shifting the ZDW which is demonstrated in fig. 5.3. On increasing d_2 and keeping parameters d_1=1.6 µm and Λ =2.5 µm fixed, the ZDW shifted drastically towards the shorter wavelength. At central wavelength 4000 nm, the dispersion value changes from -9.18ps/nm/km to 1.36 ps/nm/km when increasing diameter d_2 from 0.2 to 0.8 µm. The effective mode area is found to be

decreased at the pump wavelength, which results in better confinement of fundamental mode in designed PCF.

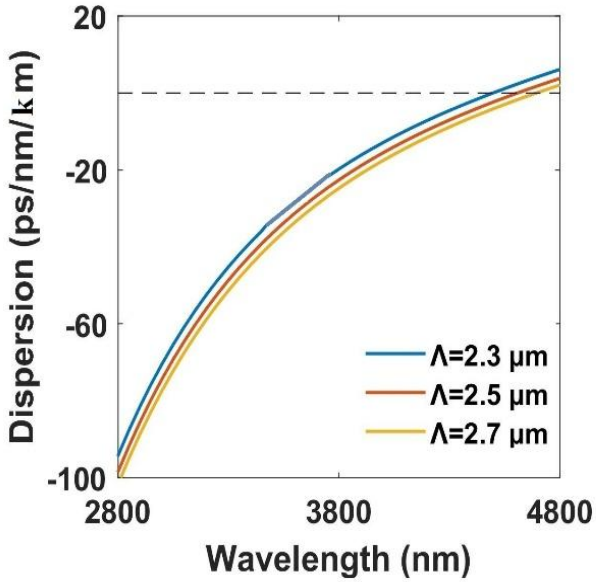

Fig. 5.4 Effect of Λ on chromatic dispersion (with d_1 = 1.6 μm, and d_2 = 0.5 μm constant).

Figure 5.4 demonstrates the variation in the dispersion characteristics by changing the pitch (Λ). If parameter Λ is increased, the ZDW shifts towards the longer wavelength side. The dispersion value is varied from -12.89 ps/nm/km to -17.54 ps/nm/km at 4000 nm. Due to smaller change in mode area, the dispersion profile nearly overlaps with an increase in the value of parameter Λ. From the above discussion, it can be noted that for the structural parameters d_1=1.6 μm, d_2=0.5 μm, and Λ =2.5 μm the dispersion value and effective mode area is minimum at 4000 nm.

The effective mode index is decreased from 2.84 to 2.36 for the wavelength range of 1000 to 14000 nm. A flat normal dispersion profile is obtained in the wavelength range of 2000 to 4700 nm to get an ultra-broadband SC spectrum and the dispersion is minimized as -15.54 ps/nm/km at 4000 nm. The proposed PCF structure possesses a normal dispersion nature at the ZDW of 4200 nm and a pump wavelength of 4000 nm. The normal dispersion regime covers

the wavelength range of 1000 to 4700 nm and the anomalous dispersion regime is beyond the wavelength of 4700 nm. The dispersion value reminds high until wavelength 2750 nm in the normal dispersion regime. The broadening of the SC spectrum arises due to the optical Kerr effect. A smooth but unstructured SC spectrum can be easily produced in the designed PCF with optimized parameters with dispersion in normal regime. The optimized parameters to get a flat normal dispersion curve in designed PCF is tabulated below:

Parameters	Value (µm)
d_1	1.6
d_2	0.5
Λ	2.5

Table 5.1. Optimized geometrical parameters of the proposed PCF design.

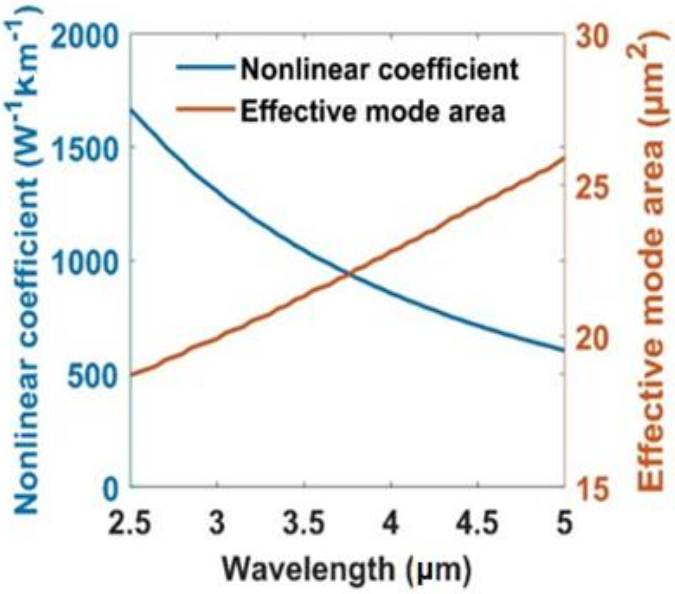

Fig. 5.5 Combined effect of nonlinear coefficient and effective mode area with wavelength.

The effect of the nonlinear coefficient and the effective mode area for optimized parameters at different wavelengths are shown in fig. 5.5. The proposed PCF structure holds the high nonlinear coefficient value as 853 $W^{-1}km^{-1}$ at 4000 nm for optimized geometrical parameters d_1=1.6 µm, d_2=0.5 µm, and Λ =2.5 µm.

The process of SCG has been analyzed with the strong dependence of dispersion parameter (β_n), where n is the order of dispersion. In our simulation, the order of dispersion coefficient goes up to the 9th order. As the limit of the order of dispersion increased beyond 9th, increasingly smaller changes are observed in the output spectrum of SC.

The broadening of SC is controlled by parameters like peak power, pulse width and length of the fiber, and their individual influence is studied and reported in figs. 5.6–5.8. The broadening of the input pulse arises due to nonlinear processes like SPM, CPM and the Raman effect. At the pump wavelength of 4000 nm, the dispersion and effective mode area are minimal, due to which the symmetrical spectral broadening of an input pulse occurred. Mainly two nonlinear factors SPM and CPM are accountable for the input pulse broadening when a short pulse is incident on the small effective mode area that confine the fundamental mode. During the simulation period, different propagating lengths of the proposed PCF are considered to study the nature of SC.

A hyperbolic secant pulse of width 90 fs is simulated initially with peak power of 8.19 kW. The propagating length is varied from 0 mm to 12 mm. During the input pulse propagation in the designed fiber length, the broadening of SC occurs due to SPM, CPM, FWM, and SRS. For propagating length of 9 mm, maximum broadening is attained from 1 to 14 µm with peak power 8.19 kW and pulse width of 90 fs.

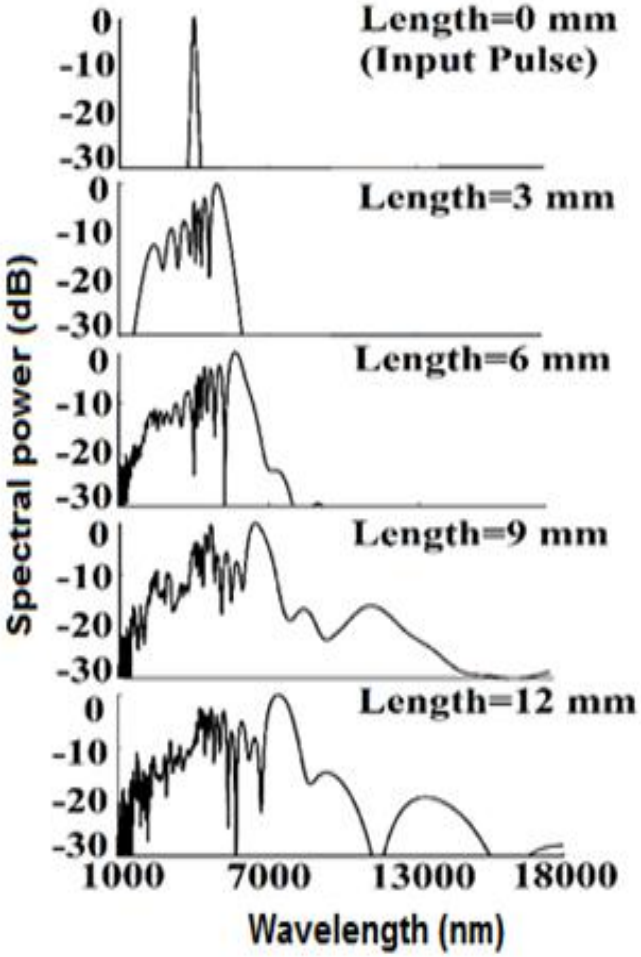

Fig. 5.6 Generated SC spectra in different propagating fiber lengths at 4000 nm with 8.19 kW pump power.

The pulse width is an important parameter which helps to control the bandwidth of SC spectra. The pulse width of the incident hyperbolic secant pulse is varied from 40 fs to 180 fs. The maximum broadening of SC spectra is even broader in a fiber length of 9 mm with peak power of 8.19 kW and a pulse width of 90 fs. For shorter pulse width, broadening of the SC spectra is mostly due to SPM, which is further followed by CPM, FWM, and SRS. With an increased pulse width the overall broadening of SC decreased.

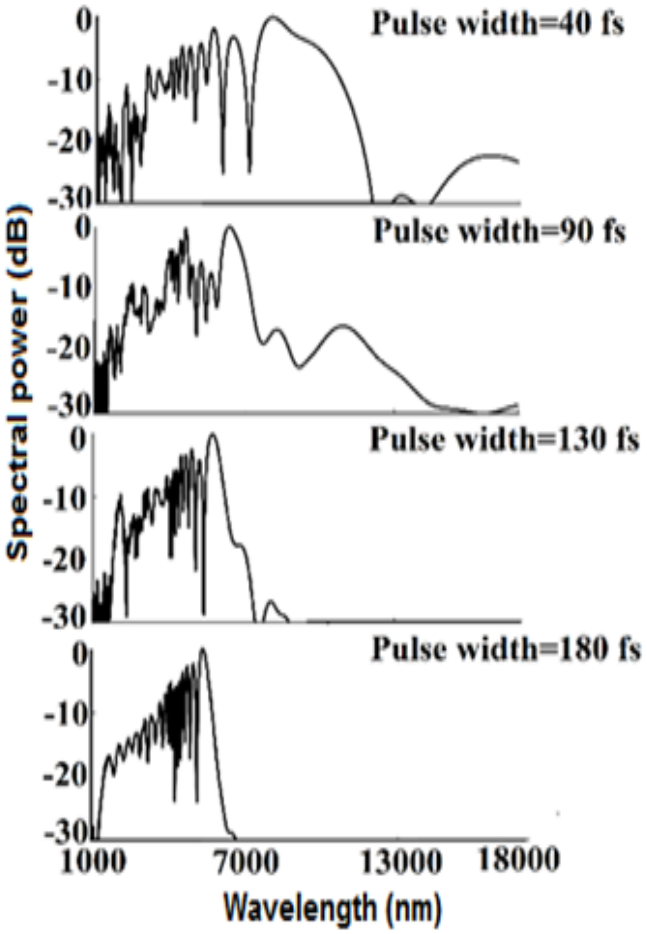

Fig. 5.7 Generated SC spectra in a 9 mm fiber length using different pulse durations at 4000 nm.

The bandwidth of SC spectra can be controlled by input peak power. The variation in input peak power (4,190 W, 8,190 W, and 12,190 W) in a 9 mm long PCF and pulse duration of 90 fs is shown in Fig. 5.8. The generated SC spectrum increases with the increase of peak power. Dispersion effect no longer exists at high peak power and only SPM dominated. For peak power of 8.19 kW, the broadening of SC spectra covers 1-14 μm with a pulse width of 90 fs propagating in a 9 mm long PCF.

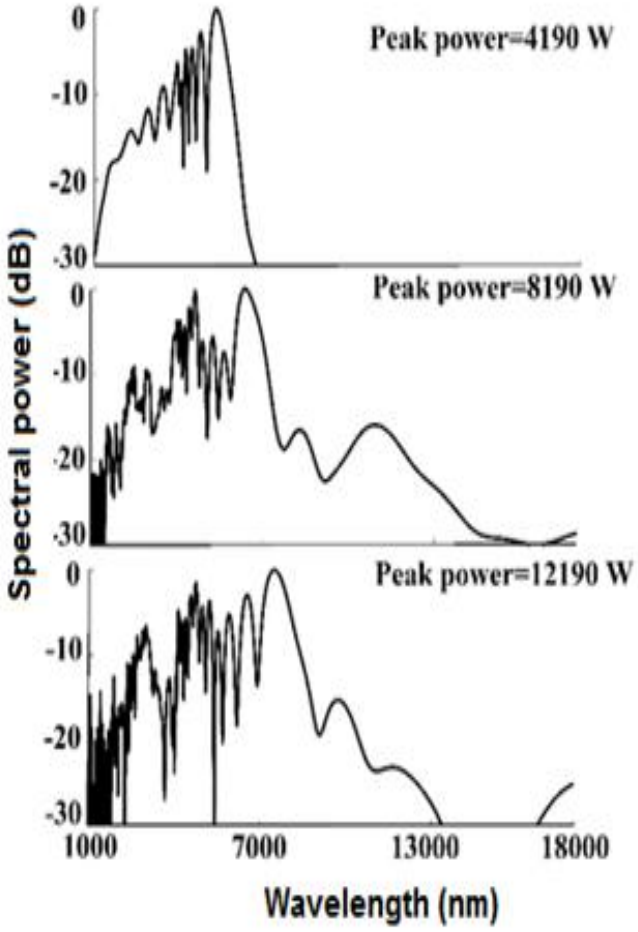

Fig. 5.8 Generated SC spectra with different peak powers in 9 mm long fiber at 4000 nm.

As per best of our knowledge, the study of SCG in PCF using $Ga_8Sb_{32}S_{60}$ chalcogenide has not been reported yet. Only Saini et al. [23] showed the numerical study of SCG in a $Ga_8Sb_{32}S_{60}$ chalcogenide based rib waveguide and generated the SC, spanning from 1 to 9.7 μm using a femtosecond laser source of wavelength 2800 nm and peak power of 6.4 kW. Our numerical findings prove that the proposed chalcogenide PCF is a better choice due to the ultra-broadband SC, spanning from 1 to 14 μm for mid-infrared nonlinear devices in comparison with previously reported PCFs in [7], [8], and [25-27].

5.4 Conclusions:

In summary, a novel design of a highly nonlinear rectangular core $Ga_8Sb_{32}S_{60}$ chalcogenide PCF is reported for ultra-broadband SCG in the mid-infrared region. The proposed PCF agreements a very high nonlinear coefficient of 853 $W^{-1}km^{-1}$ at 4000 nm for optimized geometrical parameters d_1=1.6 µm, d_2=0.5 µm, and Λ =2.5 µm. A supercontinuum spanning, 1 to 14 µm is obtained using a 9 mm long fiber pumped with a 90 fs laser pulse at peak power of 8.19 kW.

References:

1. G.P. Agrawal, "Nonlinear Fiber Optics", fifth ed., Elsevier Academic Press, 2013.

2. P. Russell, "Photonic crystal fibers", Science 299, pp. 358–362, 2003.

3. J.M. Dudley, G. Genty, and S. Coen, "Supercontinuum generation in photonic crystal fiber", Review of Modern Physics 78, pp. 1135–1184, 2006.

4. J. Herrmann, U. Griebner, N. Zhavoronkov, A. Husakou, D. Nickel, J.C. Knight, W.J. Wadsworth, P.S.J. Russell, and G. Korn, "Experimental evidence for supercontinuum generation by fission of higher-order solitons in photonic fibers", Physical Review Letters 88, p. 173901, 2002.

5. B.J. Eggleton, B.L. Davies, and K. Richardson, "Chalcogenide photonics", Nature Photonics 5, pp. 141–148, 2011.

6. V. Shiryaev, and M. Churbanov, "Trends and prospects for development of chalcogenide fibers for mid-infrared transmission', Journal of Non-Crystalline Solids 377, pp. 225–230, 2013.

7. L.B. Shaw, V.Q. Nguyen, J.S. Sanghera, I.D. Aggarwal, P.A. Thielen, and F.H. Kung, "IR supercontinuum generation in As–Se photonic crystal fiber", Proc. Adv. Solid-State Photonics paper TuC5, 2005.

8. J. Hu, C.R. Menyuk, L.B. Shaw, J.S. Sanghera, and I.D. Aggarwal, "Maximizing the bandwidth of supercontinuum generation in As_2Se_3 chalcogenide fibers", Optics Express 18, pp. 6722–6739, 2010.

9. C.R. Petersen, U. Møller, I. Kubat, B. Zhou, S. Dupont, J. Ramsay, T. Benson, S. Sujecki, N.A. Moneim, Z. Tang, and D. Furniss, "Mid-infrared supercontinuum covering the 1.4–13.3 μm molecular fingerprint region using ultra-high NA chalcogenide step-index fibre", Nature Photonics 8 (11), p. 830, 2014.

10. M. Liao, C. Chaudhari, L. Shuo, and L.S. Guang, "Numerical analysis of photonic crystal fiber with chalcogenide core tellurite cladding composite microstructure", Chinese Physics B 22, p. 074206, 2013.

11. T.S. Saini, A. Baili, A. Kumar, R. Cherif, M. Zghal, and R.K. Sinha, 'Design and analysis of equiangular spiral photonic crystal fiber for mid-infrared supercontinuum generation", Journal of Modern Optics 62, pp. 1570–1576, 2015.

12. A.B. Salem, R. Cherif, and M. Zghal, "Tapered As_2S3 chalcogenide photonic crystal fiber for broadband mid-infrared supercontinuum generation", in Frontiers in Optics 2011/Laser Science XXVII, OSA Technical Digest (Optical Society of America), paper FMG6, 2011.
13. T.S. Saini, A. Kumar, and R.K. Sinha, "Design and modeling of dispersion engineered rib waveguide for ultra-broadband mid-infrared supercontinuum generation", Journal of Modern Optics 64(2), pp. 143–149, 2017.
14. J.W. Choi, Z. Han, B.U. Sohn, G.F.R. Chen, C. Smith, L.C. Kimerling, K.A. Richardson, A.M. Agarwal, and D.T.H. Tan, "Nonlinear characterization of Ge-Sb-S chalcogenide glass waveguides", Scientific Reports 6, p. 39234, 2016.
15. D.J. Jones, S.A. Diddams, J.K. Ranka, A. Stentz, R.S. Windeler, J.L. Hall, and S.T. Cundiff, "Carrier-envelope phase control of femtosecond mode-locked lasers and direct optical frequency synthesis", Science 288, pp. 635–639, 2000.
16. T. Udem, R. Holzwarth, and T.W. Hansch, "Optical frequency metrolog"y, Nature 416, p. 233, 2002.
17. F. Quochi, M. Dinu, L.N. Pfeiffer, K.W. West, C. Kerbage, R.S. Windeler, and B.J. Eggleton, "Coulomb and carrier-activation dynamics of resonantly excited InAs/ GaAs quantum dots in two-color pump-probe experiments", Physical Review B 67, p. 235323, 2003.
18. I. Hartl, X.D. Li, C. Chudoba, R.K. Ghanta, T.H. Ko, J.G. Fujimoto, J.K. Ranka, and R.S. Windeler, "Ultrahigh-resolution optical coherence tomography using supercontinuum generation in an air-silica microstructure optical fiber", Optics Letters 26, pp. 608–610, 2001.
19. S.V. Smirnov, J.D. Ania-Castanon, T.J. Ellingham, S.M. Kobtsev, S. Kukarin, and S.K. Turitsyn, "Optical spectral broadening and supercontinuum generation in telecom applications", Optical Fiber Technology 12(2), pp. 122–147, 2006.
20. S. Dupont, C. Petersen, J. Thogersen, C. Agger, O. Bang, and S.R. Keiding, "IR microscopy utilizing intense supercontinuum light source", Optics Express 20(5), pp. 4887–4892, 2012.
21. F. Keilmann, C. Gohle, and R. Holzwarth, "Time-domain mid-infrared frequency-comb spectrometer", Optics Letters 29(13), pp. 1542–1544, 2004.
22. A. Yang, M. Zhang, L. Li, Y. Wang, B. Zhang, Z. Yang, and D. Tang, "Ga–Sb–S chalcogenide glasses for mid-infrared applications", Journal of the American Ceramic Society 99, pp. 1–4, 2015.
23. T.S. Saini, U.K. Tiwari, and R.K. Sinha, "Rib waveguide in Ga-Sb-S chalcogenide glass for on-chip mid-IR supercontinuum sources: design and analysis", Journal of Applied Physics 122, p. 053104, 2017.

24. M. Liao, C. Chaudhari, G. Qin, X. Yan, C. Kito, T. Suzuki, Y. Ohishi, M. Matsumoto, and T. Misumi, "Fabrication and characterization of a chalcogenide-tellurite composite microstructure fiber with high nonlinearity", Optics Express 17, pp. 21608–21614, 2009.

25. W. Yuan, "2–10 μm mid-infrared supercontinuum generation in As_2Se_3 photonic crystal fiber", Laser Physics Letters 10(9), p. 095107, 2013.

26. G. Qin, X. Yan, C. Kito, M. Liao, C. Chaudhari, T. Suzuki, and Y. Ohishi," Ultrabroadband supercontinuum generation from ultraviolet to 6.28 μm in a fluoride fiber", Applied Physics Letters 95(16), p. 161103, 2009.

27. H. Saghaei, H.M. Ebnali, and M.K.M. Farshi, "Midinfrared supercontinuum generation via As_2Se_3 chalcogenide photonic crystal fibers", Applied Optics 54(8), p. 2072, 2015.

CHAPTER-6

NUMERICAL EXPLORATION OF COHERENT SUPERCONTINUUM GENERATION IN MULTICOMPONENT $GeSe_2$-As_2Se_3-PbSe CHALCOGENIDE BASED PHOTONIC CRYSTAL FIBER*

6.1 Introduction:

The demand of coherent supercontinuum sources is growing rapidly due to their broad practical applications in the visible and infrared wavelength regions. Numerous theoretical and experimental works have been reported by silica, tellurite, fluoride and chalcogenide glasses based step-index fibers, PCFs, and waveguides for SCG [1-24].

Hu et al. have reported the SCG generation of the bandwidth of 4 μm in an As_2Se_3 PCF at a pump wavelength of 2.5 μm [6]. An As_2Se_3 equiangular spiral PCF has been investigated by Saini et al. for generating broadband SCG [9]. Coherent SC has been generated by Xu et al. in a CS_2 filled PCF by optimizing the fiber length and, pump pulse parameters [13]. A Ga-Sb-S based PCF has been studied for coherent SCG by injecting a laser pulse of 50 fs pulses with 20 kW peak power in 1 cm fiber length at 4.5 μm [14]. The SCG of bandwidth 1-6 μm has been computationally analyzed by Seifouri et al. in a PCF made up of As_2Se_3-MgF_2 composition [15].

*** Pooja Chauhan**, Ajeet Kumar, and Yogita Kalra, "Numerical exploration of coherent supercontinuum generation in multicomponent $GeSe_2$–As_2Se_3–PbSe chalcogenide based photonic crystal fiber", Optical Fiber Technology, 54, p. 102100, 2020.

Xing et al. have performed the numerical simulations with an extensive experimental study to generate SCG spanning, 1.9-2.34 μm in a 2 cm long fiber at -20 dB power level [16]. An ultra-broadband SCG spectrum of bandwidth 0.8-4.5 μm has been proposed by Balani et al. in a 10 mm long PCF [17]. Karim et al. has numerically investigated the effect of higher-order dispersion parameters on SCG in an As_2Se_3 based chalcogenide PCF [18]. A multi-material PCF has been numerically designed and simulated a SCG of spanning 1.6-4.2 μm using 85 fs laser source at 2.5 μm wavelength [19]. The effect of higher modes is effectively studied by Wang et al. for SCG in a multimode fiber [20]. A multimaterial PCF has been numerically reported by Diouf et al. to study the coherent mid-infrared SCG [21]. Vyas et al. have performed numerical simulations to generate the SC spectrum in a 100 mm long Ge-As-Se based PCF [22]. A Ge- Sb- Se/Ge- Se fiber has been fabricated and produced SCG spectrum covering 2.2-12 μm infrared range in 11 cm long PCF at 4.485 μm [23]. A 150 mm long $Ge_{11.5}As_{24}Se_{64.5}$ based PCF is numerically simulated for effective SC spanning, 1.4-10 μm using 85 fs input laser pulse at 3.1 μm [24]. An ultra-high numerical-aperture step-index fiber has been experimentally practiced for generating two SC spans, 1.5-11.7 μm and 1.4-13.3 μm at 4.5 μm and 6.3 μm respectively by Petersen et al. [30]. In a low-loss telluride fiber, Zhao et al. [31] determined the experimental proofs for SC range of 2.0-16 μm at pump wavelength of 7 μm using extrusion technique. Numerical simulations have been reported by Saini et al. for mid-infrared SCG covering 2-15 μm in a PCF at 4.1 μm [32].

A highly nonlinear chalcohalide based fiber is fabricated by Zhao et al. using peeling-extrusion method for producing the SC spanning, 1.05-13 μm in mid-infrared wavelength region [33]. A coherent SCG ranging 1.7-12.7 μm has been reported by Zhang et al. in a 7 cm long Te-based tapered fiber consisting $Ge_{20}As_{20}Se_{15}Te_{45}$-$Ge_{20}As_{20}Se_{20}Te_{40}$ chalcogenide glasses at a pump wavelength of 5.5 μm [34]. Jamatia et al. has performed numerical simulations to get SCG of span 0.4-4.7 μm by 3 kW input peak power at 2.8 μm in a composite

PCF [35]. In ref. [36], the numerical design of triangular-core As_2Se_3 PCF has been proposed for SCG with high nonlinear characteristics at 4.4 μm. Using As_2Se_3 chalcogenide glass, an optical rib waveguide design has been reported by Saini et al. [37] and generated the mid-infrared SC spans 1-10.9 μm and 1-11.88 μm at pump wavelength of 2.8 μm. A highly coherent SCG covering 1.28-3.31 μm, has been obtained in a 3.2 cm long tapered step-index fiber of tellurite glass at 2 μm [38]. A $Ge_{15}Sb_{15}Se_{70}$ circular PCF is used for numerical demonstration of an ultraflat-top with coherent property SCG 1.86─5.35 μm in a 10 mm long at 3 μm input pulse [39]. To date, many photonic crystal fibers with chalcogenide glass system have been reported by researchers and scientists for mid-infrared SC but with GAP-Se glass, the work based on PCFs for coherent SCG has not been reported yet.

Recently, a novel $GeSe_2$-As_2Se_3-PbSe (GAP-Se) covalently bonded chalcogenide glass has been reported by Goncalves et al. for SCG applications [25]. The GAP-Se chalcogenide has very excellent optical linear and nonlinear properties such as very high nonlinear refractive index (n_2= 7.14 ×10^{-6} cm^2/GW), high linear refractive index (n= 2.8387 at λ= 3 μm), high viscoelasticity, the high nonlinear figure of merit, and offers a very broad transparency window range (1-12 μm). Such large ion glasses have greater importance in controlling low laser damage resistance, photosensitivity, and reducing thermal or mechanical properties. This glass system gives a strong attribute for mid-infrared laser systems.

In this chapter, we have numerically simulated a PCF in a GAP-Se glass system as a cladding material for highly coherent SCG in the mid-infrared region. This chapter is categorized majorly in four sections. Section 1 is related to the introduction of coherent SCG, and an overview of previous research work in this concern is also discussed. The modeling of proposed photonic crystal fiber is framed in Section 2. In Section 3, the results of coherent SCG is explained briefly on the basis of produced simulation findings. Section 4 is dedicated for highlights of the effectiveness of proposed fiber. Our study will be useful in realizing the

potential applications of PCF in mid-infrared as well as provides insights for future theoretical and experimental research efforts.

6.2 Multicomponent PCF model:

We have designed a rectangular shaped PCF model for numerical simulation of fundamental propagating mode in the core to produce the highly coherent SC spectrum in the infrared wavelength region. The air-holes are patterned periodically in a rectangular shape, and the diameter and center-to-center distance of air-holes are considered as d, and Λ respectively. For the confinement of fundamental mode, one air-hole from the center of PCF has been removed during the simulation. The cross-sectional view of simulated multicomponent PCF is illustrated in fig. 6.1 which is surrounded by a perfectly matched layer.

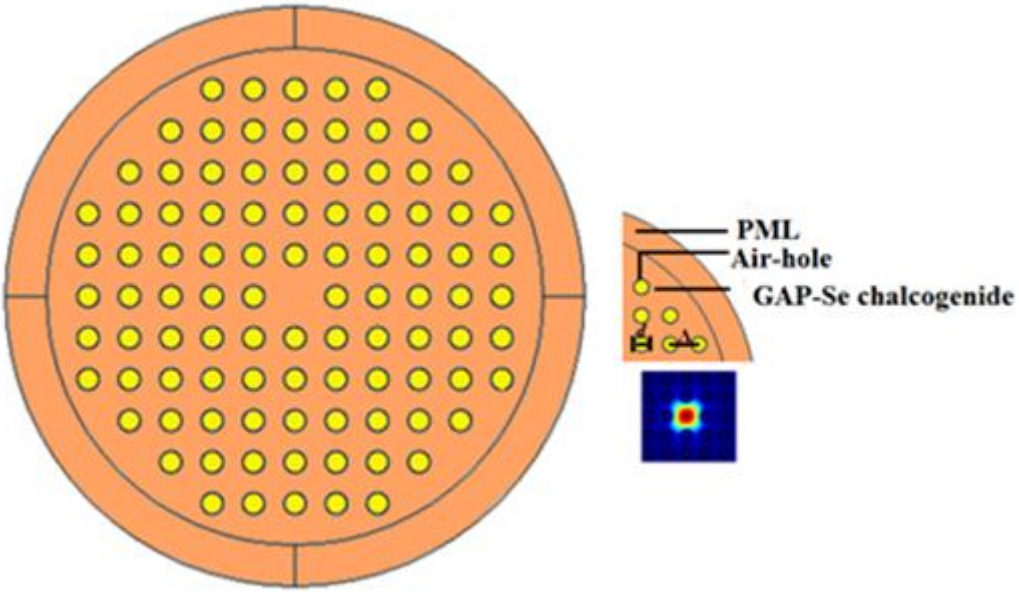

Fig. 6.1 Proposed multicomponent PCF model. Inset top: a small cross-section of PCF with parameter definitions and material used; and Inset down: fundamental mode confinement at 3.1 µm.

Our aim is to design and simulate a multicomponent GAP-Se PCF model to get high coherent ultra-broad and flat SC spectrum in the wide range of mid-infrared wavelength region. The linear refractive index of GAP-Se (with 20mol% PbSe) is taken according to the Sellmeier equation reported by Goncalves et al. [25]. With this aim, the initial step is to numerically tailor

the geometrical parameters i.e. *d* and *Λ* of the designed PCF by tuning these parameters to set the fundamental limit of dispersion regime (either normal or anomalous dispersion). The cladding material is chosen a highly nonlinear GAP-Se chalcogenide glass composition.

6.3 Results and Discussion:

The modal characteristics of n_{eff} have been numerically performed using a FEM-based software i.e. COMSOL Multiphysics. The chromatic dispersion plays an important role to study the linear and nonlinear interactions in PCFs. Initially, we have studied the effect of *d* on dispersion by varying the values of the diameter of air-holes from 0.9 to 1.7 µm keeping *Λ* fixed (=2.5 µm) as shown in fig. 6.2. It is clearly seen that the designed fiber exhibits both the normal and anomalous dispersion with a larger shift of ZDWs towards the longer wavelength region. On increasing the dimension of *d* parameter, the dispersion curve shifts from normal to anomalous dispersion very rapidly.

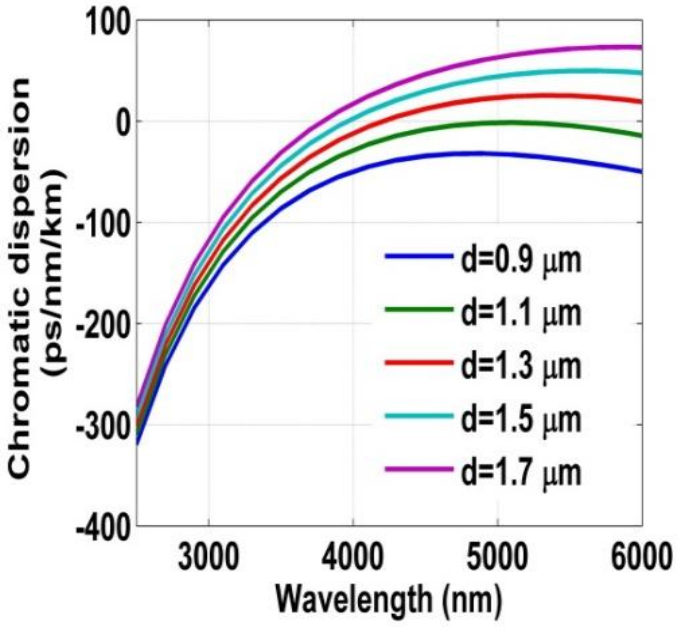

Fig. 6.2 Study of dispersion characteristics with a variation of *d* and keeping *Λ*=2.5 µm as constant.

In fig 6.3, the effect on dispersion profile by increasing the pitch i.e. *Λ* from 2.3 to 2.7 µm has been illustrated. With the increment of the pitch, while keeping the diameter of air-holes fixed as 1.3 µm, we have observed that there is a very least significant effect on the shift of

dispersion profile. Therefore, we can conclude that the flatness of the dispersion curve is controlled more effectively by *d* (air-hole diameter) rather than *Λ* (pitch). After the optimization process of geometrical parameters, we have obtained an ultra-flat dispersion profile in both normal and anomalous regime of the infrared wavelength region. The designed PCF has offered the ZDW around 4200 nm and dispersion at a pump wavelength of 3100 nm has been calculated as -100 ps/nm/km for optimized parameters *d*=1.3 µm, and *Λ*=2.5 µm fixed.

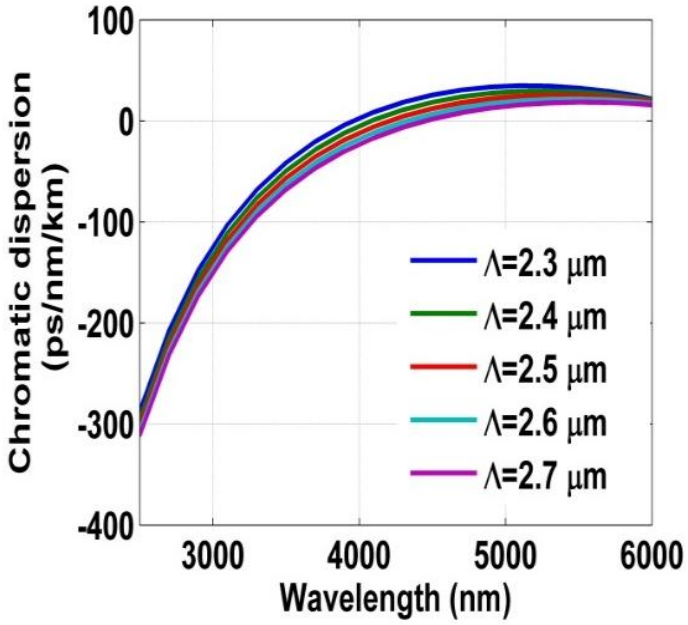

Fig. 6.3 Study of dispersion characteristics with a variation of *Λ* and keeping *d* =1.3 µm as constant.

The figs. 6.4 (a) and (b) are showing the effect of increased value of diameters of air holes on nonlinear coefficient and effective mode area at different wavelengths. As we increased the *d* parameter from 0.45 µm to 0.85 µm with interval of 0.10 µm, the values of nonlinear coefficient also increased and effective mode area are found decreased.

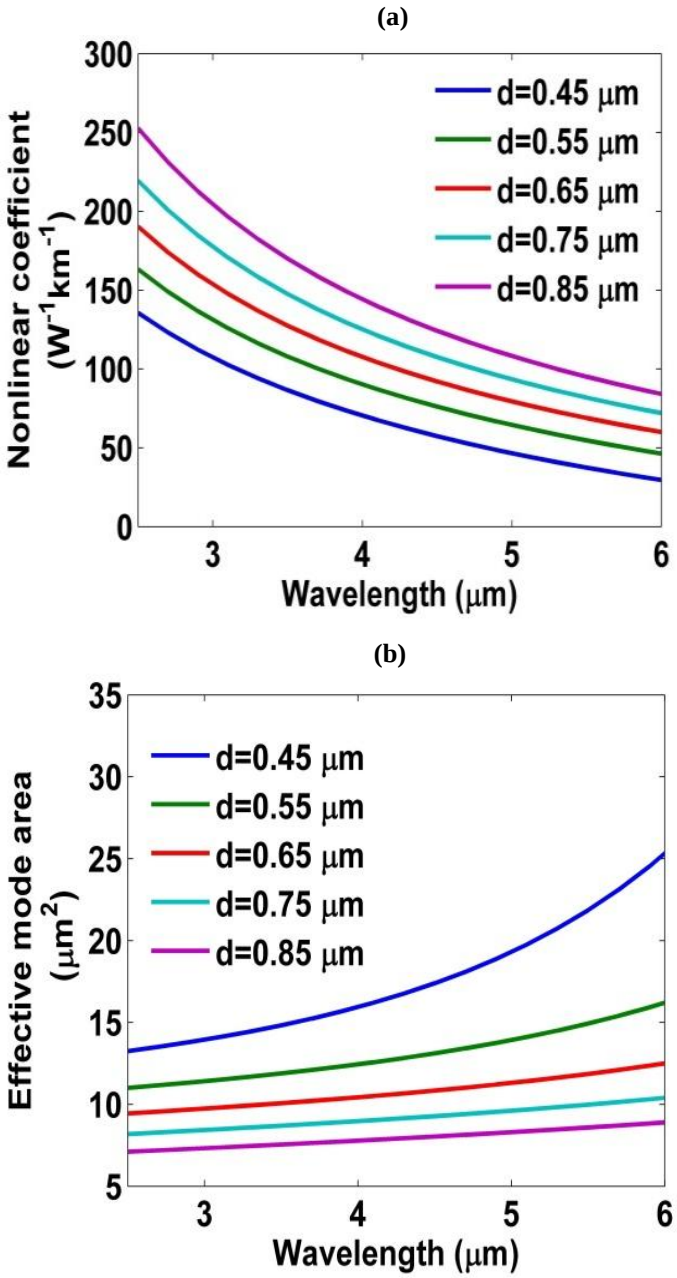

Fig. 6.4 Study of effect of variation of *d* parameter on **(a)** nonlinear coefficient, and **(b)** effective mode area with wavelength.

For the optimized parameters (d=1.3 μm, and Λ=2.5 μm) of proposed PCF, we have numerically simulated the GNLSE equation by launching an input femtosecond laser pulse of wavelength 3.1 μm with a pulse width of 85 fs, peak power of 950 W to initiate the process of SCG effectively [40, 41].

Figures 6.5 and 6.6 represent the spectral growth of SCG spectra with its degree of coherence at different fiber lengths. As we increased the fiber length from 5 mm to 15 mm with period of 5 mm, we have found that the SC spectrum increased towards longer wavelength side. The maximum bandwidth of SC has been identified in a 10 mm long PCF which covered the SC spanning, ~2-11 μm in the mid-infrared wavelength region. The symmetrical broadening of SC spectrum is mainly occurred due to the nonlinear SPM effect along the shorter and longer wavelengths. Simultaneously, we have considered the effect of degree of coherence with its spectral evolution at different fiber lengths. The generated SC spectrum is found highly coherent along the spanning, 2-11 μm in the mid-infrared region for 10 mm long PCF length.

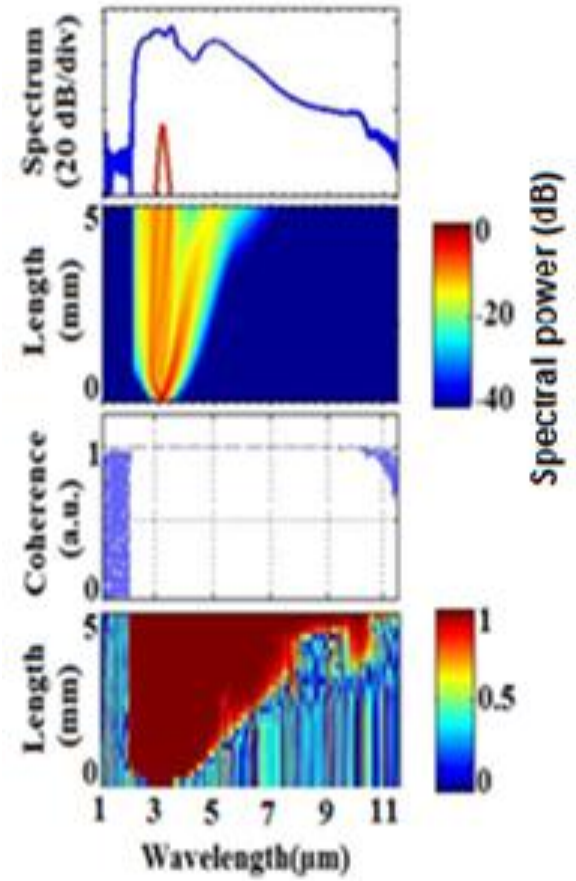

Fig. 6.5 Effect of spectral broadening of SCG, spectral evolution of SCG, degree of coherence and spectral coherence evolution with wavelength (from top to bottom) in 5 mm long PCF with E_{pulse}= 0.092 nJ (pulse width= 85 fs, and peak power= 950 W).

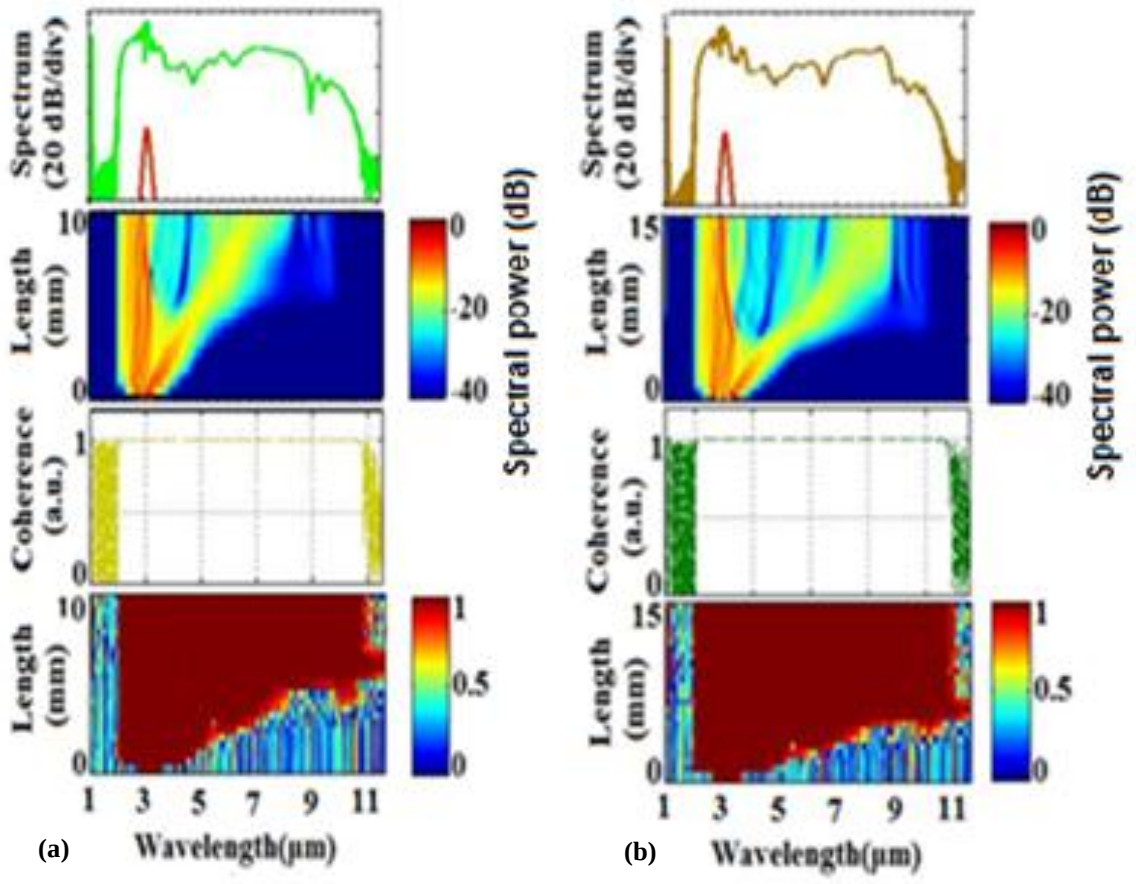

Fig. 6.6 Effect of spectral broadening of SCG, spectral evolution of SCG, degree of coherence and spectral coherence evolution with wavelength (from top to bottom) in **(a)** 10 mm, and **(b)** 15 mm long PCF with E_{pulse}= 0.092 nJ (pulse width= 85 fs, and peak power= 950 W).

Further, we have studied the effect of peak power on the SC. Numerical simulations with 85 fs laser pulse have been analyzed for different peak powers as illustrated in fig. 6.7 (a). It is observed that when we increase the peak power from 950 W to 2550 W, the SC spectrum is increasing. At higher peak power, the SC started deteriorate. This happened due to the absorption at the coating. Then, the impact of increased pulse widths on SC has been analyzed. Fig. 6.7 (b) shows the SC output spectrum generated for different pulse width at 3.1 μm with peak power of 950 W in 10 mm long PCF. As we increased the pulse width from 45 fs to 165 fs, the SC bandwidth gets reduce.

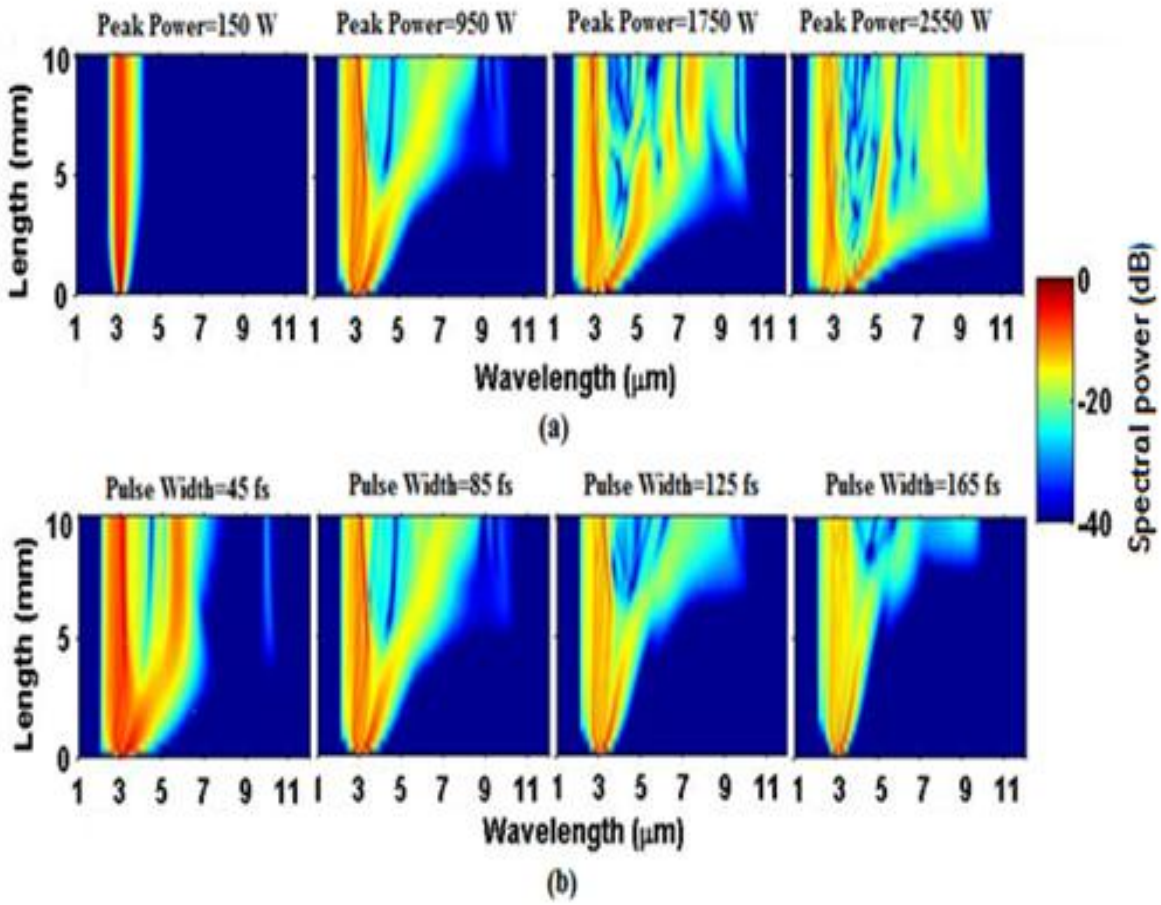

Fig. 6.7 Effect of spectral evolution of SCG with wavelength **(a)** peak power= 150 W (E_{pulse}= 0.014 nJ), 950 W (E_{pulse}= 0.092 nJ), 1750 W (E_{pulse}= 0.169 nJ), and 2550 W (E_{pulse}= 0.246 nJ) when pulse width fixed as 85 fs and pump wavelength as 3.1 μm, and **(b)** pulse width= 45 fs (E_{pulse}= 0.049 nJ), 85 fs (E_{pulse}= 0.092 nJ), 125 fs (E_{pulse}= 0.135 nJ), and 165 fs (E_{pulse}= 0.178 nJ) when peak power is fixed as 950 W and pump wavelength as 3.1 μm in 10 mm long PCF.

Then, we have carried out the simulations for different pump wavelengths (2.6 μm, 3.1 μm, 3.6 μm and, 4.1 μm) to study the effect on SCG as presented in fig 6.8. Subsequent enhanced broadening is noticed as the pump wavelength increased from 2.6 μm to 4.1 μm with 85 fs laser pulses and peak power of 950 W. The impact of fiber length on spectrograms of output pulse has been investigated and same is demonstrated in fig. 6.9. We have performed the numerical simulations for fiber length of 5 mm, 10 mm, and 15 mm with 85 fs pulse duration and peak power of 950 W. It has been observed that, the generated SC gets broadened in the

longer wavelength side at -40 dB power level. Initially, the symmetrical broadening of SC spectrum has been occurred due to SPM and later dominated by optical wave breaking.

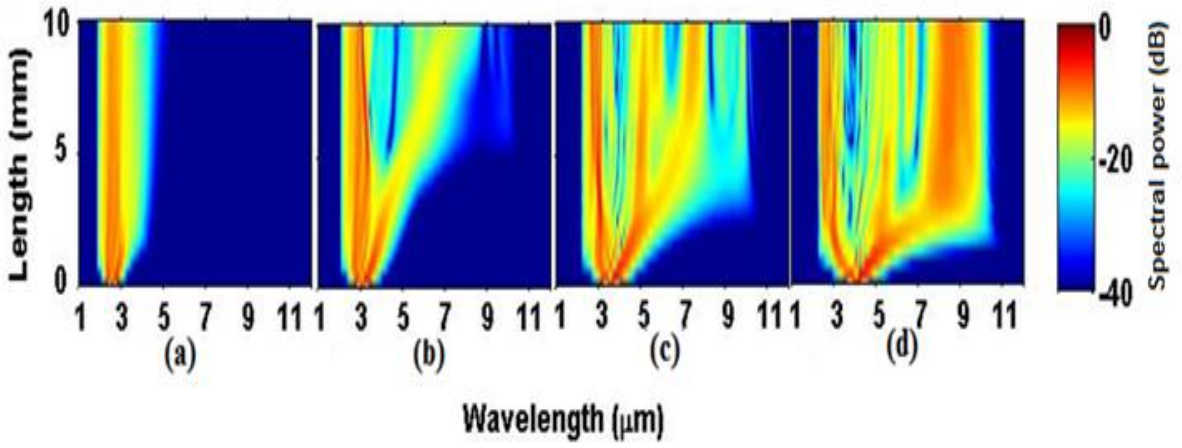

Fig. 6.8 Effect of spectral evolution of SCG at pump wavelength **(a)** 2.6 μm **(b)** 3.1 μm **(c)** 3.6 μm and, **(d)** 4.1 μm with 85 fs pulse width and peak power of 950 W.

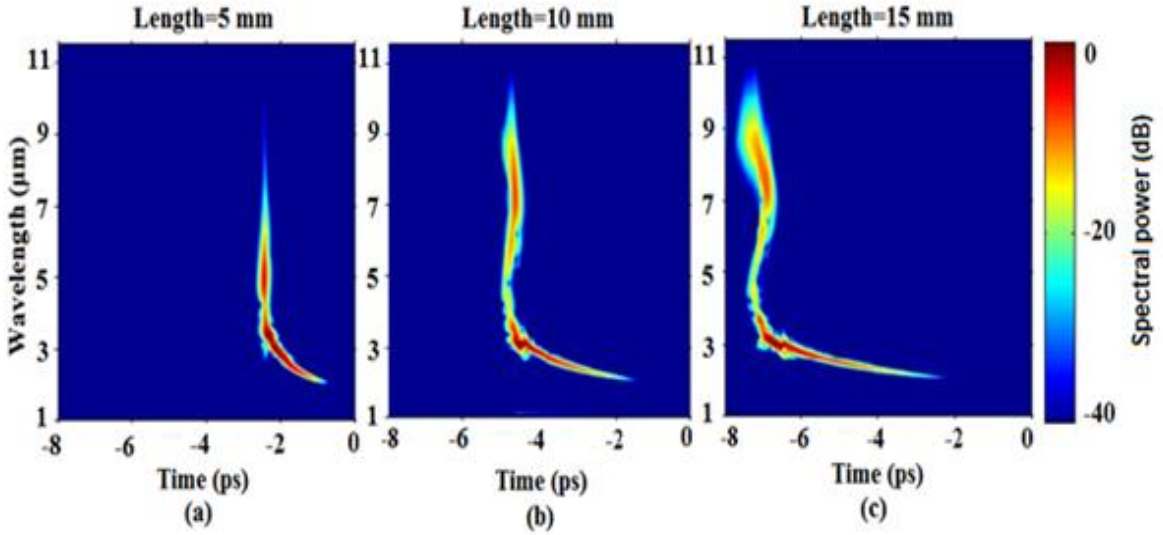

Fig. 6.9 Time-wavelength spectrogram generated for fiber lengths **(a)** 5 mm, **(b)** 10 mm and, and **(c)** 15 mm.

The Lorentz function coefficients (f_R, τ_1, and τ_2) of $GeSe_2$-As_2Se_3-PbSe chalcogenide glass is not known yet. In our simulations, we have considered the values of f_R, τ_1, and τ_2 of As_2Se_3 chalcogenide. We have demonstrated the variation in SCG when changing the values of f_R, τ_1,

and τ_2 by ±0.05, ±5 fs, and ±10 fs respectively in fig. 6.10. There is no significant change is observed in the SC span during variation of f_R, τ_1, and τ_2.

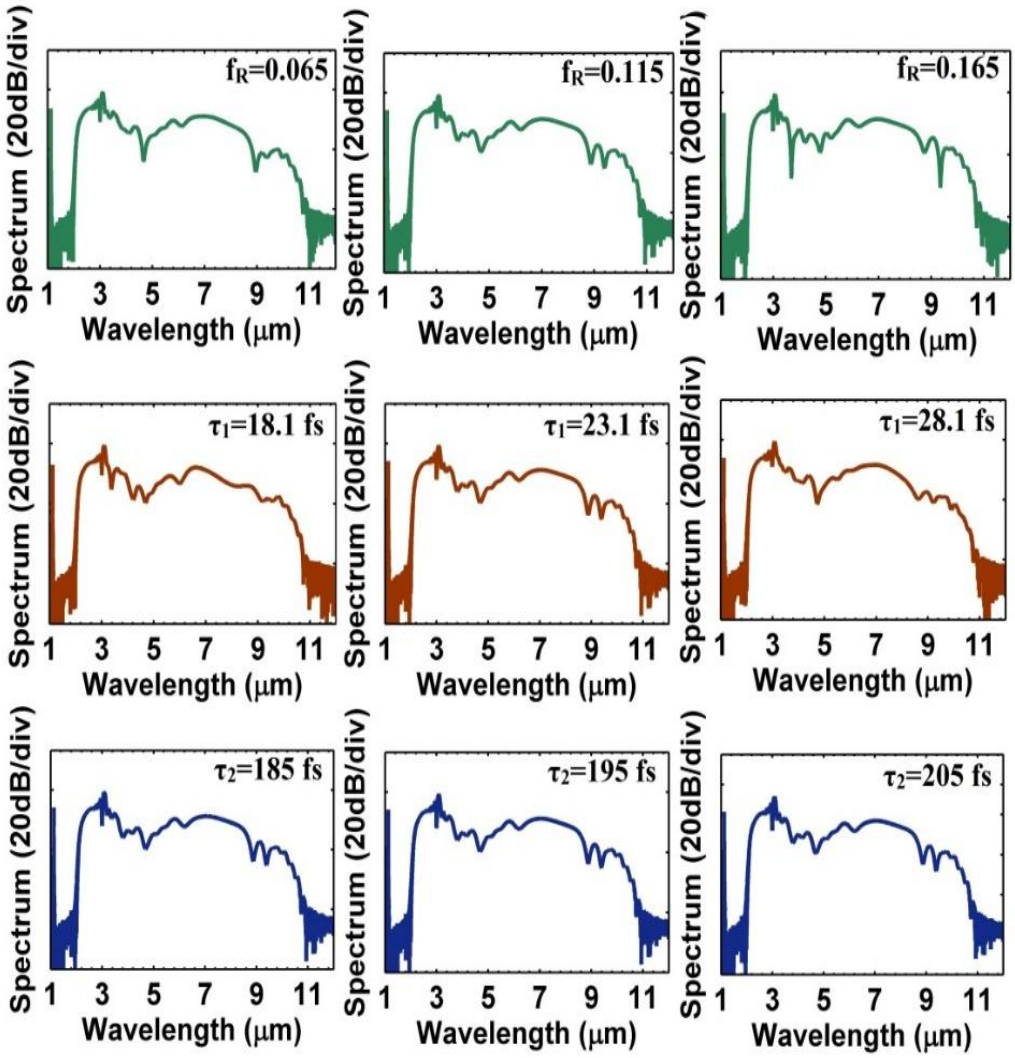

Fig. 6.10 Effect of variation of f_R, τ_1 and τ_2 on SC spectrum with pump wavelength of 3.1 μm having pulse width of 85 fs and peak power of 950 W.

The proposed PCF made from chalcogenide glass compositions can be fabricated by the extrusion and drilling techniques [43-45]. Both the methods are particularly suitable for the PCFs with rectangular periodic symmetry of air-hole arrangements. The extrusion method gives more flexibility in fabrication of PCFs prepared from chalcogenide glasses as they can accept the high dopant concentrations which gives a pathway to alter the optical as well the mechanical properties more easily in comparison of silica glass.

Finally, we can conclude based on our number of numerical simulations, the proposed fiber is able to produce a highly coherent broadband SC spectrum ranging from 2 µm to 11 µm in the mid-infrared wavelength region in a 10 mm fiber length with peak power of 950 W and pulse width of 85 fs which is much broader in comparison of previously reported SCG works as seen in table 6.1.

Reference	**Chalcogenide type**	**Pump wavelength (µm)**	**Fiber length**	**Peak Power (kW)**	**SCG bandwidth (µm)**
[26]	$As_{38.8}Se_{61.2}$ PCF	3.7	5 cm	0.88	2.9-4.575
[27]	As_2S_5-Borosilicate PCF	2.5	4 mm	28.16	1-5
[28]	As_2S_3 PCF	2.5	10 mm	20	1-10
[14]	$Ga_8Sb_{32}S_{60}$ PCF	4.5	1 cm	20	1.65-9.24
[42]	$Ge_{11.5}As_{24}Se_{64.5}$ PCF	3.1	1 cm	5	2-5.5
Proposed work	**$GeSe_2$-As_2Se_3-PbSe PCF**	**3.1**	**10 mm**	**0.95**	**1-11**

Table 6.1: Comparison of SC spectrum generated in proposed PCF with previously reported in chalcogenide PCFs.

6.4 Conclusions:

In summary, we have numerically modeled a PCF in GAP-Se glass for highly coherent supercontinuum generation. We have engineered the dispersive properties by varying the defined geometrical parameters in order to obtain an ultra-flat dispersion profile in normal and anomalous dispersion regimes. We have achieved an ultra-broadband coherent supercontinuum spectrum of the bandwidth of 10 μm by injecting an input laser pulse (85 fs pulse width) with peak power of 950 W in a 10 mm long designed fiber in the mid-infrared region.

References:

1. X. Yu, P. Shum, N.Q. Ngo, W.J. Tong, J. Luo, G.B. Ren, Y.D. Gong, and J.Q. Zhou, "Silica-based nanostructure core fiber", IEEE Photonics Technology Letters 20, pp. 162-164, 2008.

2. F. Begum, and Y. Namihira, "Design of supercontinuum generating photonic crystal fiber at 1.06, 1.31 and 1.55 μm wavelengths for medical imaging and optical transmission systems", Natural Science 3(5), p. 401, 2011.

3. Y. Namihira, M.A. Hossain, T. Koga, M.A. Islam, S.A. Razzak, S.F. Kaijage, Y. Hirako, and H. Higa, "Design of highly nonlinear dispersion-flattened hexagonal photonic crystal fibers for dental optical coherence tomography applications", Optical Review 19(2), pp.78-81, 2012.

4. L. Ferhat, L. Cherbi, and I. Haddouche, "Supercontinuum generation in silica photonic crystal fiber at 1.3 μm and 1.65 μm wavelengths for optical coherence tomography", Optik 152, pp.106-115, 2018.

5. F. Begum, and P. E. Abas, "Near-infrared supercontinuum generation in silica-based photonic crystal fiber", Progress in Electromagnetics Research 89, pp.149-159, 2019.

6. J. Hu, C. R. Menyuk, L.B. Shaw, J.S. Sanghera, I.D. Aggarwal, "Maximizing the bandwidth of supercontinuum generation in As_2Se_3 chalcogenide fibers", Opt. Express 18, pp. 6722-6739, 2010.

7. C.R. Petersen, U. Møller, I. Kubat, B. Zhou, S. Dupont , J. Ramsay , T. Benson , S. Sujecki, N.A. Moneim , Z. Tang , D. Furniss, "Mid-infrared supercontinuum covering the 1.4-13.3 μm molecular fingerprint region using ultra-high NA chalcogenide step-index fibre", Nature Photonics 8(11), p. 830, 2014.

8. M. Liao, C. Chaudhari, L. Shuo, and L.S. Guang, "Numerical analysis of photonic crystal fiber with chalcogenide core tellurite cladding composite microstructure", Chinese Physics B 22, p. 74206, 2013.

9. T.S. Saini, A. Baili, A. Kumar, R. Cherif, M. Zghal, and R.K. Sinha, "Design and analysis of equiangular spiral photonic crystal fiber for M-IR supercontinuum generation", Journal Modern Optics 62, pp. 1570-1576, 2015.

10. A.B. Salem, R. Cherif, and M. Zghal, "Tapered As_2S_3 chalcogenide photonic crystal fiber for broadband M-IR supercontinuum generation", Frontiers in Optics 2011/Laser Science XXVII, OSA Technical Digest (Optical Society of America), paper FMG6, 2011.

11. T.S. Saini, A. Kumar, and R.K. Sinha, "Design and modeling of dispersion engineered rib waveguide for ultra-broadband M-IR supercontinuum generation", Journal Modern Optics 64(2), pp. 143-149, 2017.

12. T.S. Saini, T.H. Tuan, L. Xing, N.P.T. Hoa, T Suzuki, and Y. Ohishi, "Coherent M-IR supercontinuum spectrum using a step-index tellurite fiber with all-normal dispersion", Applied Physics Express 11 (10), p. 102501, 2018.

13. F. Xu, J. Yuan, C. Mei, B. Yan, X. Zhou, Qi.Wu, K. Wang, X. Sang, C. Yu, and G. Farrell, "Highly coherent supercontinuum generation in a polarization-maintaining CS_2-core photonic crystal fiber", Applied Optics 58(6), pp. 1386-1392, 2019.

14. A. Medjouri, D. Abed, and Z. Becer, "Numerical investigation of a broadband coherent supercontinuum generation in $Ga_8Sb_{32}S_{60}$ chalcogenide photonic crystal fiber with all-normal dispersion", Opto-Electronics Review 27(1), pp. 1-9, 2019.

15. M. Seifouri, and M.R. Alizadeh," Supercontinuum generation in a highly nonlinear chalcogenide/MgF_2 hybrid photonic crystal fiber", International Journal of Optics and Photonics 12(1), pp. 69-78, 2018.

16. S. Xing, S. Kharitonov, J. Hu, and C.S. Brès, "Linearly chirped mid-infrared supercontinuum in all-normal-dispersion chalcogenide photonic crystal fibers", Optics Express 26(15), pp. 19627-19636 2018.

17. H. Balani, G. Singh, M. Tiwari, V. Janyani, and A.K. Ghunawat, "Supercontinuum generation at 1.55 μm in As_2S_3 core photonic crystal fiber", Applied Optics 57(13), pp. 3524-3533, 2018.

18. M.R. Karim, H. Ahmad, S. Ghosh, and B.M.A. Rahman, "M-IR supercontinuum generation using As_2Se_3 photonic crystal fiber and the impact of higher-order dispersion parameters on its supercontinuum bandwidth," Optical Fiber Technology 45, pp. 255-266, 2018.

19. S. Kalra, S. Vyas, M. Tiwari, and G. Singh, "Multi-material photonic crystal fiber in M-IR region for broadband supercontinuum generation", In Optical and Wireless Technologies, Springer, pp. 199-209, 2018.

20. N. Wang, M.S. Habib, F. Jia, G. Li, and R.A. Correa, "Near-IR to Mid-IR supercontinuum generation for high-order modes using As-Se multimode fiber", IEEE Photonics Society Summer Topical Meeting Series (SUM), IEEE, pp. 135-136, 2018.

21. M. Diouf, A. Wague, and M. Zghal, "Numerical investigation of an ultra-broadband coherent M-IR supercontinuum in a chalcogenide $AsSe_2$-As_2S_5 multimaterial photonic crystal fiber", Journal of Optical Society of America B 36(2), pp. A8-A14, 2019.

22. S. Vyas, T. Tanabe, M. Tiwari, and G. Singh, "Chalcogenide photonic crystal fiber for ultraflat M-IR supercontinuum generation," Chinese Optics Letters 14(12), p. 123201, 2016.

23. B. Zhang, Y. Yu, C. Zhai, S. Qi, Y. Wang, A. Yang, X. Gai, R. Wang, Z. Yang, and B.L. Davies, "High brightness 2.2-12 μm mid-infrared supercontinuum generation in a nontoxic chalcogenide step-index fiber", Journal of the American Ceramic Society 99(8), pp. 2565-2568, 2016.

24. S. Vyas, T. Tanabe, G. Singh, and M. Tiwari, "Broadband supercontinuum generation and Raman response in $Ge_{11.5}As_{24}Se_{64.5}$ based chalcogenide photonic crystal fiber", International Conference on Computational Techniques in Information and Communication Technologies (ICCTICT), IEEE, pp. 607-611, 2016.

25. C. Goncalves, M. Kang, B.U. Sohn, G. Yin, J. Hu, D. Tan, and K. Richardson, "New candidate multicomponent chalcogenide glasses for supercontinuum generation", Applied Sciences 8(11), p. 2082, 2018.

26. M. Diouf, A. Ben Salem, R. Cherif, H. Saghaei, and A. Wague, "Super-flat coherent supercontinuum source in $As_{38.8}Se_{61.2}$ chalcogenide photonic crystal fiber with all-normal dispersion engineering at a very low input energy", Pure Applied Optics: Journal of the European Optical Society Part A 56 (2), pp. 163-169, 2017.

27. A.B. Salem, M. Diouf, R. Cherif, A. Wague, and M. Zghal, "Ultraflat-top mid infrared coherent broadband supercontinuum using all normal As_2S_5-borosilicate hybrid photonic crystal fiber", Optical Engineering 55(6), p.066109, 2016.

28. M. Kalantari, A. Karimkhani, H. Saghaei, "Ultra-Wide M-IR supercontinuum generation in As_2S_3 photonic crystal fiber by rods filling technique", Optik 158, pp. 142-151, 2018.

29. A. Medjouri, A. Djamel, and Z. Becer, "Numerical investigation of a broadband coherent supercontinuum generation in $Ga_8Sb_{32}S_{60}$ chalcogenide photonic crystal fiber with all-normal dispersion", Opto-Electronics Review 27(1), pp.1-9, 2019.

30. C.R. Petersen, U. Møller, I. Kubat, B. Zhou, S. Dupont, J. Ramsay, T. Benson, S. Sujecki, N. Abdel-Moneim, Z. Tang, and D. Furniss, "Mid-infrared supercontinuum covering the 1.4–13.3 μm molecular fingerprint region using ultra-high NA chalcogenide step-index fibre", Nature Photonics 8(11), p.830, 2014.

31. Z. Zhao, B. Wu, X. Wang, Z. Pan, Z. Liu, P. Zhang, X. Shen, Q. Nie, S. Dai, R. and Wang, "Mid-infrared supercontinuum covering 2.0-16 μm in a low-loss telluride single-mode fiber", Laser & Photonics Reviews 11(2), p.1770023, 2017.

32. T.S. Saini, A. Kumar, and R.K. Sinha, "Broadband mid-infrared supercontinuum spectra spanning 2-15 μm using As_2Se_3 chalcogenide glass triangular-core graded-index photonic crystal fiber", Journal of Lightwave Technology 33(18), pp. 3914-3920, 2015.

33. Z. Zhao, P. Chen, X. Wang, Z. Xue, Y. Tian, K. Jiao, X.G. Wang, X. Peng, P. Zhang, X. Shen, and S. Dai, "A novel chalcohalide fiber with high nonlinearity and low material zero-dispersion via extrusion", Journal of the American Ceramic Society 102(9), pp. 5172-5179, 2019.

34. N. Zhang, X. Peng, Y. Wang, S. Dai, Y. Yuan, J. Su, G. Li, P. Zhang, P. Yang, and X. Wang, "Ultrabroadband and coherent mid-infrared supercontinuum generation in Te-based chalcogenide tapered fiber with all-normal dispersion", Optics Express 27(7), pp.10311-10319, 2019.

35. P. Jamatia, T.S. Saini, A. Kumar, and R.K. Sinha, "Design and analysis of a highly nonlinear composite photonic crystal fiber for supercontinuum generation: visible to mid-IR", Applied Optics 55(24), pp. 6775-6781, 2016.

36. T.S. Saini, A. Kumar, and R.K. Sinha, "Highly nonlinear triangular-core photonic crystal fiber with all-normal dispersion for supercontinuum generation", Proc. Frontiers in Optics 2014; Tucson, AZ (USA), Long Wavelength Mid-IR to THz Fiber Devices I, paper FW1D. 4, October 19-23, 2014.

37. T.S. Saini, U.K. Tiwari, and R.K. Sinha, "Design and analysis of dispersion engineered rib waveguides for on-chip mid-infrared supercontinuum", Journal of Lightwave Technology 36(10), pp. 1993-1999, 2018.

38. T.S. Saini, N.P.T. Hoa, T.H. Tuan, X. Luo, T.Suzuki, and Y. Ohishi, "Tapered tellurite step-index optical fiber for coherent near-to-mid-IR supercontinuum generation: experiment and modeling", Applied Optics 58(2), pp. 415-421, 2019.

39. A. Medjouri, and D. and Djamel, "Mid-infrared broadband ultraflat-top supercontinuum generation in dispersion engineered Ge-Sb-Se chalcogenide photonic crystal fiber", Optical Materials 97, p. 109391, 2019.

40. A. Thai, M. Hemmer, P.K. Bates, O. Chalus, and J. Biegert, "Sub-250-mrad, passively carrier-envelope-phase-stable mid-infrared OPCPA source at high repetition rate", Optics Letters 36, pp. 3918-3920, 2011.

41. F. Silva, D.R. Austin, A. Thai, M. Baudisch, M. Hemmer, D. Faccio, A. Couairon, and J. Biegert, "Multi-octave supercontinuum generation from mid-infrared filamentation in a bulk crystal", Nature Communications 3, p. 807, 2012.

42. M.R. Karim, H. Ahmad, B.M.A. Rahman, "All-normal dispersion chalcogenide PCF for ultraflat mid-infrared supercontinuum generation", IEEE Photonics Technology Letters 29(21), pp. 1792–1795, 2017.

43. R. Buczynski, "Photonic crystal fibers", Acta Physica Polonica Series A 106(2), pp.141-168, 2004.

44. V.R.K. Kumar, A. K. George, W. H. Reeves, J. C. Knight, P. S. J. Russell, F. G. Omenetto, and A. J. Taylor, "Extruded soft glass photonic crystal fiber for ultrabroad supercontinuum generation", Optics Express 10(25), pp.1520-1525, 2002.

45. P. Zhang, J. Zhang, P. Yang, S. Dai, X. Wang, and W. Zhang, "Fabrication of chalcogenide glass photonic crystal fibers with mechanical drilling", Optical Fiber Technology 26, pp.176-179, 2015.

CHAPTER-7

FLUIDIC INFILTRATED CORE BASED PHOTONIC CRYSTAL FIBER FOR COHERENT SUPERCONTINUUM GENERATION*

7.1 Introduction:

In recent times, the advent of coherent supercontinuum sources is up-surging the attention among researchers and scientists for the visible and infrared nonlinear applications. The fundamental mechanism of SCG in optical fibers is elucidated by the dispersion effect in the normal and anomalous dispersion regimes. The appropriate pumping scheme plays a vital role in generating the spectral broadband of SC. The femtosecond, picosecond, and nanosecond optical laser pulses are used in instigating the process of SCG in fibers [1, 2]. The occurrence of broadband of SC is due to the domination of soliton dynamics and dispersion waves when a femtosecond pumping source is chosen in anomalous dispersion wavelength regime. If the pumping is considered in a normal dispersion regime then the spectral broadening of SCG emerges due to the SPM and optical wave breaking [1, 2].

The most promising application of PCF is in the field of optofluidics. It is an emerging technology that combines microfluidics and optics [3]. The microfluidic technology enables one to abridge the optical elements, gives the flexibility to tune and reconfigure the optical properties of fluids.

*** Pooja Chauhan**, Ajeet Kumar, and Yogita Kalra, "Fluidic infiltrated core based photonic crystal fiber for coherent supercontinuum generation". (under communication)

The PCFs are the absolute option to infiltrate with optofluids that possess high linear and nonlinear refractive indices and also useful in manipulation with micro-objects [4]. The silica fibers can generate the SC till NIR wavelength region which is due to the smaller nonlinear refractive indices, limited transmission window, and high optical losses. The optofluids such as nitrobenzene, toluene, carbon tetrachloride, ethanol, etc. are ideal choices for the study of SCG which comparatively hold the high linear and nonlinear refractive indices and broad transmission window in comparison to pure/fused silica glasses. The value of nonlinear coefficient of nitrobenzene is taken from Kedenburg et al. [27].

Recently, the scientists and researchers are drawing much attention with the latest technique of fluidic infiltration for improving the broadband of SC in silica fibers and waveguides. Vieweg et al. have demonstrated experimentally the solitonic SCG over 600 nm span with pump source as compact femtosecond oscillator in a 26 cm long PCF with a core composition of CCl_4 [5]. Zhang et al. have numerically explored a carbon disulphide and nitrobenzene core-based PCFs and produced SC of range 0.7-2.5 μm using sub-picosecond pulses at 1.55 μm pump wavelength [6]. Bethge et al. have obtained broadband of SC of spanning 0.41-1.64 μm using their numerical and experimental skills in water-filled PCF at 1.2 μm pump wavelength [7]. Kedenburg et al. have explored a PCF with carbon disulfide filled core and generated SCG of bandwidth 1.2-2.4 μm [8]. Numerical simulations of SCG of broadband 500-2500 nm has been reported by Raei et al. in 10 mm long liquid-liquid PCF at pump wavelengths 1032 nm and 1560 nm with 10 kW input peak power and 50 fs pulse width [9]. An optofluidic infiltrated PCF has been proposed for SCG by Saghaei et al. with spanning 800-2000 nm by using pulse width and peak power as 50 fs and 10 kW at 1550 nm [10]. Hoang et al. [11] has performed the theoretical and experimental explorations to generate the all-normal dispersion SC in toluene infiltrated core PCF design. The authors succeeded in obtaining SC spanning, 850-1250 nm in a carbon tetrachloride based all-normal PCF at 1030 nm laser pulse with 400 fs

pulse width [12]. Van et al. [13] presented a PCF with chloroform infiltration and generated coherent SC spans 600-1260 nm and 600-1400 nm using a 400 fs laser pulses of 1030 nm wavelength. The numerical investigation of SCG has been presented by Van et al. in nitrobenzene infiltrated based PCF and successfully reported three SC spans of 0.8–1.8 μm, 0.8–2.1 μm, and 1.3–2.3 μm [14]. Peniewski et al. have manifested the numerical analysis of a PBG-08 based PCF with 17 different highly nonlinear organic solvents to study the SCG [15]. Xu et al. [16] has procured a broadband coherent SCG of bandwidths 820 nm and 1260 nm in a polarization maintained PCF infiltrated with CS_2 at 1760 nm. A carbon disulphide based PCF has been numerically developed by the Munera et al. [17] for the practical applications in optical switching and to develop the broadband source. Churin et al. [18] have used experimentally a CS_2 liquid-filled PCF for developing SC source of bandwidths 640 nm and 610 nm at pump wavelengths 1560 nm and 1910 nm respectively. Porsezian et al. [19] has theoretically exhibited the soliton generation of SC in a liquid core-based PCF and studied the nonlinear responses. The experimental demonstration of coherent SCG has been performed by Hoang et al. [20] in a carbon tetrachloride PCF and recorded two SC bandwidths 1350-1900 nm and 1000-1900 nm at a pump wavelength of 1560 nm using a pulse width of 90 fs and peak power of 5500 W. Chemnitz et al. [21] has inquired the step-index fibers with CCl_4 and C_2Cl_4 liquid cores for the infrared SCG at pump wavelength 1.92 μm. Xu et al. [22] have performed the numerical simulations of linear and nonlinear properties and SCG in the optical fiber filled with different organic liquid at 800 nm pump wavelength. Canh et al. have experimentally reported the all-normal SC of bandwidth 435-1330 nm at 1330 nm with peak power 150 kW in a suspended core fiber composed of water core [23]. Karasawa et al. [24] has studied the dispersion properties in the PCFs with core infiltration using CS_2, toluene, chloroform, and water using multiple methods.

In this chapter, we have computationally proposed a design of PCF for the ultra-broadband SCG in the visible and near-infrared wavelength regions. We have briefly studied the effect of inorganic liquids infiltration on the linear and nonlinear effects. The simulation results shows the possibility to generate a broadband supercontinuum spanning, 1-2.6 μm by using a femtosecond laser pulse with peak power of 5 kW in a 2.5 cm long proposed fiber.

7.2 Proposed PCFs Design:

The transverse cross-sectional view of distinguished PCF structures is demonstrated in Fig. 7.1.

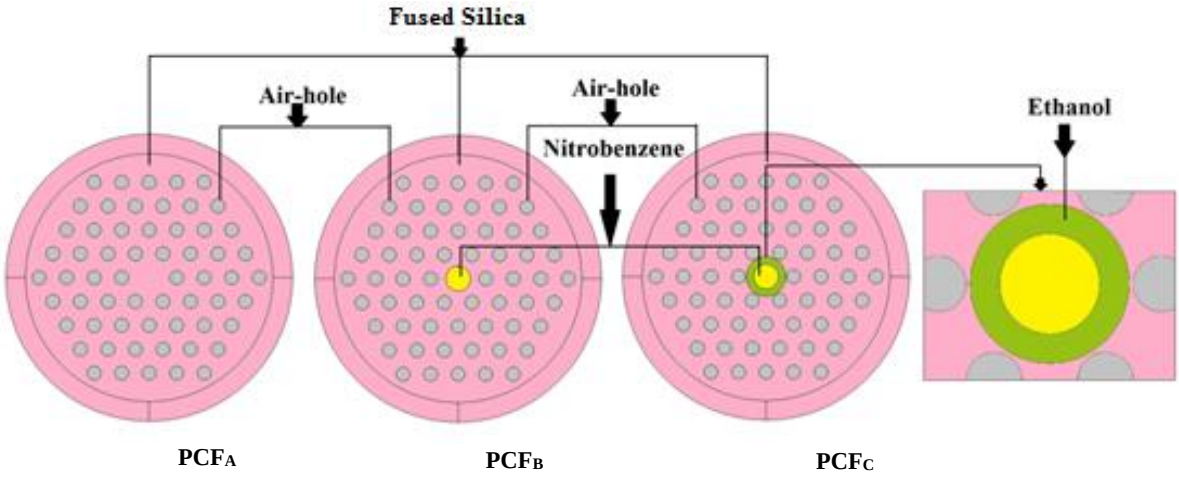

Fig. 7.1: Schematic cross-sectional view of proposed fiber designs.

We have considered three basic PCFs design and named them as PCF_A, PCF_B, and PCF_C on the basis of their core material composition. In PCF_A design, the core material is formed by the fused silica glass similar to the cladding material. The second fiber i.e. PCF_B consists of the core and cladding materials as nitrobenzene and fused silica respectively. Lastly, the core of PCF_C design is made up of composite liquid material as nitrobenzene and ethanol. The number of rings (04 rings) is kept constant in all PCFs structures and enclosed with a perfectly matched layer of thickness as 2 μm in order to reduce the effect of confinement loss. In common cladding regions of PCFs structures, the diameter and pitch of air-holes are defined by d and Λ

respectively. While the diameters d_{c1} and d_{c2} have the geometrical definitions of the diameter of the first core and second core respectively.

The wavelength-dependent refractive indices of fused silica, ethanol and nitrobenzene are taken from Malitson et al. [25], Raei et al. [9], and Kedenburg et al. [26] respectively. Figure 7.2 compares the refractive indices of fused silica, ethanol, and nitrobenzene at different wavelengths.

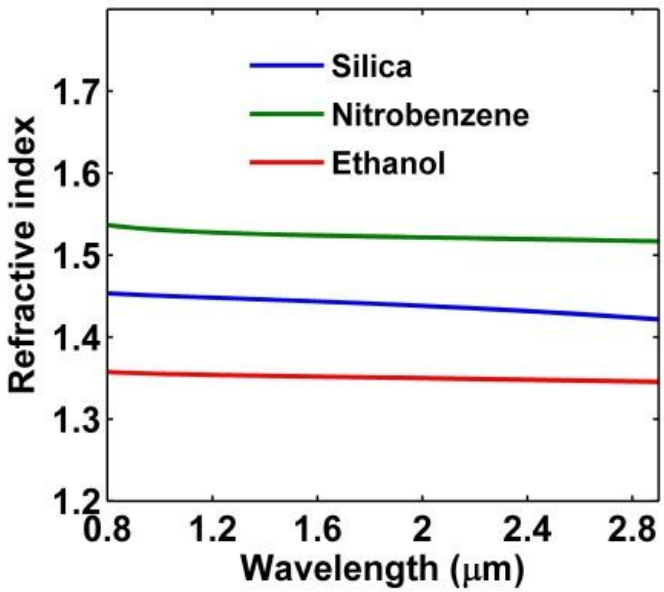

Fig. 7.2: Spectral variation of refractive indices of fused silica and organic liquids (nitrobenzene and ethanol).

7.3 Results and Discussion:

We have considered three different fiber designs (PCF_A, PCF_B, and PCF_C) for the computational analysis of the linear and nonlinear properties that control the generation of SC broadband which are listed in table 7.1 with their core compositions and parameters.

Proposed PCF Nomenclature	Type of Core	Structural Parameters Definition	
		Core	Cladding
PCF_A	Fused Silica		d, Λ
PCF_B	Nitrobenzene Infiltrated	d_{c1}	d, Λ
PCF_C	Nitrobenzene + Ethanol Infiltrated	d_{c1}, d_{c2}	d, Λ

Table 7.1: List of parameters defined in different PCFs during computational simulations.

The n_{eff} depends upon the propagation constant (β) and propagation constant in vacuum (k_0) exclusively. For the fundamental mode, the power confinement inside the core is more in comparison of higher propagated mode which is due to the highest β constant values. The chromatic dispersion being the linear effect participates in the complex dynamics of the SCG process that in result influences the propagation of the optical wave in a fiber. The dispersion occurs due to the variability of the n_{eff} for the propagated fundamental mode at different wavelengths.

Firstly, we have considered the PCF_A design to study the influence of diameter by pitch ratio (d/Λ) on dispersion characteristics by keeping pitch constant as 2.8 µm and it is presented in fig. 7.3. With the increase of the d/Λ ratio from 0.3571 to 0.5714, the ZDWs corresponding to dispersion curves are slightly shifted towards the shorter wavelengths side and the most of the dispersion values are found in anomalous region. The values of ZDWs are obtained as 1078 nm, 1049 nm, 1020 nm, and 996 nm for d/Λ values as 0.3571, 0.4286, 0.5000, and 0.5714 respectively.

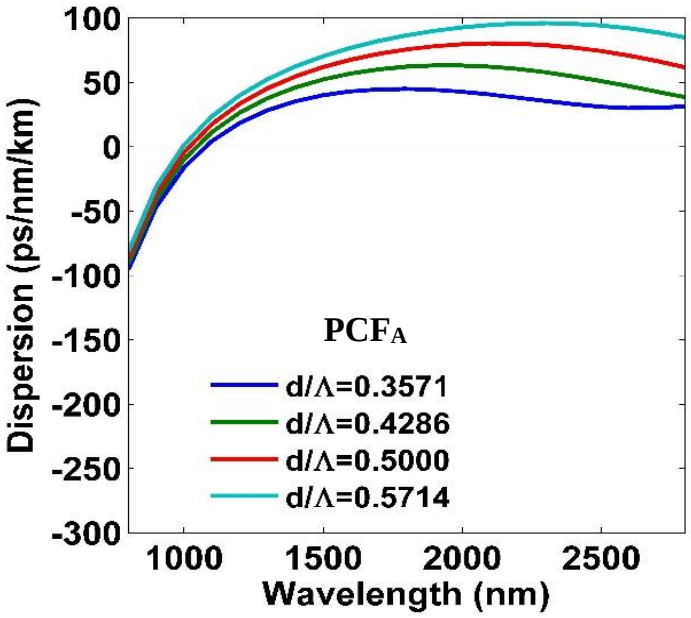

Fig. 7.3: The spectral variation of parameters d/Λ with Λ=2.8 µm constant in PCF_A to study the dispersion characteristics.

Then, we have inspected the PCF_B design and tailored the parameters d, Λ, and d_{c1} to get the flat dispersion profile. Figures 7.4 and 7.5 depict the effect of d/Λ and d_{c1} on dispersion characteristics in PCF_B.

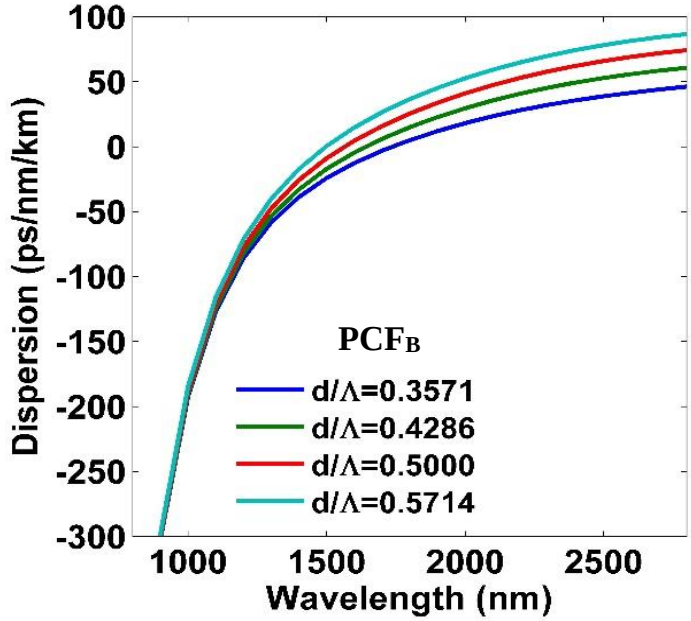

Fig. 7.4: The spectral variation of parameters d/Λ with Λ=2.8 µm, and d_{c1}=2.514 µm fixed in PCF_B to study the dispersion characteristics.

By increasing the d/Λ, we observed that the ZDWs are moved towards the shorter wavelength while d_{c1} kept constant as 2.514 µm. For the d/Λ values as 0.3571, 0.4286, 0.5000, and 0.5714, the anomalous dispersion region has started above the ZDWs values 1737 nm, 1642 nm, 1564 nm, and 1500 nm respectively.

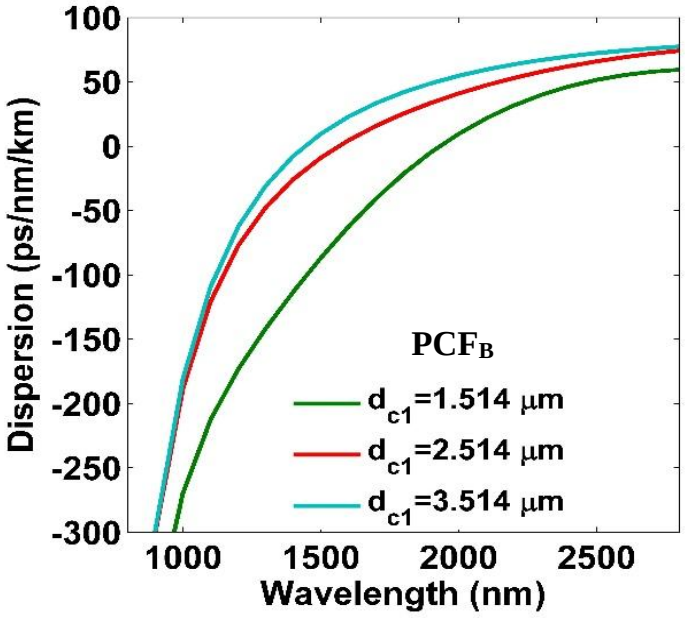

Fig. 7.5: The spectral variation of parameters d_{c1} with d/Λ=0.5000 (Λ=2.8 µm constant) in PCF_B to study the dispersion characteristics.

When we increased the values of d_{c1} parameter from 1.514 µm to 3.514 µm (kept d/Λ=0.5000), the ZDWs shifted drastically towards the shorter wavelength region and the ZDWs values are recorded as 1936 nm for d_{c1}=1.514 µm, 1567 nm for d_{c1}=2.514 µm, and 1439 nm for d_{c1}=3.514 µm and the corresponding dispersion curves covered both the normal and anomalous regions.

Next, we have optimized the PCF_C by modulating the geometrical parameters such as d/Λ, d_{c1}, and d_{c2} and studied their impacts on dispersion characteristics which are depicted in figs. 7.6 – 7.8. We have analyzed the dispersion characteristics related to the variation of d/Λ of air-holes present in the cladding region which is shown in fig. 7.6. We have retained the other parameters constant as d_{c1}=2.514 µm, d_{c2}=4 µm, and Λ =2.8 µm. While we varied the

dimension of d/Λ ratio from 0.3571 to 0.5714 (d_{c1}=2.514 µm and d_{c2}=4 µm), we noticed a slight shift in the dispersion curve towards the longer wavelengths. Also, the dispersion curve moved from normal dispersion region to anomalous dispersion region. A flattened dispersion profile is obtained for d/Λ=0.5000 value with two ZDWs at 1562nm and 1890 nm.

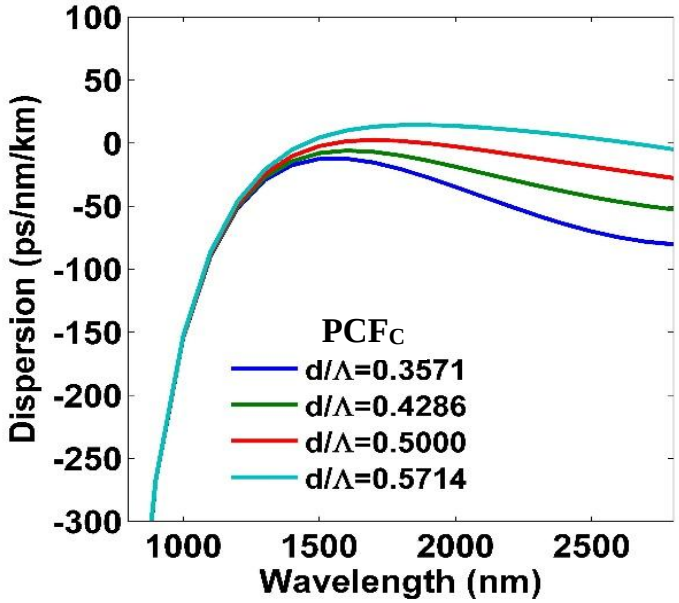

Fig. 7.6: The spectral variation of parameters d/Λ while keeping Λ=2.8 µm, d_{c1}=2.514 µm, and d_{c2}=4 µm fixed in PCF_C to study the dispersion characteristics.

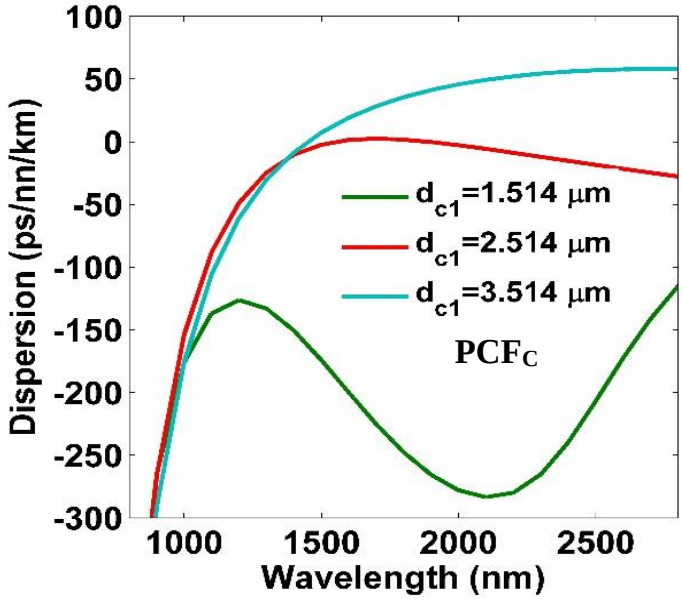

Fig. 7.7: The spectral variation of parameters d_{c1} when d/Λ=0.5000 with Λ=2.8 µm, and d_{c2}=4 µm constant in PCF_C to study the dispersion characteristics.

Then, we have studied the effect of d_{c1} on dispersion which is depicted in fig. 7.7. With the increment in the parameter d_{c1} values (1.514 µm to 3.514µm), a greater shift in the dispersion profile is noticed when the other parameters kept constant as d/Λ=0.5000 and d_{c2}=4 µm. We have obtained an ultra-flat dispersion curve for d_{c1}=2.514 µm in comparison with other d_{c1} values.

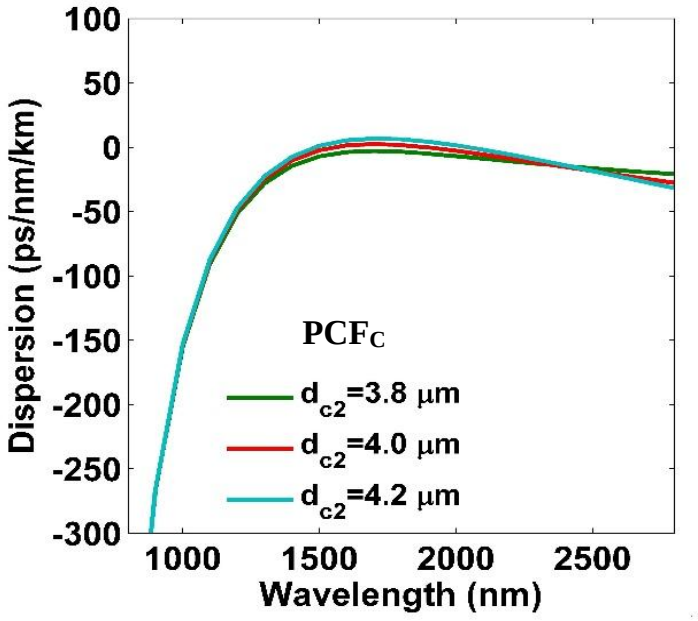

Fig. 7.8: The spectral variation of parameters d_{c2} by keeping d/Λ=0.5000 (Λ=2.8 µm), and d_{c1}=2.514 µm in PCF_C to study the dispersion characteristics.

And, we have also analyzed the effect of d_{c2} on dispersion which is demonstrated in fig. 7.8. As we increased the values of d_{c2} from 3.8 µm to 4.2 µm (with d/Λ=0.5000 and d_{c1}=2.514 µm constant values), the dispersion curve shifted slightly from normal to anomalous region and the negligible shift occurred towards the longer wavelengths. For d_{c2}=4.0 µm, we have achieved a flat dispersion profile which characterized by two ZDWs with minimum dispersion value.

Further, we have compared the best results of the effective mode index, dispersion, effective mode area, and nonlinear coefficient in the PCF_A, PCF_B, and PCF_C designs individually that are consist of un-filtrated solid silica core, nitrobenzene core, and combination of ethanol with nitrobenzene in the core respectively. Figure 7.9 (a) represents the variation of the n_{eff} in PCF_A,

PCF_B, and PCF_C designs. The range of n_{eff} in PCF_A, PCF_B, and PCF_C has been found as 1.448-1.376, 1.523-1.431, and 1.521-1.411 respectively in the wavelength range of 800 nm to 2800 nm. It is noted that the values of the n_{eff} are recorded high in the PCF_B structure in comparison to the PCF_A, and PCF_C structures.

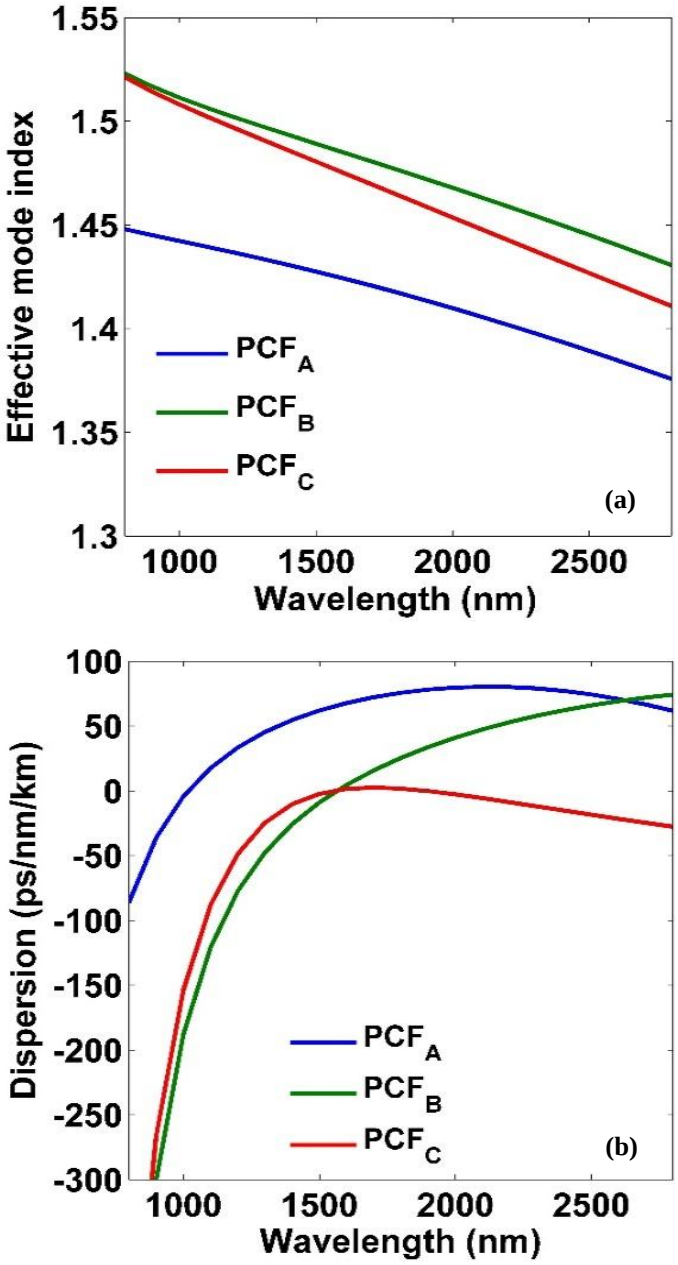

Fig. 7.9: Spectral variation of **(a)** effective mode index; **(b)** chromatic dispersion in PCF_A, PCF_B, and PCF_C.

The effect of the un-infiltrated core of PCF_A and infiltrated cores of PCF_B and PCF_C on the dispersion profile is demonstrated in fig. 7.9 (b). The more profound analysis of dispersion

management has been conducted to reduce the dispersion effect at pump wavelength by tuning the geometrical parameters associated with the fiber designs. The computational results of the dispersion profiles divulge that the PCF_C structure composed of infiltrated core (nitrobenzene and ethanol) holds the special characteristics to diminish the effect of dispersion in comparison to the PCF_A (un-infiltrated solid core of silica), and PCF_B (infiltrated core nitrobenzene) structures. It is also noticed that the dispersion profile corresponding to PCF_C is more flattened than the dispersion profiles of PCF_A, and PCF_B.

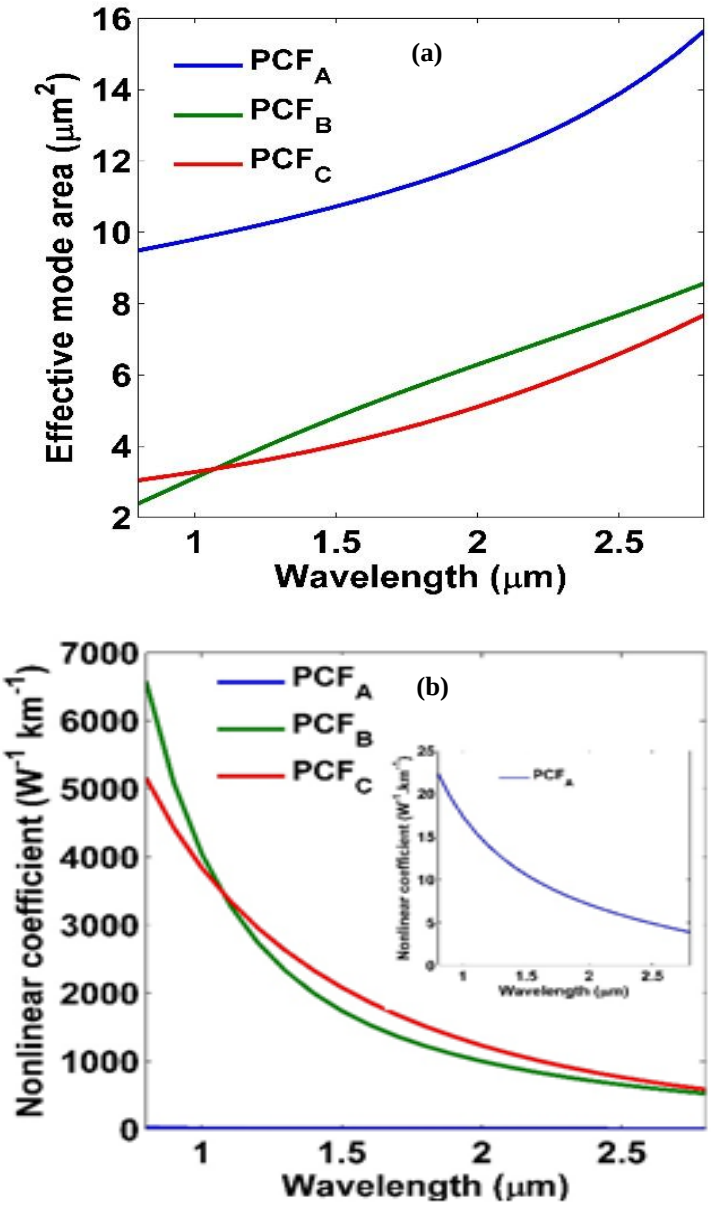

Fig. 7.10: Spectral variation of **(a)** effective mode area; **(b)** nonlinear coefficient chromatic in PCF_A, PCF_B, and PCF_C.

The effective mode area and the nonlinearity associated with the fundamental mode propagation inside core are having great importance in process of SCG in fibers. We further investigated the effect of liquid infiltration in the proposed PCF designs, with the study of effective mode area and nonlinear coefficients. Figure 7.10 (a) demonstrates the variation of effective mode area with the wavelength in PCF_A (d/Λ=0.5000), PCF_B (d/Λ=0.5000, and d_{c1}=2.514 µm), and PCF_C (d/Λ=0.5000, d_{c1}=2.514 µm, and d_{c2}=4 µm). There is a slight variation noticed in the effective mode area values in PCF_B, and PCF_C. It is observed that the effective mode area values of PCF_A (with silica core) are high in comparison of PCF_B (with nitrobenzene core infiltration), and PCF_C (with ethanol and nitrobenzene core infiltration). As a result of the low effective mode area in the PCF_B, and PCF_C, the nonlinear coefficient values are higher in PCFs with nitrobenzene, and ethanol with nitrobenzene infiltrated cores as displayed in fig. 7.10 (b). The nonlinearity reported for the PCF_A is very low in comparison to PCF_B, and PCF_C. This is due to the high linear and nonlinear refractive indices of the organic fluids in comparison to silica glass.

The comparison results validated that the infiltration of nitrobenzene and ethanol organic solvents in the core of PCF_C facilitates one to design the PCF structure for SCG in the visible and near-infrared wavelength regions. Based on the preceding analysis of the linear and nonlinear properties in PCF_A, PCF_B, and PCF_C, we have found that PCF_C is an excellent fit to generate a coherent SC broadband in the visible and near-infrared wavelengths. The optimized parameters of PCF_C are tabulated in table 7.2.

PCF_C Parameters	**Pump Wavelength**	**n_{eff}**	**A_{eff}**	***D(λ)***	**Nonlinearity**
d_{c1}=2.514 µm d_{c2}=4 µm d/Λ=0.5 Λ=2.8 µm	1550 nm	1.4778	4.08 µm^2	+0.856 ps/nm/km	1986 W^{-1}km^{-1}

Table 7.2: Numerical findings of linear and nonlinear parameters in optimized PCF_C design.

Our computational analysis is focused on the study of the influences of peak power and pulse width to obtain the highly efficient coherent SC spectrum in the visible and near-infrared wavelength regions. We have considered the optimized geometrical parameters (d_{c1}=2.514 µm, d_{c2}=4 µm, d/Λ=0.5000 with Λ=2.8 µm constant) of PCF_C for looking the possibility to generate the ultra-coherent SC broadband light source by using few femtosecond input laser pulses with low input peak power in a shorter proposed fiber length.

With this aim, we have assumed a chirpless hyperbolic secant input pulse to generate highly coherent SC broadband in the proposed PCF_C structure. An available input laser pump source of pump wavelength 1.55 µm has been used throughout our numerical simulation study which is characterized by the repetition rate of 100 kHz, pulse energy as 0.426 nJ and the average power as 0.0426 mW.

Initially, the simulations have been performed for different input peak power variations from 1 kW to 7 kW with a period of 2 kW in a 2.5 cm long fiber length of PCF_C. A hyperbolic secant input pulse of 1.55 µm wavelength has been selected having a pulse width of 75 fs during simulation analysis which is lying in the anomalous dispersion region. The spectral evolution of SC and its corresponding spectrograms of an output pulse of different peak powers are displayed in figs. 7.11 (a) and (b). It is seen that with the increase of peak power, the bandwidth of SC is found to be increased. We have successfully attained SC broadband of range 1-2.6 µm covering the visible and near-infrared wavelength regions at -40 dB power level in a 2.5 cm long proposed PCF_C structure using 5 kW peak power. The symmetrical spectral broadening occurred due to SPM and SRS nonlinear processes when pumping is considered in the anomalous region and afterward, the soliton fission materializes due to small perturbations. The spectrograms in fig. 7.11 (b) elucidated concisely the formation SCG in the proposed PCF_C. The spectral energy is presented in between the ZDWs range 1.531-1.919 µm

(anomalous dispersion region) and symmetrical spectral broadening is secured appropriately in the shorter and longer wavelength sides.

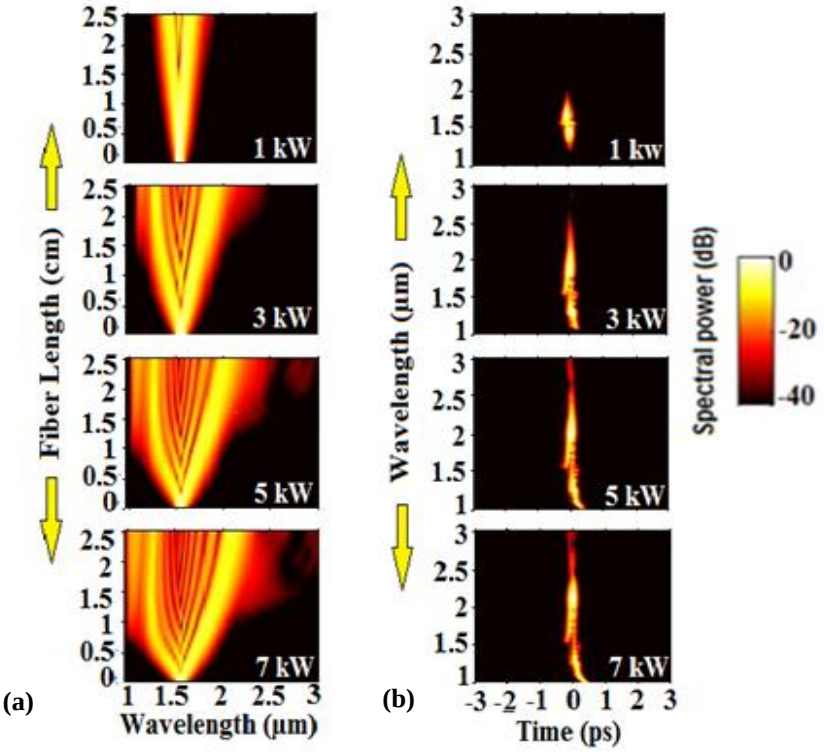

Fig. 7.11: (a) Spectra of generated SC, and **(b)** pulse spectrograms for different peak power variation using pulse width as 75 fs in 2.5 cm long fiber length at 1.55 µm.

We further investigated the impact of the input pulse width on SCG in proposed fiber design which is presented in fig. 7.12 (c). We performed the numerical simulations for different pulse widths as 35 fs, 55 fs, 75 fs, and 95 fs. We have chosen a 2.5 cm long proposed fiber and peak power as 5 kW to carry out the simulation at pump wavelength 1.55 µm. We have noticed that with the enhancement of pulse width values from 35 fs to 95 fs, the bandwidth of SC narrowed. The shorter pulses can generate the wider SC band in the proposed fiber design. Figure 7.12 (d) reveals the spectrograms generated due to nonlinear effects responsible for SCG. As we mentioned earlier that the initial broadening is dominated by SPM and later due to the higher-order dispersion, SRS, etc. In the propagation of shorter pulses, the intensity of spectral energy diminished.

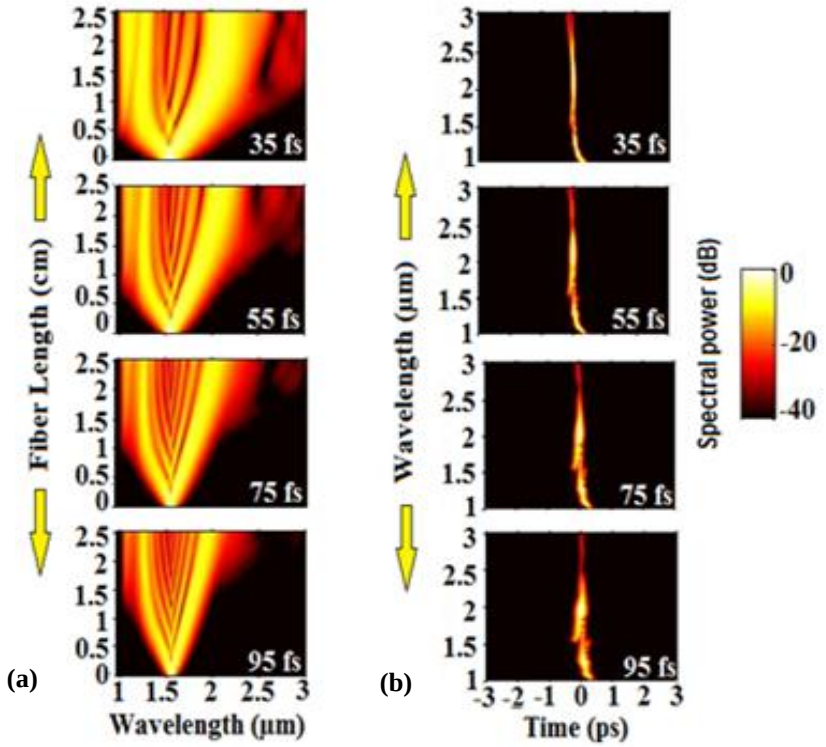

Fig. 7.12: (a) Spectra of generated SC, and **(b)** pulse spectrograms for different pulse width using peak power as 5 kW in 2.5 cm long fiber length at pump wavelength of 1.55 µm.

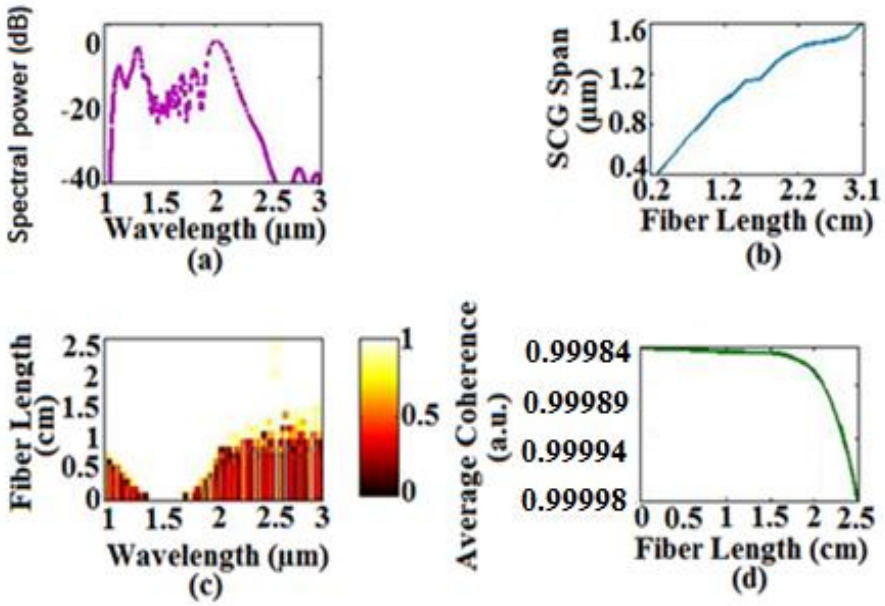

Fig. 7.13 (a) Generated spectral SC broadband at 1.55 µm with peak power 5 kW and pulse width 75 fs in 2.5 cm long PCF_C, **(b)** plot of SCG span obtained in different fiber length, **(c)** evolution of coherence in the proposed fiber design, and **(d)** plot of average coherence vs fiber length.

Next, we have shown the spectral broadening of SCG generated in a 2.5 cm long fiber at 1.55 µm pump wavelength which is illustrated in fig. 7.13 (a). At -40 dB, we have achieved a SC broadband of spanning, 1 µm to 2.6 µm when an input laser pulse of order 75 fs is pumped with peak power of 5 kW. Figure 7.13 (b) is displayed for the SCG spans generated in different propagating fiber length of PCF_C. The spanning is found to be increased for longer fiber lengths. Lastly, the effect of coherence is outlined in figs. 7.13 (c) and (d). It is seen that the resulted SC spectrum is extremely coherent in the complete wavelength range of 1-2.6 µm.

PCF composition	**Pump wavelength (µm)**	**Pulse width (fs)**	**Peak power (kW)**	**Fiber length (cm)**	**SCG spanning (µm)**
Silica PCF (methanol/ethanol core) [10]	1.55	50	20	10	0.8-2
Silica PCF (Toluene core) [11]	1.03	400	25	10	0.95-1.1
Silica PCF (Nitrobenzene core) [14]	1.03	120	0.83	5	0.8–1.8
	1.56	90	5.55	5	0.8–2.1
	1.56	90	0.66	5	1.3–2.3
Optical Fiber (Carbon disulphide core) [34]	1.95	150	4	10	1.8-2.4
Silica PCF (Chloroform core) [35]	1.06	100	47	1	0.34-1.36
Silica PCF(Nitrobenzene-Toluene core) [proposed work]	**1.55**	**75**	**5**	**2.5**	**1-2.6**

Table 7.3: Comparison table for the justification of uniqueness of the proposed fiber design with previously reported results based on organic liquid infiltration fibers.

Our presented numerical simulation results of the proposed PCF_C has several advantages in comparison to previously reported works in infiltrated organic solvents based fibers which are organized in table 7.3. The selective features such as high nonlinearity, flat chromatic

dispersion, propagation in shorter fiber length, low peak power, broader SC bandwidth, and good coherence property are offered by our proposed fiber design.

In the end, we shall discourse the possibility and challenges of fabrication methods for our proposed fiber design. Few authors reported the similar PCF design for dispersion compensation using a composite core of Ge and F dopants in a hexagonal lattice with pure silica [28] and Huang et al. [29] has also suggested a CS_2 doped PCF for the large negative dispersion with tunable ZDW at 1.55 μm wavelength. The general methods to fabricate a PCF with hexagonal lattice pattern are feasible with Stack-and-draw [30] and mechanical drilling [31]. Nielsen et al. [32] reported the selective filling technique to fabricate PCF in the hybrid-material core. The authors in reference [33] has developed a technique named selective-filling to fabricate an organic solvent-based microstructured optical fiber.

7.4 Conclusions:

In summary, we have numerically simulated a hexagonal-shaped photonic crystal fiber structure to generate supercontinuum broadband in the visible and near-infrared wavelength regions. The numerical investigation of ultraflat dispersion profile with and without organic liquids core has been followed with nanoscale variation in geometrical parameters. The proposed fiber design with a liquid core of nitrobenzene and ethanol exhibits an ultra-flatness of dispersion curve and high nonlinearity at 1.55 μm. Our simulation results prove the effectiveness of proposed 2.5 cm long designed fiber to generate the coherent supercontinuum spectrum with spanning from 1-2.6 μm by using an input pulse of pulse width and peak power as 75 fs and 5 kW respectively.

References:

1. J. Dudley, and R. Taylor, “Supercontinuum Generation in Optical Fibers”, Cambridge University Press, New York, pp. 32-51, 2010.

2. J. Dudley, G. Genty, and S. Coen, “Supercontinuum generation in Photonic Crystal Fiber”, Review of Modern Physics 78(4), pp. 1135-1184, 2006.

3. C. Monat, P. Domachuk, and B.J. Eggleton, "Integrated Optofluidics: A New River of Light”, Nature photonics 1(2), pp. 106-114, 2007.

4. C. Monat, P. Domachuk, C. Grillet, M. Collins, B.J. Eggleton, M. Cronin-Golomb, S. Mutzenich, T. Mahmud, G. Rosengarten, and A. Mitchell, "Optofluidics: a novel generation of reconfigurable and adaptive compact architectures", Microfluidics and Nanofluidics 4(1-2), pp. 81-95, 2008.

5. M. Vieweg, T. Gissibl, S. Pricking, B.T. Kuhlmey, D.C. Wu, B.J. Eggleton, and H. Giessen, "Ultrafast nonlinear optofluidics in selectively liquid-filled photonic crystal fibers", Optics express 18(24), pp. 25232-25240, 2010.

6. R. Zhang, J. Teipel, and H. Giessen, "Theoretical design of a liquid-core photonic crystal fiber for supercontinuum generation", Optics express 14(15), pp. 6800-6812, 2006.

7. J. Bethge, A. Husakou, F. Mitschke, F. Noack, U. Griebner, G. Steinmeyer, and J. Herrmann, "Two-octave supercontinuum generation in a water-filled photonic crystal fiber", Optics express 18(6), pp. 6230-6240, 2010.

8. S. Kedenburg, T. Gissibl, T. Steinle, A. Steinmann, and H. Giessen, "Towards integration of a liquid-filled fiber capillary for supercontinuum generation in the 1.2–2.4 μm range", Optics Express 23(7), pp. 8281-8289, 2015.

9. R. Raei, Rasoul, M.E. Heidari, and H. Saghaei, "Supercontinuum generation in organic liquid-liquid core-cladding photonic crystal fiber in visible and near-infrared regions", Journal of Optical Society of America B 35(2), pp. 323-330, 2018.

10. H. Saghaei, "Supercontinuum source for dense wavelength division multiplexing in square photonic crystal fiber via fluidic infiltration approach", Radioengineering 26(1), pp. 16-22, 2017.

11. R. Kasztelanic, A. Anuszkiewicz, G. Stepniewski, A. Filipkowski, S. Ertman, D. Pysz, T. Wolinski, K.D. Xuan, M. Klimczak, and R. Buczynski, "All-normal dispersion supercontinuum generation in photonic crystal fibers with large hollow cores infiltrated with toluene", Optical Materials Express 8(11), pp. 3568-3582, 2018.

12. R. Kasztelanic, A. Filipkowski, G. Stępniewski, D. Pysz, M. Klimczak, S. Ertman, T.R. Woliński et al., "Supercontinuum generation in an all-normal dispersion large core photonic crystal fiber infiltrated with carbon tetrachloride", Optical Materials Express 9(5), pp. 2264-2278, 2019.

13. C.V. Lanh, K. Borzycki, K.D. Xuan, V.T. Quoc, M. Trippenbach, R. Buczyński, and J. Pniewski, "Optimization of optical properties of photonic crystal fibers infiltrated with chloroform for supercontinuum generation", Laser Physics 29(7), p. 075107, 2019.

14. C.V. Lanh, K. Borzycki, K.D. Xuan, V.T. Quoc, M. Trippenbach, R. Buczyński, and J. Pniewski, "Supercontinuum generation in photonic crystal fibers infiltrated with nitrobenzene", Laser Physics 30(3), p. 035105, 2020.

15. J. Pniewski, T. Stefaniuk, H.L. Van, L.C. Van, R. Kasztelanic, G. Stępniewski, A. Ramaniuk, M. Trippenbach, and R. Buczyński, "Dispersion engineering in nonlinear soft glass photonic crystal fibers infiltrated with liquids", Applied optics 55(19), pp. 5033-5040, 2016.

16. F. Xu, J. Yuan, C. Mei, B. Yan, X. Zhou, Q. Wu, K. Wang, X. Sang, C. Yu, and G. Farrell, "Highly coherent supercontinuum generation in a polarization-maintaining CS_2-core photonic crystal fiber", Applied optics 58(6), pp. 1386-1392, 2019.

17. N. Munera, S. Vergara, C.A. Alvarez, and R.A. Herrera, "Liquid-core photonic crystal fiber for supercontinuum generation based on hybrid soliton dynamics", In 2018 International Conference on Electromagnetics in Advanced Applications (ICEAA), IEEE, pp. 546-549, 2018.

18. D. Churin, T.N. Nguyen, K. Kieu, R.A. Norwood, and N. Peyghambarian, "Mid-IR supercontinuum generation in an integrated liquid-core optical fiber filled with CS_2", Optical Materials Express 3(9), pp. 1358-1364, 2013.

19. K. Porsezian, K. Nithyanandan, R.V.J. Raja, and R. Ganapathy, "A theoretical investigation of soliton induced supercontinuum generation in liquid core photonic crystal fiber and dual core optical fiber", The European Physical Journal Special Topics 222(3-4), pp. 625-640, 2013.

20. R. Kasztelanic, G. Stępniewski, K.D. Xuan, M. Trippenbach, M. Klimczak, R. Buczyński, and J. Pniewski, "Femtosecond supercontinuum generation around 1560 nm in hollow-core photonic crystal fibers filled with carbon tetrachloride", Applied Optics 59(12), pp. 3720-3725, 2020.

21. M. Chemnitz, C. Gaida, M. Gebhardt, F. Stutzki, J. Kobelke, A. Tünnermann, J. Limpert, and M.A. Schmidt, "Carbon chloride-core fibers for soliton mediated supercontinuum generation", Optics express 26(3), pp. 3221-3235, 2018.

22. Y. Xu, X. Chen, and Y. Zhu, "Modeling of micro-diameter-scale liquid core optical fiber filled with various liquids", Optics express 16(12), pp. 9205-9212, 2008.
23. T.L. Canh, H.L. Van, D. Pysz, T.B. Dinh, D.T. Nguyen, Q. H. Dinh, M. Klimczak et al., "Supercontinuum generation in all-normal dispersion suspended core fiber infiltrated with water", Optical Materials Express 10(7), pp. 1733-1748, 2020.
24. N. Karasawa, "Dispersion properties of liquid-core photonic crystal fibers", Applied Optics 51(21), pp. 5259-5265, 2012.
25. I.H. Malitson, "Interspecimen comparison of the refractive index of fused silica", Journal of Optical Society of America 55(10), pp. 1205-1209, 1965.
26. S. Kedenburg, M. Vieweg, T. Gissibl, and H. Giessen, "Linear refractive index and absorption measurements of nonlinear optical liquids in the visible and near-infrared spectral region", Optical Materials Express 2(11), pp. 1588-1611, 2012.
27. S. Kedenburg, A. Steinmann, R. Hegenbarth, T. Steinle, and H. Giessen, "Nonlinear refractive indices of nonlinear liquids: wavelength dependence and influence of retarded response", Applied Physics B 117(3), pp. 803-816, 2014.
28. H. Xu, X. Wang, X. Huang, C. Zhou, H. Zhu, and X. Cai, "All-solid photonic crystal fiber for dispersion compensation over S+ C+ L wavelength bands", IEEE Photonics Technology Letters 30(17), pp. 1499-1502, 2018.
29. D. Huang, Z. Huang, and D. Zhan, "Novel large negative dispersion and tunable zero dispersion wavelength of photonic crystal fiber," Waves in Random and Complex Media 28(4), pp. 624-629, 2018.
30. D. Pysz, I. Kujawa, R. Stępień, M. Klimczak, A. Filipkowski, M. Franczyk, L. Kociszewski, J. Buźniak, K. Haraśny, and R. Buczyński, "Stack and draw fabrication of soft glass microstructured fiber optics", Bulletin of the Polish Academy of Sciences. Technical Sciences 62(4), 2014.
31. P. Zhang, J. Zhang, P. Yang, S. Dai, X. Wang, and W. Zhang, "Fabrication of chalcogenide glass photonic crystal fibers with mechanical drilling", Optical Fiber Technology 26, pp. 176-179, 2015.
32. K. Nielsen, D. Noordegraaf, T. Sørensen, A. Bjarklev, and T.P. Hansen, "Selective filling of photonic crystal fibres", Journal of Optics A: Pure and Applied Optics 7(8), p. L13, 2005.
33. Y. Huang, Y. Xu, and A. Yariv, "Fabrication of functional microstructured optical fibers through a selective-filling technique", Applied Physics Letters 85(22), pp. 5182-5184, 2004.

34. C. Wang, G. Feng, W. Li, and S. Zhou, "Highly coherent supercontinuum generation in CS_2-infiltrated single-core optical fiber", Journal of Optics 21(10), p. 105501, 2019.

35. C. Wang, W. Li, N. Li, and W. Wang, "Numerical simulation of coherent visible-to-near-infrared supercontinuum generation in the $CHCl_3$-filled photonic crystal fiber with 1.06 μm pump pulses", Optics & Laser Technology 88, pp. 215-221, 2017.

CHAPTER-8

CONCLUDING REMARKS AND FUTURE RESEARCH SCOPE

In this work, we have demonstrated the numerical simulations of visible, near and mid-infrared ultra-broadband coherent SCG in highly nonlinear PCF designs based on silica, tellurite, chalcogenide, and organic liquids for the major applications in spectroscopy, gas sensing, medical, optical coherence tomography, wavelength-division multiplexing, and free space communications.

A hexagonal shaped photonic crystal fiber in silica glass has been proposed which generated a supercontinuum broadband spanning, ~0.67-2.4 μm in 37 cm long fiber length with peak power of 8 kW at pump wavelength of 1300 nm. A golden spiral shaped PCF in tellurite glass has been investigated and we achieved an ultra-broadband supercontinuum of bandwidth 1000-5500 nm at 1350 nm pump wavelength in a 5.5 cm long fiber length. We have obtained a supercontinuum spanning, 1-14 μm in 9 mm long $Ga_8Sb_{32}S_{60}$ chalcogenide based PCF at 4 μm pump wavelength and peak power of 8.19 kW. We have reported a coherent supercontinuum broadband of bandwidth 10 μm in 10 mm long GAP-Se based photonic crystal fiber using peak power of 950 W and pulse width of 85 fs at 3.1 μm. At the end we proposed a hexagonal-shaped photonic crystal fiber infiltrated with organic liquids to generate the coherent supercontinuum spectrum with spanning, 1-2.6 μm with peak power of 5 kW at 1.55 μm.

This work can further be extended:

- To design and model the chalcogenide based photonic crystal fibers to generate the supercontinuum at longer wavelengths.
- To design and model the chalcogenide based photonic crystal fibers with flattened dispersion profile for supercontinuum generation.
- To study the high power supercontinuum generation in photonic crystal fibers for newly reported chalcogenides.